Doctoral Dissertation

Doctoral Program in Energy Engineering (34th Cycle)

Newly designed single-ion conducting polymer electrolytes enabling advanced Li-metal solid-state batteries

By

Gabriele Lingua

Supervisor:
Prof. Claudio Gerbaldi

Doctoral Examination Committee:
Prof. Maria Assunta Navarra , Referee, University of Rome "La Sapienza"
Prof. Robert Dominko, Referee, National Institute of Chemistry, Department for Materials chemistry

Politecnico di Torino
2022

Declaration

I hereby declare that the contents and organization of this dissertation constitute my own original work and does not compromise in any way the rights of third parties, including those relating to the security of personal data.

Gabriele Lingua

2022

To whom believes in miracles

Contents

List of Figures

List of Tables

Preface

Nowadays, nobody would be astonished to see a young girl/boy connected with her/his mobile phone while searching online for a new electric or hybrid car as the old one cannot circulate anymore in the city centre due to carbon dioxide (CO_2) emission limits. To understand how we came to this scenario, that would have been considered incredibly futuristic even only 15-20 years ago, it is necessary to walk back in time to find the first example of electric vehicle, precisely to the 1830s, when R. Anderson conceived the first, real horseless electric carriage. Since then, many efforts have been spent in the research and development of innovative energy storage and conversion materials and related devices, eventually leading to the commercialization, in 1991, of the first lithium-ion battery (Li-ion battery, LIB) by SONY® and then its evolution, which resulted into the current generation of advanced energy power sources.

LIBs have a central role in our daily lives for their widespread use in smart mobile devices, electric vehicles, and large-scale energy storage from renewables. The technology seems to be mature in terms of energy and power density, reliability and cyclability; unfortunately, this is still not enough to satisfy the always growing demand and voracious energy needs by our modern, global society. Indeed, there is an ever-increasing demand for batteries, especially from the automotive field, with greatly enhanced energy and power density (fast performance upon discharging and charging). Moreover, the legislation is forcing car manufacturers to sizeably reduce CO_2 emissions of their vehicles. This burden has driven the effort of the research community to focus on new propulsion concepts with rechargeable batteries at their core. Accordingly to the climate investigations, it was estimated that 496 (282 to 701 in lower- and upper-bounding scenarios) gigatons (Gt) of CO_2 (Gt CO_2;1 Gt = 10^{12} kg) will be emitted from the combustion of fossil fuels by the current

infrastructure between 2010 and 2060. Actually, the scenario which assumes continuous expansion of fossil fuel-based infrastructure and vehicles predicts cumulative emissions of 2986 to 7402 Gt CO_2 during the remainder of this century, leading to dramatically increasing global warming (foreseen Earth's surface temperature increase in the range of 2.4 to 4.6 °C by 2100 and atmospheric concentrations of CO_2 greater than 600 ppm). In this context, the need for advanced batteries is evident and urgent, thus revolutionizing the market by combining high-voltage cathode materials (HVCMs), high-capacity anodes and innovative solid-state electrolytes (SSEs). The stringent requests of European legislation along with technological progress led to the discovery of several LIB configurations involving innovative electrodes and electrolytes. In the past years, tremendous research efforts have been focused on the development of safer electrolytes to replace current toxic and flammable organic carbonate solvents. Following the discovery of ion conductivity in poly(ethylene oxide) (PEO) with alkali metal salts, the use of solid polymer electrolytes (SPEs) gathered much attention, which resulted in sizeable developments towards its practical application. Among the wide variety of SPEs, single ion-conducting polymer electrolytes (SICPEs) are currently at the forefront of the research by the scientific community because of their promising prospects of targeting high energy density at high current rate due to the transference number close to unity. In addition, the tunability of the macromolecular structure in the polymer network by means of controlled polymerization and monomer selection allows easy control over the final SICPE properties, which may be finely tuned and optimized depending on the final envisaged application.

Considering the abovementioned scenario, the research efforts in the three years of Ph.D. course were focused on developing innovative SICPE networks with easily tuneable properties obtained by exploring the combination of different monomers with different chemical characteristics. Different copolymers with Li^+ single ion conducting features were prepared in order to investigate several aspects, such as: the use of polycarbonate to increase the oxidative stability of the SICPE, the effects of phase separation on SICPE electrochemical and mechanical properties and the advantages resulting from novel ionic monomers. All the samples were fully characterized from the chemical-physical and electrochemical viewpoints resulting promising candidates for application in the solid-state Li metal batteries. Most of the syntheses were carried out in the Luxemburg Institute of Science and Technology (LIST-Luxemburg) laboratories during a six months visiting stage carried out in the first year of Ph.D., as well as upon continuous collaboration with

the Prof. Alexander S. Shaplov further on along the whole Ph.D. course. The initial research efforts were mainly dedicated to preparing novel SICPEs for application in advanced, high-voltage Li-metal batteries. The goal was achieving SICPEs with suitable ionic conductivity, high transference number and enhanced resistance towards anodic oxidation allowing safe operation when combined with high voltage cathodes, such as lithium nickel manganese cobalt oxides (NMC). Based on the obtained initial outcomes, the efforts were then focused on optimising the systems by preparing different SICPEs with well-defined block copolymer structure and specifically designed ionic monomer characteristics, which allowed investigating the influence of both phase separation and chemical nature of the monomers.

The outcome of the work is organised in 7 chapters, comprising the introductory section and concluding remarks; in addition, the description of the experimental setup used in reported in chapter 3. Chapter 1 briefly overviews the present global energy scenario, while also introducing modern energy storage technologies, particularly LIBs. Furthermore, the time evolution, the basic concepts, the present status and limitations of LIBs are discussed to update the reader with the present and future trends in the field of research.

In Chapter 2, solid-state electrolytes (SPEs) for LIBs are introduced, chiefly highlighting the beneficial effects and the future development prospects of SPEs. SPEs based on polyethylene oxide and polycarbonate are discussed, also pointing out the most relevant literature outcomes. In addition, the family of SICPEs is discussed, detailing its time evolution and the most impactful recent achievements in the field.

Chapter 3 briefly describes the polymerization techniques used for the preparation of SICPEs and the description of the experimental setup used during this Ph.D. work.

Chapter 4 thoroughly details the synthesis and characterization of the novel family of block copolymers obtained by coupling the ring opening polymerization (ROP) of trimethylene carbonate (TMC) monomer and the RAFT polymerization of methacrylate monomers. The chapter includes the preparation of a poly(carbonate) macro-RAFT precursor and its subsequent application in the RAFT copolymerization of the lithium ionic monomer and the poly(ethylene glycol) methyl ether methacrylate (PEGM). The resulting SICPEs were characterised in their electrochemical behaviour in real laboratory-scale cell configuration, demonstrating enhanced compatibility and stable performance with both average-

and high-voltage composite cathodes, *viz.* $LiFePO_4 - LFP$ and $LiNiMnCoO_2 - NMC$, as well as with the lithium metal anode.

In Chapter 5, the synthesis procedure and the characterization are reported for a series of single ion conducting block copolymers obtained by reversible addition-fragmentation chain transfer (RAFT) copolymerization of lithium ionic monomer, PEGM and 2-phenylethyl methacrylate (PhEtM). The resulting SICPEs displayed partial incompatibility between blocks along with well-defined phase separation character. The effect of long-range-ordered microphase segregation on mechanical properties and ionic conductivity was investigated, evidencing the ability of the system to maintain suitable ionic conductivity values despite the huge amount of non-ionic monomers. Moreover, the SICPE achieved high rate capability, up to C/5 rate, in lab-scale Li-metal cell with $LiFePO_4 - LFP$ composite cathode along with excellent Coulombic efficiency.

Finally, Chapter 6 details the synthesis of a novel lithium monomer characterized by a long and flexible ethylene oxide chain with an anchored anionic moiety. The monomer was used to prepare a set of polymers (homopolymers and copolymers) including PEGM by free radical polymerization. The resulting new family of SICPEs was characterized from the chemical-physical and electrochemical viewpoints The comparison of the innovative SICPE with the most recent literature reports highlighted the beneficial effect of the newly designed monomer structure on electrochemical performances. Indeed, the enhanced stability and ionic conductivity of SICPE were successfully demonstrated by excellent rate capability and highly stable prolonged cycling at C/5 current rate in lab scale Li metal cell with LFP.

In the modern scenario of increasing demand for energy storage devices, which should enable the forthcoming electric revolution, the present work represents a concrete step forward towards the development of new solid-state electrolyte with single Li^+ ion conducting features, enhanced electrochemical stability and ion mobility. In this respect, the results obtained during the 3-years of Ph.D. research sizeably contribute to improving the amount of knowledge in the field of SICPEs, which is rather new and actually definitely promising for paving the way towards the next generation of high performing, safe and durable lithium-based batteries for being successful in achieving the goals of a sustainable global energy transition.

Chapter 1

1 Energy storage

1.1 Global scenario and a look to the future

Energy storage is a critical component of manufacturing, the service industry, the future renewable energy industry, and all the portable electronics that have become fundamental elements of our daily lives. Without modern energy storage and conversion devices, such as lithium-ion batteries (LIBs), the growth and consolidation of smart portable technologies, including smartphones, laptops, smartwatches, as well as electromobility solutions, would not have been possible. Thinking bigger, large-scale energy storage from renewables (*viz.* grid energy storage) plays a critical role in high-tech manufacturing, where it is essential to have a constant power supply. Indeed, to avoid short dips, spikes and/or interruptions, many industries are equipped with large power storage backups, comprising batteries and supercapacitors, respectively, for energy and frequency regulation in such critical applications. Smart grid technology allows us to store the excess of energy during production peaks and use it back when needed, with flexibility at different timescales (seconds/minutes, hours, weeks, and even months, see Figure 1.1).
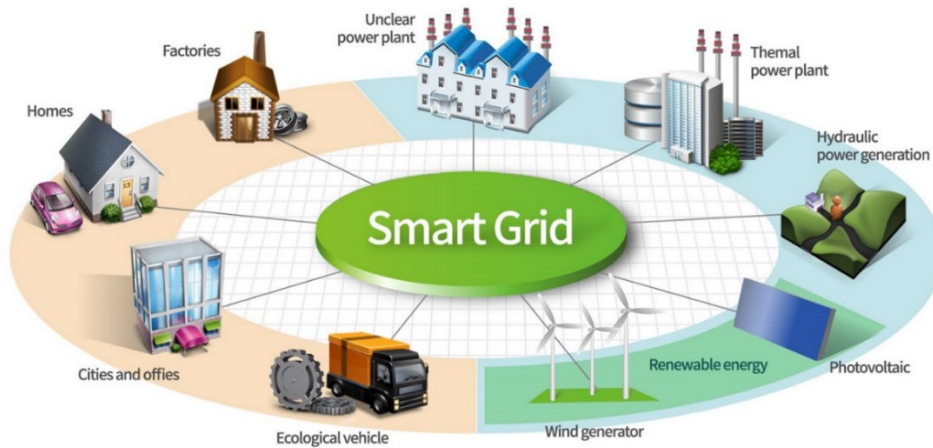
Figure 1.1 Smart Grid example of efficient electricity network, which allows to connect different user's behaviours and energy production sources.

The development of these innovative technologies is directly connected to novel renewable sources, which are under continuous evolution/optimisation to make possible a change in the steady rise of greenhouse gases and air pollutants in the atmosphere. In the last decade, even more attention has been dedicated to global climate change and depletion of natural resources mainly ascbribed to industrial activities, transportation, and electricity production. As reported by the Intergovernmental Panel on Climate Change (IPCC), the severe industrial growth has raised atmospheric carbon dioxide (CO_2) levels from 280 parts per million to about 417 parts per million in the last 151 years, which resulted in global temperature increase. As a direct consequence of the introduction of stringent regulations by national and international legislation, hybrid, plug-in and fully electric vehicles are rapidly growing in popularity, being road transportation one of the most impactful sectors concurring to CO_2 emission.[1]
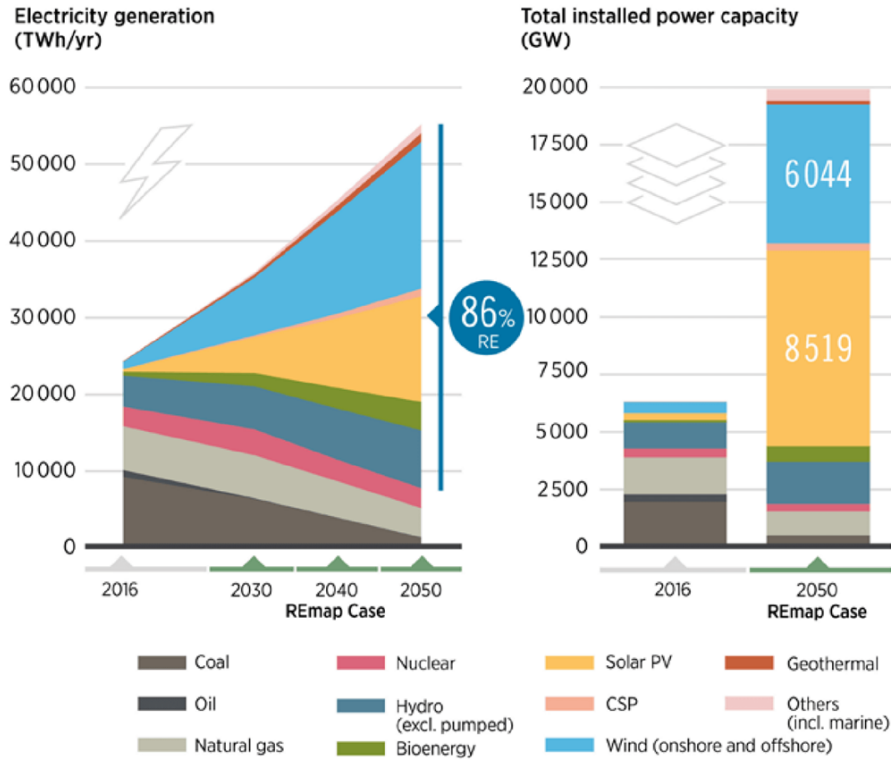
In this scenario, the development of novel, efficient materials for electrochemical energy storage (EES) devices is the key point for exploiting only renewable energy sources, especially solar and wind power sources, instead of fossil fuel, thus ensuring the safeguard of our planet (Figure 1.2). The term "EES" has been popular in the literature from more than a decade, and it is comparable with, but not identical to, the traditional term "electrochemical energy conversion and storage", which emphasises 'conversion between electrical and chemical energy', considering also fuel cells.[2] This is because currently popular EES technologies mainly include rechargeable batteries and electrochemical capacitors (ECs), widely known as supercapacitors. Nevertheless, it is worth to mention

emerging ESS technology, such as hybrids of battery and supercapacitor, namely supercapatteries.[2]

1.2 Electrochemical energy storage devices

As above mentioned, systems for electrochemical energy storage and conversion include batteries, fuel cells, and ECs. Although there are several differences among energy storage and conversion mechanisms, there are "electrochemical similarities" between these systems. Common features are that the energy-providing processes occur at the phase boundary of the electrode/electrolyte interface and that transport of electrons and ions is separated.

In order to explain the reason why fuel cells do not belong to the category of EES devices, it is worth reminding that this technology implies utilizing hydrogen pumped from a storage tank and oxygen from the outside air to generate electric power, almost like a battery. However, unlike batteries, fuel cells do not actually store energy in the form of electric potential, but they are more similar to active devices, which convert potential energy (hydrogen tank) into electrical one.[3] In other words, energy storage and conversion occur in different compartments.

Regarding EES devices, both EC and battery technologies consist of two electrodes, the anode and the cathode, separated by an ion-permeable and electronic insulating electrolyte, which can be liquid (needs a separator to avoid physical contact of the electrodes) or solid. The anode is the negative electrode, from which electrons flow during discharge through the external circuit towards the cathode, the positive electrode. The separating electrolyte is a fundamental component of EES devices that ionically connects the electrodes, allowing conduction of ions (cations) between them, which balances (compensates) the negative electron charges. The working principle of both batteries and supercapacitors is similar and the main difference is that in batteries Faradaic reactions occur at the electrodes. Indeed, in supercapacitors, when electrodes are polarized by an applied voltage, the ions in the electrolyte form an electric double layer of opposite polarity to the electrode polarity (capacitive reactions). For example, positively polarized electrodes will have a layer of negative ions (anions) at the electrode/electrolyte interface along with a charge-balancing layer of cations adsorbing onto the negative

layer. In the case of batteries, at the electrode/electrolyte interface, specific mechanisms, which will be discussed more in details below, such as cation de/insertion or de/intercalation (depending on the electrode structure and properties) take place, with consequent electrons transfer from or into the electrodes (respectively oxidation or reduction process, *viz.* Faradaic process).

Supercapacitors, namely *electrical double layer capacitors* (EDLCs), can directly store electrical energy via electrostatic adsorption of ions at the interface between the electrodes and the electrolyte under an applied cell voltage, without any reversible Faradaic reaction. Therefore, the capacitance mainly depends on the active surface area of electrodes, which can be accessed by the electrolyte. Indeed, important factors controlling the electrochemical activity of electrodes are the specific surface area, pore size distribution, pore shape, morphology, conductivity, and surface functionality.[4] Among these, the pore size of electrode materials should be very close to the size of ions in the electrolyte to yield maximum double layer capacitance. In addition, being electrodes not involved in ions insertion/de-insertion reactions, the structural integrity of common active materials is maintained, which allows supercapacitors to be charged and discharged even millions of times without any significant material degradation. On the contrary, in batteries, structural changes in the active materials upon ions insertion/deinsertion occur, affecting their overall operational life. For long time, batteries and supercapacitors have been compared by performance criteria. Supercapacitors exhibit unprecedented power density and possess a longer life expectancy, while batteries offer superior energy density and higher breakdown voltage (Figure 1.3).
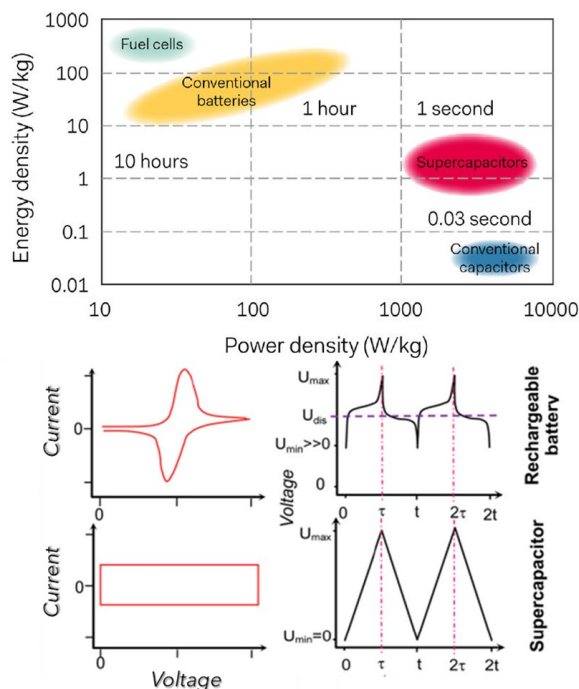
Figure 1.3 Ragone plot showing energy density vs. power density for various energy-storing devices and comparison between supercapacitor and rechargeable battery in terms of current vs voltage and charging/discharging profiles. Figure adapted/reprinted with permission from Chen, G. Z.[2].

Indeed, as mentioned above, the charging and discharging processes in EDLCs do not involve any Faradaic reaction. The current *vs*. voltage profile is characterized by flat plateaus and rectangular shapes because of accumulation phenomena at the interface without oxidation/reduction reactions. Conversely, the rechargeable battery current *vs*. voltage profile evidences the occurrence of reversible oxidation and reduction reactions, respectively, accompanied by positive and negative current increases (oxidation/reduction peaks) (Figure 1.3).[2] The most relevant electrode materials for supercapacitors are based on carbon: activated carbon, carbon nanotubes (CNTs) and graphene; but also several metal oxides with high conductivity, such as RuO_2, V_2O_5, MoO_x and MnO_2. Meanwhile, regarding the electrolyte, which plays a fundamental role in EDCLs performance, especially in terms of conductivity, the chemistry ranges from aqueous or organic liquid electrolytes to the use of ionic liquids (ILs) and gel/dry solid polymer electrolytes.[2,5–9]

Despite encouraging results in the field of energy storage, the development of new generations of supercapacitors is still at the preliminary stage, and the limited energy density (which is just a fraction of that of LIBs) reduces the possibility of building an efficient, fully electric vehicle solely based on this technology. Nevertheless, the combination of supercapacitors and batteries is being increasingly explored by researchers to improve the driving range and battery lifetime of fully electric or hybrid-electric vehicles (EVs, HEVs, respectively). The coupling between batteries and supercapacitors in an integrated system makes it more robust and performing, as they cover each other's weaknesses. Supercapacitors protect batteries from power fluctuations and lead to a longer lifespan, while batteries can provide higher energy-density allowing longer-range of utilization as needed by EVs.

Batteries are by far the most common and studied device for storing electrical energy, and the first example of an accumulator is the *Voltaic cell* discovered in 1800 by the Italian physicist Alessandro Volta, who demonstrated the formation of a voltage difference when two different metals (copper and zinc) are put in contact through an ion conductive membrane (cloth soaked in brine) with the production of external electric current. The Volta cell prototype evolved into the Daniel electrochemical cell (1836)), a great improvement over the existing technology as it eliminated the issue of H_2 bubbles formation. Lately, in 1859, Gaston Planté realised the first rechargeable (secondary) battery, the well known *lead-acid battery*. From that point onwards, to address the problem of overall low energy density of the devices, the scientific efforts and the technological progress led to the discovery of *Nickel Cadmium* (NiCd) *battery*.

This transition was fundamental to get lighter batteries, but their use and production drastically decreased because of cadmium toxicity, up to the complete replacement with its "green version" in 1990: the *Nickel-Metal Hydride battery* (NiMH). NiMH batteries rapidly conquered the portable electronic device market, maintaining the same working voltage (1.2 volts) and charging characteristics of NiCds, but with a 50 % higher energy density and the elimination of toxic and expensive metals. NiMH cells were characterised by a self-discharge greater than NiCds, but the improvements in the separator, switching from polyamides to polyolefins, enabled NiMH cells to have a lower self-discharge than that of NiCds. The performance of NiMH batteries has seen continuous improvements over the years through a combination of different approaches, such as thin and high-density

negative electrodes, thinner separators, upgraded cathode and improved packaging efficiencies, which finally brought to the use of this secondary battery in early hybrid EVs, such as the Toyota Prius in 1997.

In the same years, continuous progress in technology and the always more connected society were among the main causes of widespread diffusion of portable electronic products, such as video cameras, mobile phones, and notebooks. This technological revolution unleashed the growing need for rechargeable batteries with greatly enhanced energy/power density and reduced size and weight, to overcome the limited performance of conventional available rechargeable batteries. As a result, the new, small, and lightweight rechargeable battery, namely the Li-ion battery (LIB) was invented, most rapidly becoming the undisputed market leader worldwide. Research on LIBs started in the early 1980s, and the first production and commercialization were achieved in the early '90s by SONY®, following Yoshino's design (Figure 1.4). Since then, LIBs have become the dominant energy storage solution for portable electronic devices and more...[10]
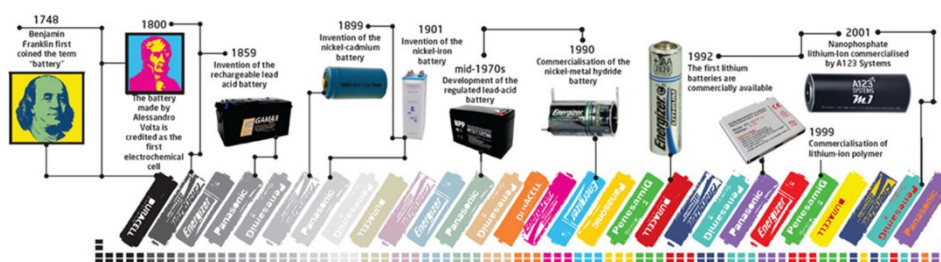
Figure 1.4 Battery timeline evolution from the fist use of the term "battery" to commercialized products. Figure adapted/reprinted from UPS battery center "History Of Batteries: A Timeline" (https://www.upsbatterycenter.com/blog/history-batteries-timeline/).

1.2.1 The development of rechargeable batteries

Rechargeable Li-ion batteries are key components in our daily life, from smart electronics to HEVs and EVs. As already discussed in the previous paragraph, the research in the field of energy storage and conversion resulted in astonishing advances in chemistry and engineering of materials and devices. However, because of their energy density values, flexibility and lightweight LIBs dominate the market,

and their diffusion and development will rapidly grow to address the requirement for the transition towards a "green" and carbon-free society.

Generally speaking, a battery is composed of several electrochemical cells, connected in series and/or parallel to provide the required voltage or capacity, converting chemical energy into electrical energy. Each cell consists of a positive and a negative electrode (both sources of chemical reactions) separated by an electrolyte solution typically containing dissociated salts, which enable ion transfer between the two electrodes. Once these electrodes are connected externally, the chemical reactions proceed in tandem at both electrodes, thereby producing electrons transfer to compensate the positive charges and enabling the current to be tapped by the user. The amount of electrical energy that a battery is able to deliver, expressed either per unit of weight (Wh kg^{-1}) or per unit of volume (Wh l^{-1}), is a function of the cell potential (V) and capacity (Ah kg^{-1}), both of which are linked directly to the chemistry of the system.

The motivation for using a battery technology based on lithium relied initially on the fact that Li is the most electropositive element (-3.04 V versus standard hydrogen electrode), which means it can be used to make batteries with higher terminal voltages than other designs (typically, ~ 3.6 volts rather than 1.5 volts of NiMH), as well as the lightest (equivalent weight M = 6.94 g mol^{-1} and density ρ = 0.534 g cm^{-3}) of all metals, thus facilitating the design of storage systems with high energy density (lithium has the capacity to store ~ 3860 mAh g^{-1} of charge).[11] In the early 1960s, there was a growing interest in the electrochemistry of non-aqueous solvents, and several solvent-solute electrolyte combinations were studied to enhance the ionic conductivity. The first primary lithium battery prototypes were characterized by the presence of organic liquid electrolyte mixtures comprising acetonitrile (ACN), 4-butyrolactone (BL), dimethyl carbonate (DMC), dimethyl formamide (DMF), dimethyl sulphoxide (DMSO), ethyl acetate (EtOAc), ethylene carbonate (EC) and propylene carbonate (PC) and, prevalently, lithium perchlorate salt ($LiClO_4$).[12]

The breakthrough in terms of conductivity and interfacial stability with lithium metal anode was the use of solvent mixtures based on PC or BL. The interaction of organic electrolyte with the lithium metal electrode allows the formation of a stable and electrochemically insulating film on the surface of the anode, which protects it from further reactions. It was established that PC could be electrochemically

decomposed quite efficiently, forming a passivating film, consising of insoluble products of the electrolyte decomposition with the metal. Its effect on the electrode kinetics was provided by Peled and coworkers [13], who coined the term "*solid electrolyte interphase*" (SEI), emphasising its functionality as an interphase between the metal and the solution, with properties of a solid electrolyte.

As will be noted later, characteristics of this film are also fundamental for realising safe secondary batteries exploiting the lithium metal anode. The research community efforts were fundamental in understanding the basic processes associated with lithium metal cells. In this respect, the 1970s were characterized by the rapid commercialization of lithium-based primary batteries. The most promising systems operating at room temperature included lithium/sulfur dioxide (Li/SO$_2$), lithium/manganese oxide (Li/MnO$_2$), lithium/polycarbon monofluoride (Li (CF$_x$)$_n$) and lithium/iodine-polyvinylpyridine (Li/I(PVP)) cells.[14] These primary systems found applications in various field, from military to medical, with the Li/MnO$_2$ cell being dominant in the consumer market.[15]

Rechargeable Li-based cells intruded the battery market when, in the mid-70s, based on the Whittingham's design, ExxonMobil announced the commercialization of the Li/TiS$_2$ system as a coin cell for electronic watches.[16] The velocity and reversibility of intercalation/deintercalation reactions at ambient temperature made TiS$_2$ the best intercalation compound available at the time. [17,18] The introduction of cathodes, which can reversibly intercalate alkali metals, drastically revolutionized the scientific research in the field of energy storage. Actually, it was the beginning of the large production and development of rechargeable lithium-based batteries (*viz.*, the Li-METAL BATTERY).

Unfortunately, despite the excellent characteristics of the intercalation positive electrode, the system was not viable for mass production, as it soon encountered the shortcomings of the Li-metal in combination with liquid-electrolyte.[19,20] While lithium can be de-/inserted with high efficiency at the cathode side, there are significant problems during the plating and stripping process of Li cation, respectively, onto and from Li metal anode. In particular, the newly plated lithium can readily react with the liquid electrolyte, thus reducing the overall cell capacity. In addition, the uniformity of the deposit may become poor, leading to dendrite formation, which pose serious safety issues. Indeed, such Li metal protuberances either lose their electrochemical activity or grow through the separator to contact

the cathode material, leading to internal short circuits and cell failure. Finally, since the passivation reaction is highly exothermic, the cell may overheat, and in extreme cases, due to the low melting point of lithium, thermal runaway may occur, which eventually cause fire and serious explosion hazards.[19,21]

All the issues related to the use of metallic lithium led, in the early 1980s, to its rapid replacement at the anode side with a second lithium intercalation compound with much lower chemical potential versus lithium (vs Li^+/Li) than the cathode.[22] $Li_xFe_2O_3$ may be considered one of the first intercalation negative electrodes. The promising negative electrode was coupled with several cathode materials such as TiS_2 and V_2O_5 to get the first examples of lithium rocking chair cells by Murphy et al.[23] and then, by Scrosati et al.[22] In such system, the Li^+ ions travel back and forth (Rocking Chair Technology) between the electrodes during charge and discharge, while Li-metal plating and related issues are prevented by the redox potential of the alternative negative electrode, which is safely higher than lithium-metal plating. This secondary battery, which avoids the use of lithium metal, is also referred to as Li-ION BATTERY.

1.2.2 The Li-ion battery: 2019 Nobel prize in chemistry

In 2019, The Royal Swedish Academy of Sciences has awarded the Nobel Prize in Chemistry to John B. Goodenough (The University of Texas at Austin), M. Stanley Whittingham (Binghamton University, State University of New York), and Akira Yoshino (Asahi Kasei Corporation), for the development of the lithium-ion battery.

As mentioned above, M. Stanley Whittingham is one of the pioneers of Li-ion battery development. While focusing his research in superconducting materials, he discovered an extremely energy-rich material, titanium disulfide (TiS_2), lately used to prepare innovative intercalation cathodes in lithium-metal batteries.[16] This discovery prompted the investigation of a series of other transition metal dichalcogenides MX_2 (M = transition metal and X = S or Se) as possible cathode materials.[24] The coupling of these innovative positive electrodes with the lithium metal anode led to developing the rechargeable TiS_2/Li cell having excellent rate capability with an open-circuit voltage (Voc) of about 2.2 V (Figure 1.5).
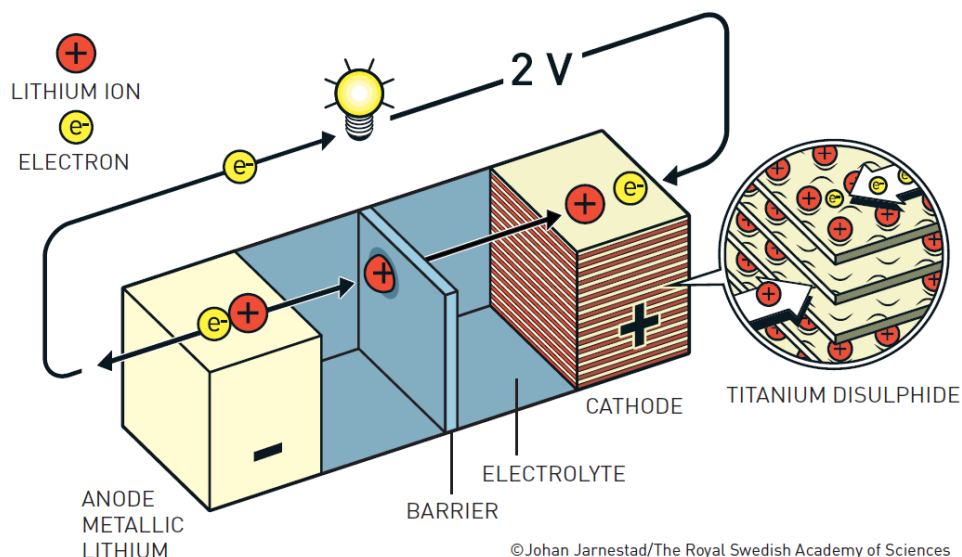
Figure 1.5 Whittingham's Li-metal battery design.

However, the replacement of Li metal with safer anode materials also exploiting an intercalation mechanism, involved a lowering of the Voc, because of their higher redox potential vs Li^+/Li than the metal anode. Thus, higher operating potential materials were needed for the cathode to compensate for the potential increase at the anode side to achieve practical overall cell voltage output.

John B. Goodenough, at the University of Texas at Austin, was the pioneer in exploring alternative insertion/intercalation cathode materials. A fundamental understanding of the redox energies in solids led him to consider layered oxide comprising lithium in which the transition metal ion (M^{n+}) could be in a high oxidation state. He focused on $Cr^{3+/4+}$, $Fe^{3+/4+}$, $Co^{3+/4+}$ and $Ni^{3+/4+}$ redox couples in layered $LiMO_2$ oxides[25] and, after a systematic search, in 1980, he demonstrated that using layered cobalt oxide with intercalated lithium ions ($LiCoO_2$) may result in a significant increase of cell voltage to ~ 4 V compared to the dichalcogenide cathodes (Figure 1.6).[26]
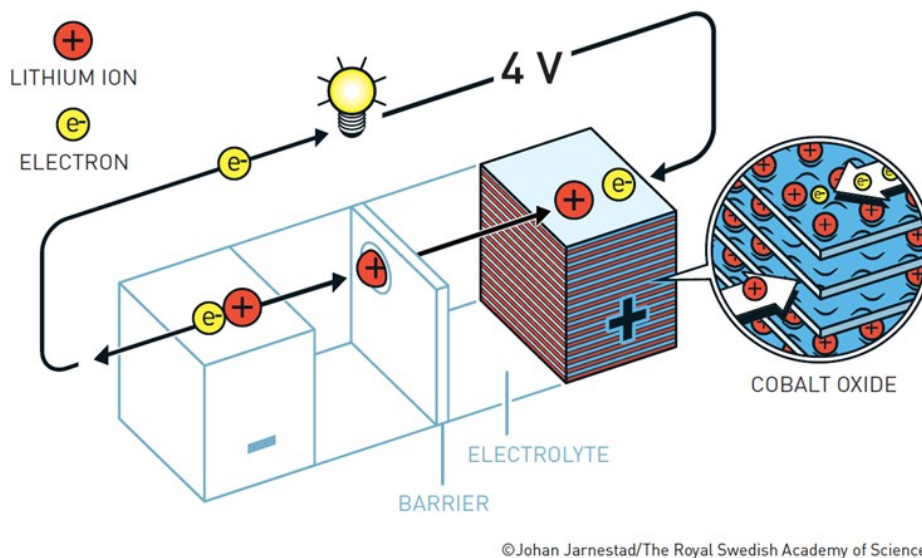
Figure 1.6 Goodenough's Li-ion battery design.

Crucially, the discovery of the $LiCoO_2$ cathode eliminated the necessity to use the hazardous metallic lithium anode because the cathode already possesses lithium, allowing the use of a lithium-free host at the anode.[14]

In the early 1980s, Akira Yoshino evaluated the characteristics of polyacetylene as anode material, and he found that this material possessed suitable electrochemical properties.[27] When the electrolyte composition was optimized, this material demonstrated a high capacity and no evidence of severe degradation reaction after repeated charging and discharging. While the cycle life property at the anode was promising, there were still several limitations at the cathode side due to the use of TiS_2. Then, based on the previous insights by Goodenough, Yoshino started his research on LIBs with $LiCoO_2$ as the cathode and polyacetylene as the anode, but he rapidly excluded polyacetylene due to its low density (1.2 specific gravity density) which precluded cell size reduction. He calculated that a suitable anode material should possess a specific gravity density of at least 2.0 to achieve small size and lightweight batteries.[27] Studying the suitability as anode of several carbonaceous materials, he found that they provided greater capacity when having

a specific layered crystalline structure, which allows Li^+ ion intercalation without causing severe structural stress/strain and electrolyte decomposition.

As a result, the first Li-ion battery cell prototype with the carbonaceous anode in combination with $LiCoO_2$ cathode was successfully fabricated. Furthermore, this development also enabled efficient and straightforward assembly in the discharged state, with no special atmosphere required because of air stability of carbonaceous anode and $LiCoO_2$, despite containing Li-ions (Figure 1.7).[10]
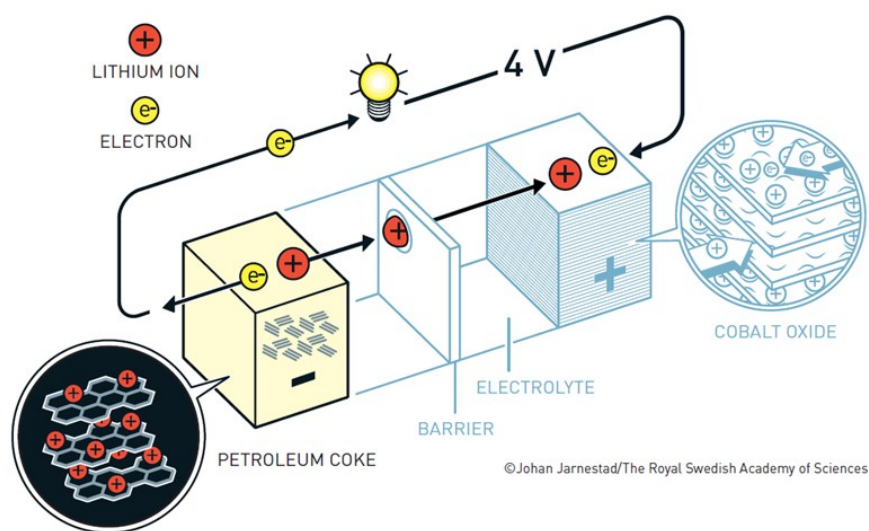
Figure 1.7 Based on the Goodenough cathode, Akira Yoshino developed the first commercially viable lithium-ion battery in 1985.

Nevertheless, the commercialization of the innovative battery system required several additional technological developments, which included electrode shape formation, adoption of suitable current collectors and, finally, the development of safe separators combined with electrolyte optimization. The first LIB was finally commercialized in 1991 by Sony and in 1992 by A&T BatteryCorp., a joint venture between Asahi Kasei and Toshiba.[27] In 1995, the most widely used anode materials were graphite and hard carbon. Graphite gathered much attention because of its relatively high specific capacity of 392 mAh g^{-1}, low redox potential of about 0.1

V vs Li^+/Li and superior discharge profile compared to hard carbon.[28] However, it was soon evident that propylene carbonate (PC), one of the common organic electrolyte solvents, decomposes during charging when graphite is used. The intercalation of PC solvated lithium ions into graphite is typically followed by gas formation. Because of intercalation and gas formation inside the graphite, material exfoliation occurs with the detachment of single layers or packages of graphene layers. The consequence of this unwanted reaction at the anode side is the continuous expansion/contraction of the internal graphite volume, along with the loss of active material and rapid specific capacity decay. The issue was then solved by using specific mixtures of organic carbonates allowing protective SEI layer formation, as detailed in the followings.

1.2.3 Inside LIBs

As in any rechargeable battery, the Li-ion cell consists of two electrodes, the anode, and the cathode, separated by an ionically conducting electrolyte. Solid electrodes are kept apart by a separator, which generally is a polyolefin microporous membrane (e.g., Celgard®).[29] The chemical reactions between the anode and the cathode, which produce electricity, occur by the movement of both electronic and ionic components. Inside the cell, the electrolyte conducts the ionic component, referred to as the working ion (*viz.*, Li^+ cation for LIBs), while concurrently forcing the electrons to flow through an external metal circuit to counterbalance the positive charges. Current collectors at the anode and the cathode, which are made of copper and aluminum, respectively, deliver the electronic current to/from large-area electrodes, and they are the terminals of the external circuit (Figure 1.8).
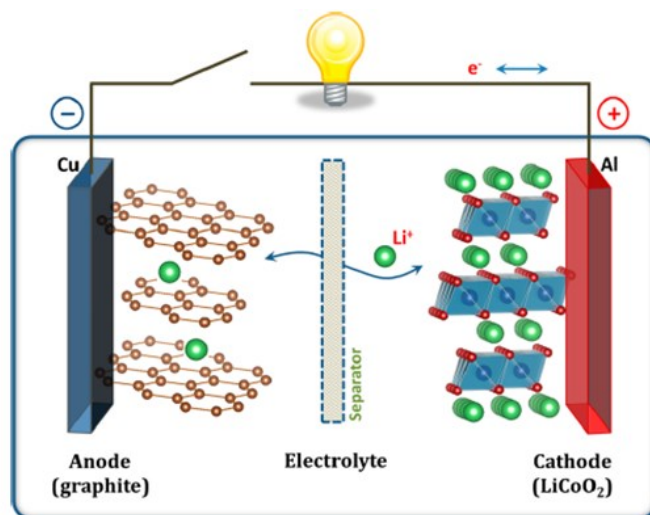
Ions and electrons flow spontaneously from the anode to the cathode during the discharge process, meanwhile during charging process, they are forced to flow in the opposite direction by application of an external applied electric field.[30,31] Once redox reactions are completed, the flow of charges stops, and the battery is fully discharged or discharged. The reversibility of the process allows the redox reactions to be repeated several times.

The typical configuration of LIBs is based on the C/Li salt in EC–DMC or PC/LiMO$_2$ sequence and operate following the reaction:

$$yC + LiMO_2 \leftrightarrow Li_xC_y + Li_{(1-x)}MO_2, \text{ where } x \sim 0.5, y = 6, \text{ voltage} \sim 3.7V;$$
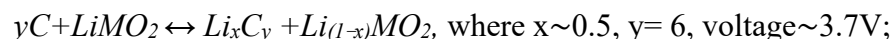
It is well known in the literature that there is a considerable imbalance of cathodic vs anodic total charge for the graphite negative electrode in LIBs during the first few (formation) cycles. This charge imbalance, also named irreversible capacity, of graphite was attributed to solvent co-intercalation, electrolyte reduction, SEI layer formation, and other side reactions accompanying intercalation and deintercalation mechanism.[32,33] During the formation cycle, the irreversible electrochemical decomposition of the electrolyte takes place at the electrode surface. The passivating layer deposited during the formation cycle, which is electrically

resistive but Li-ion conductive, is fundamental to guarantee the formation of an effective protecting layer on the top of the graphite anode (Figure 1.9), which excludes further electrolyte decomposition and avoids graphite exfoliation, thus guaranteeing prolonged charge-discharge cycles with negligible capacity fading.[34,35]
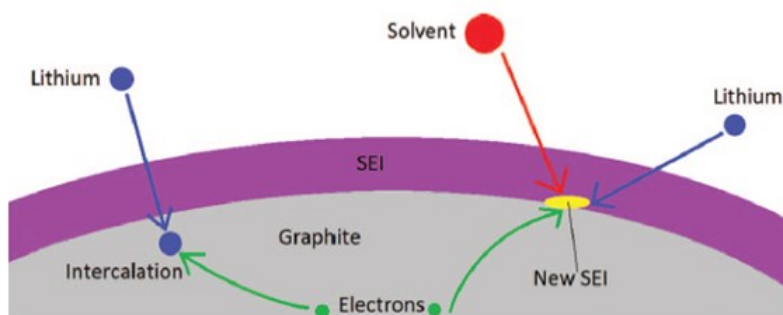
Figure 1.9 The typical electrochemical intercalation of lithium and the competitive reactions with electrolyte components to form a solid-electrolyte interphase (SEI). Figure adapted/reprinted from Pinson, M. B. et al.[35]

Besides being a fundamental procedure, battery formation and conditioning is a time-consuming and expensive process involving long galvanostatic cycling at low charge/discharge rates, and it takes between 2 and 4 weeks.[36] As previously mentioned, the ethylene carbonate (EC) was found to be the most efficient organic solvent for a stable SEI layer formation.[32,33] Thus, it rapidly became an essential component in all commercial electrolyte formulations. Unlike PC, the SEI layer deriving from EC decomposition, effectively prevents graphite exfoliation caused by co-intercalation of lithium ions and solvent molecules. Moreover, it is essential to remind that the SEI composition and its efficiency are strictly linked to the composition of the electrolyte solution, which also involves the nature of the Li salt used.[37] Noteworthy, several types of carbonaceous materials can be used to produce anodes, e.g. natural and synthetic graphite, activated carbon, coke, carbon fibres, carbon nanotubes, etc.[38,39] These materials can be roughly classified into two groups: soft carbons (graphite and graphitised carbons), which are made of small crystallites stacked nearly in the same direction, and hard carbons (non-graphitised, chiefly amorphous glass-like carbons), which are randomly oriented and amorphous. Indeed, the extent of lithium ions intercalation and the reversibility of the intercalation process both depend strongly on the morphology and structure of

the carbonaceous host material.[40] Actually, practical batteries show well-balanced performances of energy density, power density, safety, and time life.

One of the most important parameters to predict the lifespan of a battery, crucial requirement especially for EVs, is the open-circuit voltage (Voc). It is related to the state of charge (Soc), which is the ratio of the available capacity Q(t) and the maximum possible charges that can be stored in a battery (the nominal capacity Q(n)).[41] As already mentioned, the Voc is defined as the potential difference between the positive and negative electrodes in the battery. Indeed, the electrolyte is considered a passive components, which plays only the role of transporting lithium ions, and it is not involved in the electrochemical reaction. Ideally, during the discharge process, only the electrodes are taking part in the redox reactions, along with electrons flowing through the external circuit from the electrode with high electrochemical potential (anode) to the one with a lower value (cathode). Therefore, the open-circuit voltage of the cell can be defined as:

$$FVoc = -\Delta E_F = \mu_A^e - \mu_C^e \quad \text{Equation 1;}$$

where F and E_F represent the Faraday's constant and the Fermi Energy level, respectively. The Fermi energy level depends on the material's work function for the common solid electrode materials.[42] The cell working voltage is affected by the Voc and the electrochemical stability voltage window of the electrolyte. The window can be represented as the energy gap (Eg), which is the energy difference between the lowest unoccupied and highest occupied molecular orbitals (LUMO and HOMO) of a liquid electrolyte (or the bottom of the conduction band and top of the valence band of a solid electrolyte). As shown in Figure 1.10, the LUMO energy level should be below the μ_A to avoid undesirable electrolyte reduction at the interface with the anode. Contrary, if the μ_A is above the LUMO, the electrolyte at the interface is reduced with consequent passivating SEI layer formation. Similarly, a μ_C located below the HOMO oxidizes the electrolyte unless reactions are blocked by forming a stable SEI layer.
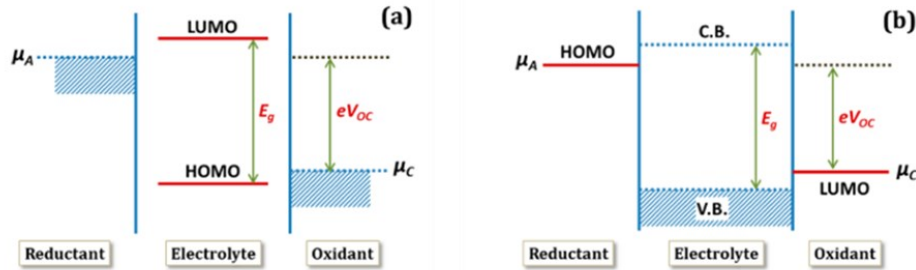
Figure 1.10 Relative energies of the electrolyte window (E_g) and the electrode electrochemical potentials μ_A and μ_C with no electrode/electrolyte reaction: (a) liquid electrolyte with solid electrodes; (b) solid electrolyte with liquid or gaseous reactants. Figure adapted/reprinted from Goodenough, J. B.[30]

The Voc, Soc, and thus the battery performances are directly linked to the mechanism and kinetic of the electrode reactions, which involve a series of physical, chemical, and electrochemical steps, including charge-transfer and charge transport processes.[3] The battery can be represented by an equivalent circuit model, which comprises resistors, capacitors and voltage sources, as shown in Figure 1.11. The use of this model helps to interpret the phenomena occurring inside the cell based on its dynamic characteristics and working principles.
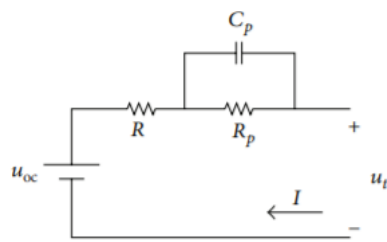
$$u_t = u_{oc} - RI - u_p \quad \text{Equation 2;}$$

Figure 1.11 The Thevenin model used to illustrate the battery equivale circuit.

The Thevenin model is the leading foundation of various circuit models, and it is widely used in EV studies. It is mainly composed of: the open-circuit voltage (u_{oc}), internal (ohmic) resistance (R), the RC-branch, comprising R_p and C_p, which are used to model battery polarization effects and u_t, the terminal voltage.

The Equation 2 allows to express the terminal voltage when the external circuit is closed, and the current flows, such as the Voc decrease due to polarization effects, which in turn are affected by different kinetics:

- **activation polarization**: related to the kinetics of the electrochemical redox reactions taking place at the electrode/electrolyte interfaces;

- **ohmic polarization**: directly linked to the resistance of individual cell components and issues arising from the non-perfect contact between them;

- **concentration polarization**: due to mass transport limitations during cell operation.

In practical batteries, the influence of the current rate on the cell voltage is controlled by all three types of polarization, and there are a variety of experimental techniques used to study internal electrochemical reactions.[3,30] Among them, the analysis of the characteristic current *vs* voltage profile of the discharge curve is most commonly used. Indeed, the detailed profile analysis makes it possible to extrapolate the cell capacity value estimating the overpotential and the effect of temperature and current rate on performances. Moreover, electrochemical impedance spectroscopy (EIS) is another commonly used technique that can add a significant amount of information about cell operation and related materials characteristics.[43]

1.2.4 LIBs present status and limitation

Today, the world faces two main energy/power-related challenges: moving from fossil fuels based to sustainable energy sources based electricity production, and moving ground transportation towards electrical propulsion, namely, using EVs instead of cars powered by internal combustion engines (ICEs). However, the current commercial LIBs are rapidly meeting their theoretical limitations (~250 Wh kg^{-1} and ~680 Wh L^{-1}).[44] Indeed, the use of graphite as anode implies limited energy/power density due to the low specific capacity of the active material (~372 mAh g^{-1}). Therefore, the innovation in the battery materials chain, including both cathode and anode, is constantly devoted to improving the energy densities for producing lighter and thinner next-generation lithium-based batteries. In this

respect, in the following paragraphs a non-exaustive list of electrode/electrolyte materials is presented, which were selected amongst the most promising and impactful for practical use in Li-based batteries in the near future, also bearing in mind their intrinsic relevance with the specific experimental work done during this PhD thesis. For more comprehensive analysis of the incredibly large variety of materials under investigation by the scientific community, the reader is referred to some of the most recent and specific reviews in the field.[45–51]

Anode

As previously mentioned in paragraph 1.2, among high-capacity anodes, Li metal is one of the most promising candidates for the realization of high energy batteries as it has the lowest electrochemical potential (−3.04 V vs. the standard hydrogen electrode) and high theoretical specific capacity (3860 mAh g^{-1}).[20,52,53] Noteworthy, fully lithiated graphite, corresponding to LiC_6 stoichiometry, with a specific capacity of ~372 mAh g^{-1}, is about one tenth of Li metal. Unlike the classical layered graphite anode, Li metal is a "hostless" anode, thus, the working mechanism is entirely different in comparison with graphite intercalation/de-intercalation process.[54] In a lithium metal battery (LMB), Li$^+$ ions reduction and deposition at the lithium metal surface on charge is often referred to as plating, while Li metal oxidation and dissolution on discharge is generally called stripping. The repeated plating/stripping process results in a significant volume variation, which can disrupt the SEI layer causing an additional electrolyte fraction to react with the Li metal surface, with losses of utilisable lithium and internal resistance increase.[44,55] The sum of these unwanted phenomena negatively affects the LMB Coulombic efficiency (CE). Dendritic lithium plating is the major problem of this anode material, which cause internal short circuits in the cell or break and lose of electric contact with the electrode ("dead" lithium), decreasing the amount of lithium available for reversible cycling (Figure 1.12).
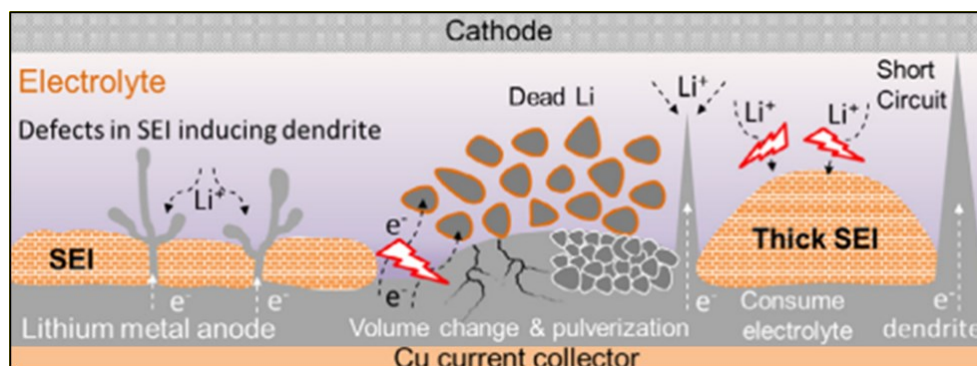
Figure 1.12 Schematic illustration of all unfavourable interactions and layer formation on the Li metal surface during cycling. Figure adapted/reprinted from Feixiang W. et al.[55]

Several factors affect dendritic growth, depending on pressure, current density, quality of the lithium metal electrode surface (surface composition and morphology), SEI and electrolyte characteristics (in terms of conductivity, thickness and mechanical properties). Inhomogeneity in the composition and morphology of the Li metal surface and at the electrode/electrolyte interface can impair the electric field causing locally high current densities. Even in battery-grade foils, a native passivation film is present, but its non-blocking characteristics allow for cycling. Indeed, the low standard redox potential of lithium metal makes it unstable in contact with moisture, promoting rapid oxidation yielding Li_3N, Li_2O, $LiOH$, and Li_2CO_3 as the main solid products on its surface. In particular, Li_2CO_3 arises from the reaction of $LiOH$ with CO_2.[44,55] Additionally, most of the electrolytes (liquid, polymer and ceramic) are chemically unstable upon contact with the Li metal, and this is one of the main limiting factors preventing the use of this anode. Noteworthy, dendrite formation is favoured by the depletion of Li^+ ions near the electrode surface on the electrolyte side caused by the concentration gradient at high current density. All the above-mentioned drawbacks limit the widespread diffusion of Li metl as a viable anode, especially in terms of safety and cyclability. In order to deal with these issues, a profound understanding of interfacial chemistry is needed, along with solid and feasible electrolyte alternatives to achieve a stable contact with Li metal. Among all possible solutions, particular attention is given to developing solid-state electrolyte (SSE) materials, artificial SEI formation and nanoscale interfacial engineering.[56–59] Moreover, solid-state polymer electrolytes (SSPEs) and artificial surface layers with high elastic modulus are also

being developed to contrast dendritic growth and allows for the fabrication of safe high-energy Li-metal batteries.[20]

In this context, besides Li metal, there are many different negative electrode materials (see Figure 1.13) under investigation to meet the ever-increasing demands in different application scenarios (such as high energy/power density and long cycle life). Common carbonaceous materials for LIBs anode generally include graphite, soft carbon, hard carbon, mesocarbon microbeads (MCMB) currently utilized in commercial applications, carbon nanotubes, and carbon nanofibers, graphene currently under study in academic research.[60] For example, the first LIB prototypes developed by Sony company used coke or hard carbon as anode materials, exhibiting good cycle stability.[27] Rapidly, graphite replaced soft carbon and hard carbon mainly because of the lower lithiation potential (~0.2 V vs Li/Li$^+$), high theoretical capacity, and lower irreversible capacity loss during the first lithiation step.[61] Among the carbon allotropes, the most promising structural, mechanical and electrochemical candidates are carbon nanotubes (CNTs).[62] Claye et al.[63] observed reversible electrochemical insertion of Li into CNTs, along with reversible Li capacity in the order of 460 mAh g^{-1}, which is 23% larger than the theoretical value for graphite (372 mAh g^{-1}). Wang et al.[64] prepared N-doped carbon nanofibers film through electrospinning and high-temperature carbonization, reaching a high capacity of 702 mAh g^{-1} after 500 cycles at a high current density of 5 A g^{-1}. The capacity improvement originated from the highly defective structure created by the N dopant in the graphite domain.

The addition of silicon to form composite Si/C anode material with high specific capacity is one of the most promising approaches for enabling high energy density LIBs.[65] Silicon is especially abundant in the earth crust, and it can be electrochemically lithiated via a two-phase mechanism to form the final phase Li$_{22}$Si$_5$ (theoretical capacity of 4200 mAh g^{-1}).[66] Indeed, silicon exhibits a relatively low delithiation potential of about 0.4 V vs. Li$^+$/Li, limiting the lithium precipitation on the surface, thus improving the safety of devices. The main drawback of Si-based anodes is the huge volume expansion/shrinkage (volumetric expansion ~300%) during lithiation/delithiation, which causes the fracture and pulverization of the electrode structure along with the loss of the electrical contact between the active material and the current collector. For these reasons, the role of the binder and the SEI film-forming ability of the electrolyte at the interface becomes fundamental to improve the cycle life of devices.[67] As for carbon, different silicon

nanostructure such as nanoparticles, nanotubes, nanowires, or thin films are under investigation. Cui et al.[68] prepared Si nanowires on the stainless steel substrates directly as the working anode for LIBs, obtaining a charge capacity of 4277 mAh g^{-1} and maintaining the high discharge capacity above 3000 mAh g^{-1} for nine cycles at C/20, indicating the promising potential of the one-dimensional nanomaterials for excellent lithium storage performance. Maranchi et al.[69] prepared a 250 nm Si film deposited by sputtering on Cu foil which delivered excellent reversible capacities close to 3500 mAh g^{-1} at a relatively high current rate (such as C/2.5) after 30 cycles with high Coulombic Efficiency.
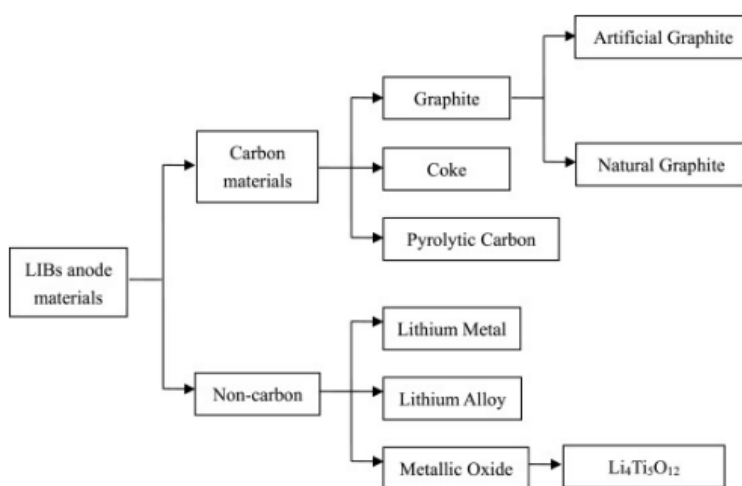
Figure 1.13 Classification of anode materials for lithium-ion secondary batteries. Figure adapted/reprinted from Yan H.[70]

Among commercial non-carbon anode materials, spinel $Li_4Ti_5O_{12}$ (LTO) covers a fundamental role due to promising prospects for powering the energy storage systems for electric vehicles due to the high safety, environmentally friendliness, relatively low manufacturing cost and excellent electrochemical performance (see Figure 1.13).[60,70] Usually, LTO shows a typical flat charge and discharge potential of approximately 1.55 V, and a theoretical capacity of 175 mAh g^{-1}. The "zero-strain" structure characteristic of this material and its nontoxicity make $Li_4Ti_5O_{12}$ an excellent negative electrode to achieve high coulombic efficiency (nearly 100%), and good compatibility with the commonly used electrolyte systems. To overcome the limited electrical conductivity of LTO, Wang et al.[71] prepared a rutile-TiO_2

carbon-free nanocoated $Li_4Ti_5O_{12}$ to improve the kinetic of lithium insertion/extraction. The galvanostatic discharge/charge voltage profiles at different current rates showed high specific capacity of 145−155 mA h g^{-1} at 1 C. As a result, the cell (with 1 M $LiPF_6$ in EC/DMC/DEC; 1:1:1 in wt % as electrolyte) can be operated at 10 C for 100 cycles with slight capacity decay and at a high rate of 30C, it can still deliver a capacity of ca. 80 mA h g^{-1}.

Cathode

At the positive electrode side of the cell, $LiCoO_2$, thanks to its simple synthesis route and high performance, it has been the most common cathode material used in the Li battery industry, especially in portable electronics market. The use of $LiCoO_2$, combined with Li metal anode, has been subject of studies and optimization for many years. $LiCoO_2$ shows good electrochemical properties: a practical specific capacity of about 150 mAh g^{-1}, with an average discharge voltage of about 3.6 V vs. Li$^+$/Li, resulting in an energy density of about 585 Wh kg^{-1} and a cycle-life extending beyond 1000 cycles. Nevertheless, the use of $LiCoO_2$ and its derivatives raises serious concerns for developers because of its inherent thermal instability. Thermal analysis revealed that partially de-lithiated Li_xCoO_2 (x = 0.49– 0.9) undergoes an exothermic reaction (decomposition starts between 200 and 300 °C) accompanied with following structure modification and oxygen release.[72] The relatively low activation energy for the decomposition process results in possible oxidization of the binder or electrolyte by the generated oxygen gas. Despite the widespread use of layered oxide $LiCoO_2$ based cathodes in rechargeable lithium-based batteries, the limited availability of cobalt,[73] and its increased cost raised concerns (Co is actually classified as Critical Raw Material – CRM). The choice of alternative materials was dictated by the need for innovative cathodes for large-scale applications, as envisioned in HEV or for load levelling.

In order to replace or limit the amount of expensive and toxic cobalt, the research focus moved on lithium metal phosphates and $LiNi_xMn_yCo_zO_2$ cathode types, which have now been widely recognized as a new generation of materials that can offer the safety, power and energy density to satisfy the fast growing Li-ion battery demand.[74] Among lithium metal phosphates, olivine structured $LiFePO_4$, also named triphylite, has attracted much attention as one of the most promising replacements for $LiCoO_2$. Compared to commercial $LiCoO_2$, $LiNiO_2$, $LiMn_2O_4$, and their derivatives, $LiFePO_4$ cathode stands out due to several

advantages, such as low cost (it contains iron, one of the most abundant elements in the Earth's crust), excellent thermal stability up to 400 °C, low toxicity, which brings about very limited safety issues.[75–78] As a polyanionic compound, it also exhibits framework structures built up from both corner-sharing (MO_6) octahedra (M = transition metal) and (XO_4) tetrahedral polyanions (X = P, S, As, Mo or W) instead of only (MO_n) polyhedra as in transition metal oxides. In $LiFePO_4$, the structure consists of corner-shared FeO_6 octahedra and edge-shared LiO_6 octahedra running parallel to the c-axis in the alternate a-c planes, which are linked together by corner- and edge-sharing PO_4 tetrahedra (Figure 1.14).[79–81]
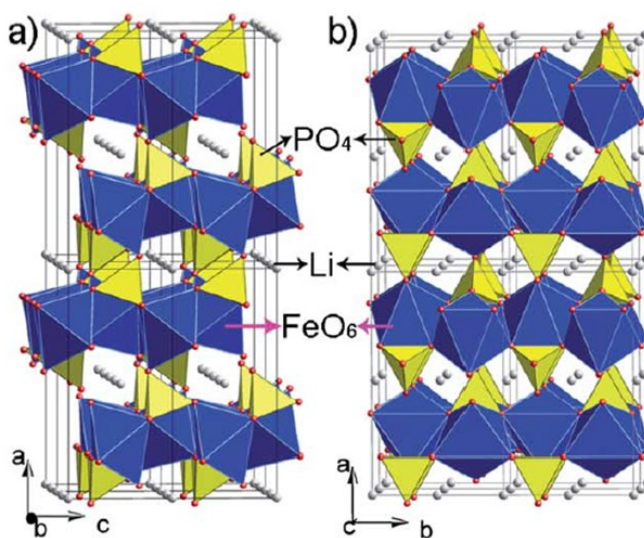
Figure 1.14 Polyhedral representation of the crystal structure of Olivine LiFePO4 cathode material. Viewed along the b- and c-axis, respectively (a) and (b). Figure adapted/reprinted from Gong Z.[81]

Upon the first charge, $LiFePO_4$ (LFP) can de-intercalate 1 Li^+ ion per formula unit, corresponding to the oxidation of Fe^{2+} to Fe^{3+}. The extraction of Li^+ ions gives rise to a new phase, $FePO_4$ (heterosite), which has the same 3-D framework with only a slight variation in the lattice parameters. This feature guarantees a highly reversible process. The key aspect of this cathode is the presence of oxygen atoms strongly bonded by both Fe and P atoms, resulting in a structure characterized by improved stability at high temperatures compared to layered oxides, such as $LiCoO_2$. $LiFePO_4$ has a relatively high theoretical specific capacity of 170 mAh g^{-1}, and an operating voltage of 3.45 V vs. Li^+/Li. The flat voltage profile of the

LiFePO$_4$ is characteristic of a two-phase Li$^+$ extraction/insertion mechanism. The LFP working voltage is highly compatible with the average ESW of commercial liquid and polymer electrolytes, thus limiting degradation reactions at the interface during the oxidation process (charging or de-lithiation).[76] However, first investigations on LiFePO$_4$ evidenced the difficulties for this material to reach the theoretical capacity at room temperature, reflecting the unavailability of part of the active material, with capacity values close to the theoretical one, achieved only at very low current density, suggesting transport limitations of both electrons and ions. Limitations are mainly related to the strong covalent oxygen bonds, leading to low ionic diffusivity and poor electronic conductivity (about 10^{-9} to 10^{-10} S cm^{-1}). Optimal charge/discharge performances have been achieved thanks to particle size reduction and residual Fe^{3+} phase elimination during the sintering process.[80] Moreover, carbonaceous materials included in the precursors during the cathode material preparation is fundamental in increasing the material performance via carbon coating of active particles, enhancing the surface electronic conductivity of LiFePO$_4$;[80] it results in the full utilization of active materials at high current rates. Additionally, carbon conductive powder added during cathode preparation improves the electronic contact between the active material particles and the current collector.[75,82,83]

Considerable attention was also given to different lithium-conducting phosphate materials, particularly compounds with Li$_3$M$_2$(PO$_4$)$_3$ stoichiometry. Their structural characteristics allow various isomorphous replacements, which are essential in increasing lithium concentration or selecting the optimal channel dimension. Several research groups have already demonstrated the feasibility of these materials as a replacement for LiCoO$_2$.[84,85] Among them, lithium vanadium phosphate (Li$_3$V$_2$(PO$_4$)$_3$, LVP)[86] is currently considered one of the most interesting candidates, characterized by superior performances at high current densities and increased average voltage of 3.8-4 V versus Li$^+$/Li, making this material an attractive candidate for the realization of high-power electrochemical devices. For these reasons, an increasing number of works are now focusing on the synthesis and application of this material in LIBs.

Readily available transition metals (TMs), such as Fe and Mn, were employed to prepare the attractive layered LiFeO$_2$ phase, and, most interestingly, the layered manganese oxide LiMnO$_2$.[11] Unfortunately, the pure compound undergoes structural modification to a spinel system upon cycling, with a consequent decay in

the electrode performance. The structural instability of the layered phase was tackled through partial cationic substitution of Mn by other metals, such as Cr or Co, obtaining $Li_{1+x}Mn_{0.5}Cr_{0.5}O_2$ and $LiMn_{1-y}Co_yO_2$.[87] The presence of manganese is beneficial to stabilize the layered structure of the TM oxides and, at the same time, to decrease the whole amount of toxic chromium and cobalt. Lithium manganese cobalt oxide compounds are characterized by a layered zig-zag structure, which is nonetheless obtained thorugh complicated synthesis procedures. However, the high initial specific capacity (> 200 mAh g^{-1}) and the promising operating charge voltage of 4.2-4.5 V made this cathode material category one of the most studied nowadays to address the requirement needed for EV and plug-in applications.[87]

Starting from the same α-$NaFeO_2$ layered structure, several alternative elements were studied instead of the critical cobalt, nickel being the most interesting one. However, the substitution by nickel leads to a system in which manganese becomes the structure stabilizer and the electrochemically active ions. These compounds are thus best described as substituted nickel oxides in which the manganese remains in the tetravalent state, and nickel is redox-active between the +2 and +4 oxidation states;[73] actually, the manganese helps in reducing the cost and stabilizing the lattice. Mixed nickel−manganese dioxide ($LiNi_{1-y}Mn_yO_2$) multielectron redox systems were deeply investigated firstly by the group of Dahn in 1992.[88] They reported a solid solution with $y \leq 0.5$ where a further increase of Mn content negatively affects the electrochemical properties of the material. Among all possible compounds of the $LiNi_{1-y}Mn_yO_2$ family, $LiNi_{0.5}Mn_{0.5}O_2$, also named 550 material (0.5 Ni, 0.5 Mn, 0.0 Co), became the most widely studied cathode material after the pioneering work performed by Ohzuku et al. in 2001, who first reported a high reversible capacity of 200 mAh g^{-1} in lithium metal cell (2.5 - 4.5 V, 0.17 mA cm^{-2}).[89] Aimed to stabilize the material structure and limit the capacity fading upon cycling; several $LiNi_{1-y}Mn_yO_2$ formulations were analyzed with y ranging from 0 to 1.[90] The higher manganese content was found to simultaneously lower the discharge capacity and ameliorate both capacity retention and thermal stability; meanwhile, nickel ions are still present in the lithium layer, which restrict the rate capability. Then, bearing in mind the above considerations and that the cobalt addition can reduce the amount of nickel in the lithium layer, the next step was mixing the three transition metals with the first report published in 1999 by Liu et al.[91] and in 2000 by Yoshino et al.[92]

Mixed nickel-manganese-cobalt dioxide (NMC or $LiNi_{1-y-z}Mn_yCo_zO_2$) represents one of the most important layered oxide cathodes for Li-ion batteries along with its parent containing aluminium instead of manganese (NCA).[93–95] The partial substitution of nickel with manganese and cobalt decreases the TM content in the lithium layer from 7.2% to 2.4%, specifically when Co and Mn amounts are around 0.3. The $LiNi_{0.33}Mn_{0.33}Co_{0.33}O_2$, also named NMC 111 (Figure 1.15), was synthesized for the first time in 2001 by Ohzuku et al. by solid-state reaction at 1000 °C starting from $LiOH \cdot H_2O$, $CoCO_3$, and a nickel manganese hydroxide. The material showed capacity values exceeding 150 mAh g^{-1} while cycling in a voltage range between 2.5 and 4.2 V at 0.17 mA cm^{-2} and 30 °C.[89] Attempts to improve the phase-purity and homogeneity of the cation distribution includes various synthetic routes such as solid-state, sol-gel, and modified co-precipitation of triple hydroxides. Currently, coprecipitation is the most widely used method for the synthesis of NMCs.[90]
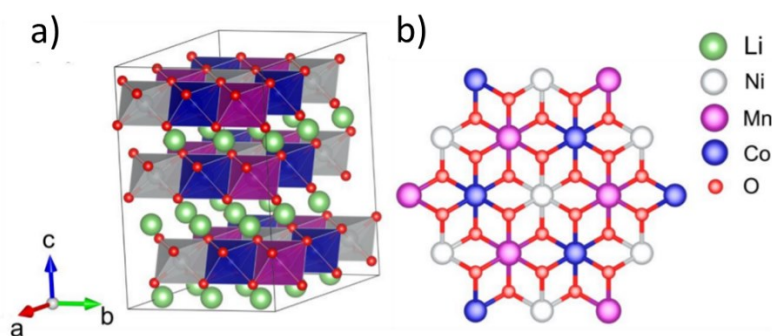
Figure 1.15 Illustration of the bulk geometry of NMC333 with R-3m symmetry. (b) Schematic representation of ion-ordering in TM layers. Figure adapted/reprinted from Garcia, J. C. et al.[96].

NMC 111 can be considered as a 1:1:1 solid solution of $LiCoO_2$, $LiNiO_2$, and $LiMnO_2$ showing limited volume variation upon cycling, excellent safety features with respect to $LiNiO_2$ and $LiCoO_2$, and a higher specific capacity approaching 200 mAh g^{-1} when the upper voltage limit is set to 5 V in lithium metal cell. There is a large number of published literature studies regarding the crystal and electronic structure of NMC 111 (Figure 1.15).[96–99] Some of them reported the structure variation of typical α-NaFeO$_2$ (space group $R\bar{3}m$)[96,97] to the [√3×√3]R30°-type superlattice with valence states of transition metals differing from that of simple

$LiMO_2$ (M =Ni, Mn, or Co) compositions, in which the oxidation state of the transition metals is 3+. Indeed, calculated and experimental data confirmed that the oxidation states of Ni, Co, and Mn in pristine NMC 111 are 2^+, 3^+, and 4^+, respectively.[97,100–102] In addition, analysis of the redox reaction mechanism during intercalation/deintercalation indicates that the main redox processes involve the Ni^{2+}/Ni^{4+} couple, while Mn^{4+}, as in mixed nickel−manganese dioxide, is electrochemically inactive.[103] Regarding the contribution of Co^{3+}/Co^{4+}, there is still an open debate; almost certainly, it causes a significant increase of voltage near the end of charge (4.5 V vs. Li^+/Li) with the possible consequent oxidation of oxygen, resulting in unsafe gas release.[104] The studies indicated 4.3 - 4.4 V as the optimum upper cutoff voltage for NMC, also well-fitting with the ESW of a wide variety of non-aqueous electrolyte.

NMC 111 could be defined as the precursor of high-energy and high voltage cathode materials, and it was subject of many systematic investigations, essential for the development of different systems, such as NMC 442, firstly studied in 2004 by Whittingham's group,[105] and the most popular NMC 532[106] characterized by good electrochemical performance and relatively low cost. However, the capacity fading associated with the high-voltage operation is still a significant challenge. Unfortunately, to achieve specific capacity values close to the theoretical one, the complete removal of lithium ion from the structure is necessary, which causes electrolyte oxidation, surface film formation, and transition metal dissolution, ultimately compromising the long-term cycling stability.[104] Aiming to improve the accessible capacity at reasonable upper cutoff voltage limits, Ni-rich layered oxides (NRLOs) (with Ni-content largely higher than Mn-and Co-contents) recently surged at the main focus of research interest by the scientific community, as a higher amount of lithium can be extracted from their structure within the same voltage window. However, Ni-rich NMC, such as NMC 622 or 811 (i.e., $LiNi_{0.6}Mn_{0.2}Co_{0.2}O_2$ or $LiNi_{0.8}Mn_{0.1}Co_{0.1}O_2$, respectively) [107,108] suffer from a shorter lifetime due to faster capacity fading compared to NMC 111 or 532 (Figure 1.16).[109]
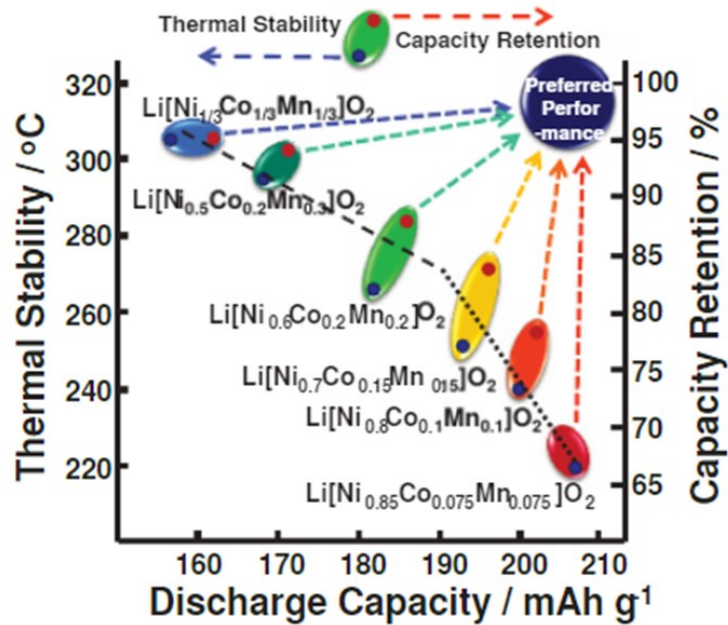
Figure 1.16 Comparison of the structural and electrochemical properties of layered Li[Ni$_x$Co$_y$Mn$_z$]O$_2$ (x = 1/3, 0.5, 0.6, 0.7, 0.8 and 0.85) cathode material for lithium-ion batteries. Figure adapted/taken from Noh, H. J.[107]

Lithium-rich layered oxides (LRLOs) belong to another class of emerging alternative materials, which is gathering increasingly high attention as potential next-generation cathodes for LIBs because it avoids the use of critical cobalt, while concurrently showing large discharge capacity of 250–300 mAh g^{-1}.[110] LRLOs have a complex structure, as they can be viewed as a combination of Li$_2$MnO$_3$ and LiMO$_2$, and, depending on synthesis conditions and composition, they can form either a single-phase solid solution or a nanocomposite. LRLOs also possess a unique first charge profile consisting of an initial region where the TM ions are oxidized, followed by a long plateau, where oxide ions are oxidized. Unfortunately, the main drawback is the partial irreversibility of this oxidation process, accompanied by high first cycle irreversible capacity (IRC) loss and structural modifications. Thus, some of the oxygen and Li vacancies created during the first charge are then eliminated through TM migration, which leads to the reduction of Mn^{4+} to Mn^{3+} ions, and a gradual transformation of the material to a spinel-like phase with subsequent voltage decay.[111,112] As mentioned in several literature reviews,[90,110] in order to solve these issues, surface coating is widely investigated,

and it is shown to improve the discharge capacity, cyclic stability, and rate capability while reducing the IRC. Other innovative synthesis methods need to be developed to solve the TM migration issue, vacancy elimination, and subsequent phase transformation to mitigate/suppress voltage decay, thus making it possible the widespread exploitation of LROLs in practical LIBs and facilitating the automotive battery transition from the commonly used LFP- and NMC-based systems (Figure 1.16) towards innovative and high-performance energy storage devices.
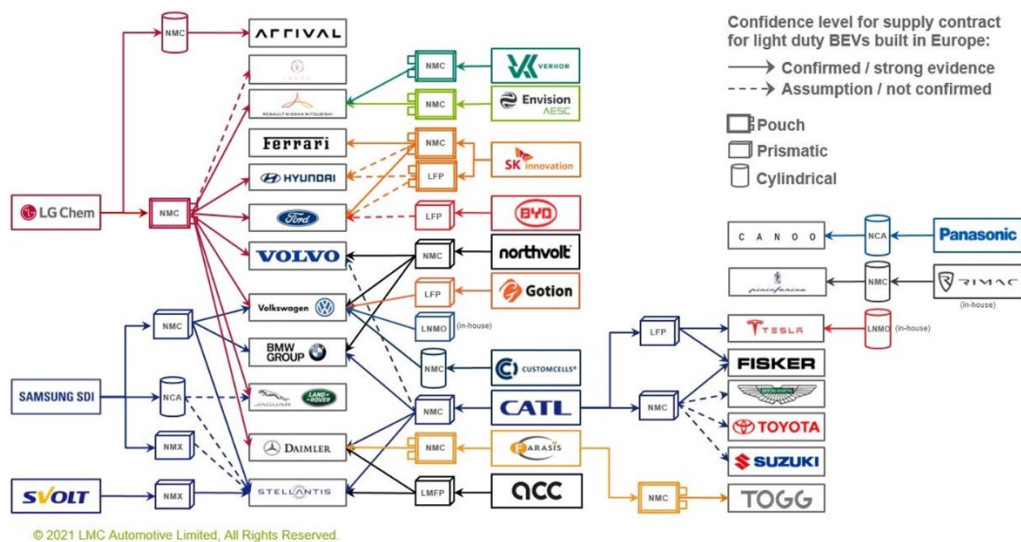
Figure 1.17 Overview about actually batteries utilization for electric, hybrid and plug-in vehicles. (Sourse: LMC Automotive Limited 2021 report)

Electrolyte

Following the electrodes, the electrolyte is amongst the most costly components in LIBs. Single-solvent formulations are very rare, and most compositions are based on lithium salt mixed with at least two or more solvents.[12] Indeed, combining several organic solvents allows obtaining the best compromise in terms of low viscosity, high dielectric constant and stable SEI formation. In liquid electrolyte solutions, the solvent dielectric constant measures the efficiency in countering the electrostatic attraction force between ions bearing opposite charges (Figure 1.18). Common organic solvents for battery electrolytes include ethers and carbonate esters (cyclic and acyclic) containing oxygen as the electronegative heteroatom inducing the dipole moment.[12] Spectroscopic and computational data identified the

carbonyl oxygen in carbonates as the binding site for Li$^+$ cation, and solvent molecules nature would play a dominant role in determining its mobility.[113] Recently, different carbonates, including fluorinated ones, became popular due to their excellent resistance again anodic decomposition, which allows high-voltage cathode materials use, despite the limited cathodic stability (artificial SEI formation required with Li metal anode).[114,115] Carbonate-based solvents are highly flammable with flash points below 30 °C.[116–118] In addition, the salt of choice at present, namely lithium hexafluorophosphate - LiPF$_6$, can undergo an autocatalytic decomposition into LiF and PF$_5$, which are extremely reactive with water.[119] These reactions often cause internal cell degradation and related safety hazards. In order to reach the high safety targets required for the application of LIBs in the automotive field, several solutions are currently under investigation, being the use of novel fluorinated sulfones, sulfoxides, phosphorus and silicon-based solvents among the most investigates ones.[113,120,121]

Aprotic room-temperature ionic liquid (RTIL) and, more recently, their protic counterparts (PRTIL),[8] represent another interesting category of electrolytes gathering increasing attention within the scientific community.[122] In the last few years, RTILs have been considered as alternative electrolytes for LIBs because they offer several advantages over carbonate-based electrolytes: a high oxidation potential (~5 V vs Li$^+$/Li), nonflammability, a low vapour pressure, elevated thermal stability, low toxicity, high boiling points, and a high Li-salt solubility. Unfortunately, they have a high viscosity, which decreases the overall Li$^+$ ion mobility. The use of additives, such as vinylene carbonate (VC) or fluoroethylene carbonate (FEC), can mitigate the elevated viscosity, thus enhancing the ion mobility and, especially for PRTILs, improve cathodic stability.[67] Noteworthy, small concentrations of carbonate additives do not negatively affect safety properties of RTIL electrolytes, which actually maintain almost completely their characteristic nonflammability.[123]

Differently from liquid organic media, in ceramic electrolytes lithium ions hop from site to site in a crystalline anionic or polyanionic framework, which define the specific accessibility and energy barrier to reach these sites. Generally, these sites are cation vacancies or metastable interstitial defects. The overall activation energy associated with the lithium-ion conduction accounts for the energy required to form these defects, and the energy barrier to lithium cations hopping is determined by the anionic framework. The most studied ceramic conductors are oxides

(perovskite-, NASICON-, LISICON-, garnet-type, etc.) and sulfides (thio-LISICON-, LGPS-, argyrodite-type, etc.).[51] Many super Li$^+$ ion conducting ceramic electrolytes have body-centred cubic anionic frameworks. Elemental substitution in these materials can affect the concentration of defects, the energy barrier to lithium cations hopping, and the migration pathway. Most syntheses of these ceramic electrolytes yield polycrystalline materials with grain boundaries between crystallites with different orientations.[124] Grain boundaries hinder lithium-cation migration in most cases, particularly in oxides. It is worth mentioning that the dimensionality of the possible pathways for lithium-ion transport affects ionic conductivity, being 3D preferred over 1D because impurities can easily block it. In this respect, differences in the composition and insulating impurities at grain boundaries negatively affect the conductivity, as well as voids in ceramic pellets also act as an insulating barrier for lithium-ion conduction. NASICON-, garnet- and perovskite-type solid electrolytes are promising candidates to replace liquid electrolytes because of their high ionic conductivity and good electrochemical stability (Figure 1.18).[125] However, improving the interfacial characteristics with electrodes and careful material selection are still needed to get suitable performance for real application in commercial LIBs.

Similarly to liquid electrolytes, ion-polymer interaction allows salt dissolution and contrasts the attractive ion-ion force. After the discovery of the first ion conducting polymeric material in 1973 by Wright et al.,[126] much efforts focused on identifying polymer electrolytes with room temperature ionic conductivity close to that of liquid electrolytes (Figure 1.18). The materials design and the development of polymer electrolytes passed through several stages. The most studied polymer hosts are polyethers, polyesters and polycarbonates, where the ether oxygen and the carbonyl oxygen coordinate lithium cations through ion-dipole interactions.[12] Coordinated cations can act as transient crosslinking points between polymer segments, increasing the glass transition temperature (T_g).[127] On the other hand, crystallization in semi-crystalline polymers can be kinetically hindered in the presence of dissolved salt depending on the concentration, particularly when large soft anions with delocalized charge are used, such as lithium bis(trifluoromethanesulfonyl)imide (LiTFSI) or bis(fluoromethanesulfonyl)imide (LiFSI). Lithium-ion mobility mainly relies on the coordinating ability of oxygen atoms coupled with the segmental motion in the amorphous phase above the T_g. Therefore, amorphous polymers with low T_g enhance ion mobility.[128] Among this huge electrolyte family, it is possible to identify different subcategories, namely:

conventional salt-in-polymer or solid polymer electrolyte (SPE), plasticized salt-in-polymer, gel-polymers, ceramic-polymer composites and the emerging class of single ion conducting polymer electrolytes (SICPEs). Plasticized SPEs and gel electrolytes differ solely in the amount of organic liquid solvent(s)/liquid plasticizer into the polymer matrix, while composites are generally prepared simply by dispersing a small fraction of micro/nanosize inorganic (ceramic)/organic filler particles into the conventional SPE host.[129] In all the case, a dissolved salt is needed to allow for ionic conduction into the matrix. A completely different category are SICPEs, characterized by the presence of anchored anionic moieties to the polymer chain responsible for cation coordination and conduction, ensuring a Li^+ ion transference number close to unity.
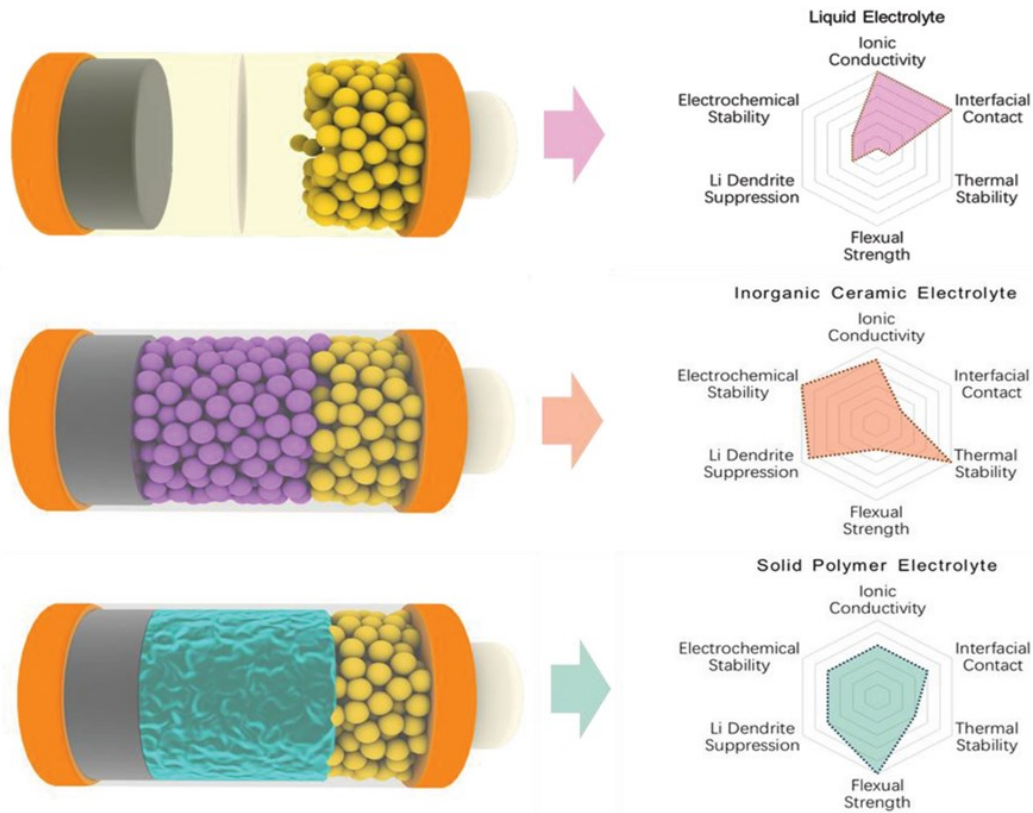
Figure 1.18 The performance comparisons of liquid electrolytes, ICEs, and SPEs. Figure adapted/reprinted from Song L. et al..[129]

SPEs are considered a key component in the development of solid-state batteries, as they allow the removal of the liquid electrolytes from the system, thus improving the safety level of the device. However, some significant drawbacks are causing this technology to lag: the low ionic conductivity and the complex interfacial interaction between the electrodes and the electrolyte.

Finally, a good SPE for LIBs must have some specific characteristics:

• possess high ionic conductivities (around 10^{-3}-10^{-4} S cm^{-1} at room temperature);

• negligible electronic conductivity (10^{-9}-10^{-12} S cm^{-1});

• have high ionic transference number ($t_{Li+} \sim 1$);

• have high mechanical and chemical stability;

• and possess a high Electrochemical Stability Window (ideally anodic oxidation limit > 5 V vs Li^{+}/Li.

The perfect balance among all these characteristics will allow suitable SPE for application at a large scale in the next generation of solid-state batteries, as more deeply detailed in the following Chapter, which is specifically focused on polymer-based electrolytes being the core subject of this Ph.D. work.

Chapter 2

2 Next-generation lithium metal batteries

2.1 Toward solid-state batteries

Considering the current status of conventional LIBs, the non-solid component is just the liquid electrolyte, being prevalently a solution of organic carbonate solvents, additives and alkaline salt. The replacement of liquid electrolytes with solid-state alternatives (e.g., ceramics, polymers or composites) is necessary to develop fully solid-state batteries.

Generally, solid-state electrolytes can be classified into two major categories: ceramics and polymers (see paragraph 1.2.4 *Electrolyte)*. Occasionally, these are also incorrectly referred to as "hard" and "soft" solid state systems, principally due to the stiff but brittle characteristics of ceramics in comparison with the rubber nature of polymers. This assumption is not often valid if the mechanical properties of the material are considered. Indeed, some polymers can be very stiff and show better mechanical properties than their ceramic counterparts. Moreover, "solid" state ceramic electrolytes, generally containing expensive rare elements, such as germanium or lanthanum, are more costly with respect to polymers.[51] However, the comprehensive description of ceramic and composite electrolytes is out of the scope of this thesis, which is mainly focused on the preparation and characterization of single ion conducting polymer electrolytes (SICPEs) belonging to the family of SPEs. Thus, the main focus of this Chapter will be on SPEs, starting with a general presentation of the LIBs limitations for the application in the automotive field and how the replacement of liquid electrolyte with polymer one could be an effective solution. Finally, a short description about the most studied SPE systems will be given, followed by a more detailed analysis of the SICPE category.

The driving force behind the liquid to solid electrolyte transition is the potential improvement of safety for these electrochemical energy storage devices, especially considering their large-scale application in the automotive field. Many polymer materials are stable up to 150 °C and the negligible vapor pressure makes potential risks of severe hazards minimal. The safety hazards would decrease dramatically by simply replacing the flammable battery components with non-flammable materials. Moreover, considering the replacement of ICEs in large-scale transportation (e.g., marine transportation and aviation), with large size and heavyweight battery packs, make the overall satefy level of battery cells fundamental. In this context, solid-state batteries can play a major role.

Another fundamental bottleneck for the widespread application of EVs is the limited performance in comparison with ICEs. Namely, the main EV target is reaching the same performance of ICEs is terms of practical operational distance range. The automotive industry targeted a two-times increase of LIBs energy density in the next decade, enabling progress in the driving range of EVs from 500 km to more than 1000 km. The energy density of a battery is the product of its capacity and potential; thus, it is possible to increment this parameter working on two main factors: decreasing the weight and the volume of the battery cell using thin solid-state electrolyte films and increasing the cell voltage utilizing higher energy density and higher voltage cathodes. The most obvious example is the employment of Li metal electrodes instead of graphite as the anode. Noteworthy, Li metal has a lower operating potential than graphite (leading to a slightly higher output voltage) and a tenfold higher capacity. Indeed, the high reactivity of liquid electrolytes with Li metal can be mitigated or even overcome using solid-state electrolytes. For example, a large improvement in terms of high energy density has been already demonstrated by Bollore Blue Solution company in France, which developed the lithium metal polymer (LMP®) technology, commercializing in 2007 an EV sharing network and now large distribution of electric buses. Moreover, SPEs engineering may lead to the development of a much thinner electrolyte separator compared to the conventional one used for liquid electrolytes, while also using materials with lower density, which results in an overall battery weight decrease.

Generally, SPEs are also among the best solutions to target low-cost production, as polymers are relatively inexpensive materials that can be easily fabricated on a large scale. Specifically, the most significant gain in cost is the

absence of solvent additives, which is also an added value in terms of sustainability and recycling. Indeed, polymer electrolytes account also for a soft, more chemically and mechanically stable separator able to mitigate the volume variation of electrodes upon the lithiation/de-lithiation process.

Nevertheless, solid-state electrolytes have not already intruded the market of LIBs due to several important drawbacks, which prevent their widespread diffusion, such as: limited ionic conductivity, poor electrode wettability and relatively narrow ESW. Despite the sizeable attenuation of the electrode volume expansion assured by SPEs, problems may arise from the non-optimal contact between electrode materials and electrolytes when porous electrodes are used. Loss of contact during reversible lithium insertion/de-insertion may occur, which causes rapid capacity decrease and eventually cell failure. Many efforts are devoted to developing an optimal SPE/electrodes interface to guarantee both stable cycling upon electrode volume variation and enhanced wettability. In this respect, in-situ polymerization has recently emerged as a powerful technique to achieve intimate contact between electrode active material particles and SPE, resulting in lower charge transfer resistance at the interface with the electrodes and, in turn, higher energy efficiency.[67,130,131]

As stated before, the main shortcoming of using SPEs is their limited ionic conductivity. Low ionic conductivity can be a significant problem also for liquid systems with high viscosity, and it becomes even more challenging when switching to the fully solid state. Indeed, differently from liquid electrolytes the ions conduction mechanism in polymers is dominated by both the coordinating ability of functional groups and the mobility of the polymer chains. In this context, the relatively high-temperature tolerance of SPEs plays a crucial role, allowing to get suitable conductivity values at elevated temperatures without drastically changing the mechanical properties of the polymer electrolyte. Thus, working on the conductivity, temperature, and mechanical properties (temperature tolerance) parameters, it may be possible to identify the best conditions (interplay/compromise), allowing excellent ambient temperature performance. Another important challenge to allow the transition towards solid-state battery is increasing the ESW of the SPEs in such a way to ensure stable cycling with high voltage cathodes (i.e., cathode materials operating at above 4.3-4.5 V vs. Li^+/Li). Similar to other properties of polymers, like conductivity and mechanical stability,

the resistance toward anodic oxidation is strictly dependent on the nature of the SPE.

A considerable amount of literature has been published on polyether-based systems due to the good ionic conductivity and high stability with cathode materials operating up to 4V, such as LiFePO$_4$.[132] However, to target the production of solid-state batteries with high energy density, more recently the attention has been focused on novel polymer systems comprising carbonate, ester, siloxane and fluorinated functional groups or even a mixture of them, exploiting grafting and/or copolymerization techniques.[133] Indeed, the possibility of tuning SPE final properties by controlled polymerization and starting monomers functionalization makes the solid-state polymer solution, in principle, definitely more attractive than a liquid electrolyte. The real breakthrough in the field would be finding the SPE or composite SPE, which can concurrently overcome all of the performance of the liquid counterpart at the same time, thus allowing for the design of high energy density solid-state Li-metal batteries operating at low temperature. To achieve this challenging target, the scientific research followed multitude approaches along the years, to cover all possible categories of SPE, from the development of gel and dry polymer electrolytes to single ion conducting polyelectrolytes and plastic crystals.[49,134]
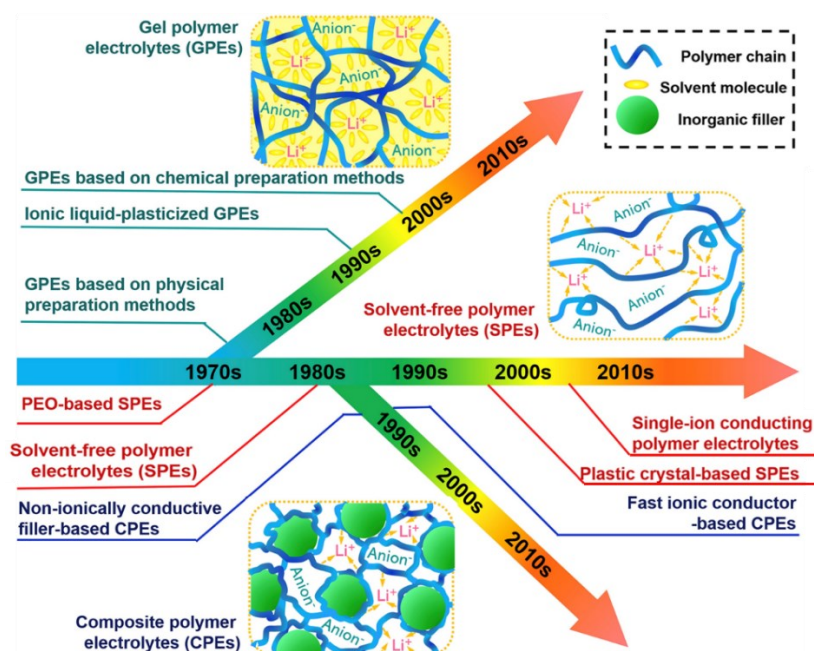
Figure 2.1 Timeline of the development of polymer electrolyte family branched in different subcategories. Figure adapted/reprinted from Zhou, D.[49]

2.1.1 Solid Polymer electrolytes (SPEs)

We can define SPEs as polymer host matrices with dissolved alkali salts, which macroscopically show good mechanical integrity and do not flow like a viscous liquid.[135] The dominant feature of this electrolyte category is the absence of any liquid or solvent additive. In this context, it should be acknowledged that the term "polymer electrolyte" is frequently used in the LIB field to indicate lithium-ion polymer battery, in which the electrolyte is more similar to gels or "quasi solid-state polymers". In general, *gel polymer electrolytes* (GPEs) contain a small fraction of liquid(s), such as solvents or plasticizers. Typically, in this kind of system, the liquid part controls the features of the resulting polymer/solvent mixture. Namely, it is the main responsible for the ionic conduction in the electrolyte, but at the same time, only mitigate the conventional liquid electrolytes issues, like poor safety and liquid leakage. It is fundamental to underline the difference between GPEs and SPEs, especially in terms of ion transport mechanism and safety. Indeed, the polymer host

matrix acts as a flame retardant in the case of thermal runaway events, and the ion conduction prevalently occurs through small molecules solvation instead of polymer chain coordination. However, the definition of SPEs refers solely to the family of salt in polymer (SIP) and to be clear, from now on, all the electrolyte systems comprising solvent or plasticizer will be referred to as quasi solid-state or gel electrolyte.

There is a large volume of published studies describing different polymer systems, such as polymethacrylate (PMMA), polyalcohol (PA), polyvinylidene fluoride (PVDF), poly(vinylidene fluoride-co-hexafluoropropylene) (PVDF-HFP), polyacrylonitrile (PAN) and polydimethylsiloxane (PDMS). Nevertheless, being this thesis work focused on investigating SICPEs with structures and characteristics more similar to SPEs based on polyethylene oxide- (PEO) and polycarbonate-based systems, these will be briefly described in the followings.[49,50,128,133,136,137]

PEO

The origin of polymer electrolytes exploration dates back in 1970s and can be attributed to the discovery of ionic conductivity in polyether-based polymers, chiefly polyethylene oxide (PEO) with dissolved alkali salts by Professor P.V. Wright.[126] A few years later, Professor M. Armand showed the first examples of PEO-based SPEs conceived for electrochemical applications, especially lithium batteries.[127,138] Armand M. can be considered the pioneer of the huge amount of research works related to the electrochemical properties investigation of PEO in its various forms and its application in energy storage/conversion field. He was the first to attribute the ionic conductivity to the amorphous phase of PEO-LiX electrolyte, which rapidly boosted the research work to find a way to suppress the crystallinity of the polymer and reach high ionic conductivity at ambient temperature. The basic structure of PEO–LiX polymer electrolytes involves Li^+ cations surrounded by PEO chains, thereby separating them from their anionic counterparts. Polymer electrolytes, therefore, require local relaxation and segmental motion of the PEO chains to allow for Li^+ ion transport, and this condition can only be obtained when the polymer is in its amorphous state, thus well above its melting temperature (*viz.*, 50-60 °C, Figure 2.2). It was demonstrated that ethoxy units (CH_2CH_2O) of PEO have a much better solvating ability toward Li salts than either methoxy (CH_2O) or propoxy ($CH_2CH_2CH_2O$) ones due to the

helical wrapping around the Li^+ ions, which is optimal when the ether oxygens are separated by exactly two carbon atoms .[132,139]
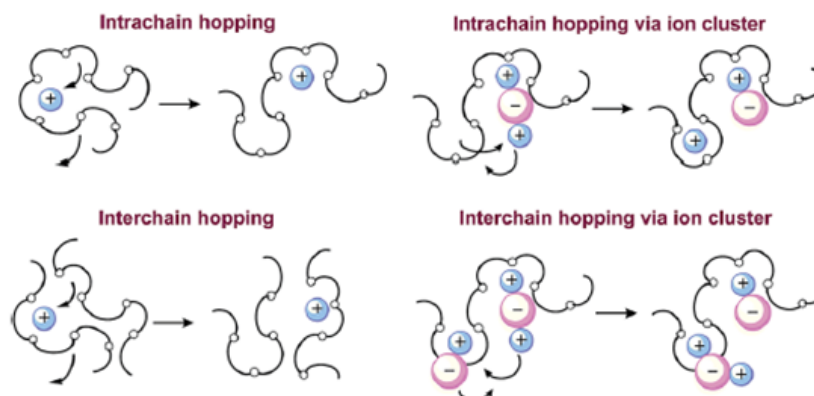
In 1998, Scrosati and coworkers proposed the addition of nanometer-sized inert ceramic particles of TiO_2 and Al_2O_3 to enhance the ionic conductivity at low temperatures.[140] The study showed that PEO-LiX with functionalised ceramics retains their amorphous state after the heating-cooling, thus preventing recrystallization of PEO and increasing the ionic conductivity at room temperature. It was found that the presence of acidic sites of ceramics particles actively competes with the lithium cations, interacting with basic oxygens of PEO and forming crosslinking centres, thus preventing the reorganization of polymer chains and promoting the Li^+ transport.[140] By far, PEO is considered one of the most attractive polymer electrolytes because of its excellent ability to dissolve Li salts. Indeed, several PEO-LiX systems have been studied, starting from the use of LiCl as dissolved salt, and the direct correlation between bulky anions and improved ionic conductivity was demonstrated.[141] The salt in LIBs plays a critical role in battery performance, being the source of lithium ions and extremely relevant in the solid electrolyte interface (SEI) formation at the electrodes. Anions with a highly delocalized negative charge and low basicity are preferred due to the weak coulombic interaction between charges. In comparison with the commonly used $LiClO_4$ and $LiPF_6$, the new generations of alkali salt bearing trifluoromethanesulfonate (triflate, TFS⁻), bis(trifluoromethanesulfonimide) (TFSI⁻), bis(fluorosulfonyl)amide (FSI⁻) and the novel fluoroborate based- and

imidazolium based- anions[142] demonstrated high solubility, high electrochemical stability and ionic conductivity (Figure 2.3). Large anions with strong electron-withdrawing groups allowed to decrease the crystallinity of the macromolecular network reaching conductivity values in the range of 10^{-3} to 10^{-4} S cm^{-1} at room temperature. Various strategies and approaches have been tried to break the crystallinity of PEO, such as the addition of different nanofillers and plasticizers, but also the preparation of polymer blends, cross-linked PEO-based polymers and grafted-block copolymer.[132,141,143]
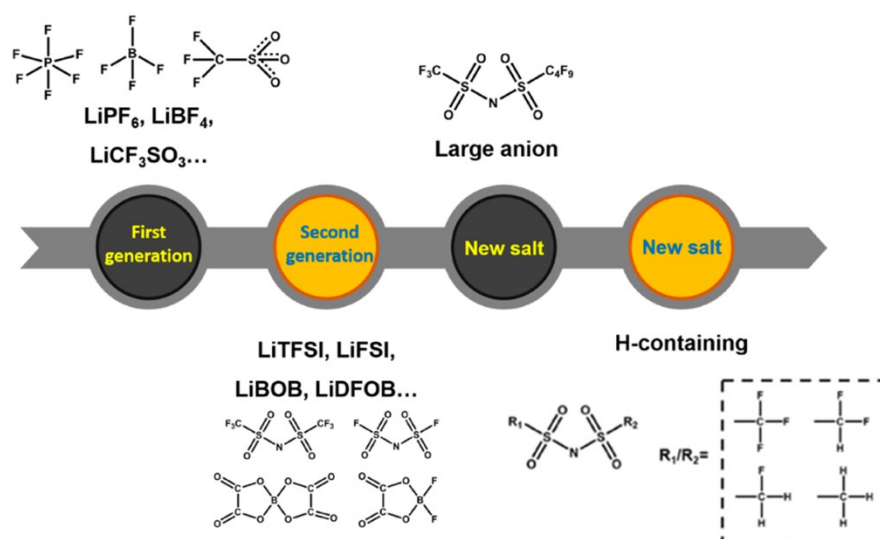
Figure 2.3 Evolution of lithium salts chemical structure to increase the negative charge delocalization. Figure adapted/reprinted from Zhao Y. et al.[141]

Despite the rapid development of PEO-based SPEs, its electrochemical stability improvement in battery systems has been the bottleneck for its widespread commercialization, so far. The hygroscopic nature of PEO and the relatively high number of terminal -OH groups for short chains polymers (named polyethylene glycols), especially used to get less viscous SPEs with high conductivity, were imputed as the main responsible for the instability at high potential values.[136] Aiming at improving the anodic stability of PEO-based electrolytes, several methods have been proposed, which included the preparation of crosslinked quasi

solid-state polymer electrolytes with highly concentrated plasticizers (ILs, organic solvents) to the synthesis of grafted PEO or blends involving fluorinated or carbonate-based polymers.[132,141] Thermally or photo-induced crosslinking has mainly been exploited to incorporate a relatively large amount of liquid or ceramic additives and to stabilize the amorphous state of linear PEO below the crystallization temperature, resulting in gel electrolytes with high ionic conductivity ($\sim 10^{-3}$ S cm^{-1} at ambient temperature) and suitable anodic oxidation resistance for stable cycling with 4V cathodes (up to $\sim$ 4.4 V vs Li$^+$/Li).[132,144]

Another interesting approach is the preparation of blend polymer electrolytes especially to improve the dimensional stability of SPE.[127] Blend preparation gathered considerable attention as a nontrivial synthesis method that allows obtaining systems with superior properties. These methods are also highly suitable for practical applications and scale-up due to easy control over compositional changes to fine tune physical and electrochemical properties. The preparation of grafted PEO or block copolymers requires specific techniques, such as controlled radical polymerization (RAFT, ATRP, etc) and click-chemistry reactions.[145–149] Although the relative complex synthesis, it is possible to obtain polymers with well-defined structures and specific desired properties due to partial immiscibility of the polymeric (monomers, oligomers, etc.) precursors. It was consistently demonstrated that the comb-like structure of the copolymer prevented the formation of lithium dendrite by phase separation between the rigid and the mobile blocks, like polystyrene (PS) and poly(ethylene glycol) methyl ether methacrylate (PEGMA), respectively.[145,149–153] Noteworthy, SPE improvements allowed to reach Li-ion transference number values in the range of 0.5-0.6, which are relatively high even if still far from unity. The outstanding results obtained by blending PEO with other polymer systems induced the research to investigate novel SPEs considering different polymer hosts to achieve superior electrolyte properties.

POLYCARBONATE

Aliphatic polycarbonates have been reported in the literature[136,141,154–161] as an alternative polymer host matrix for SPEs to the well-investigated PEO-based systems. The interest of the research community switched on this polymer family because of the similarity to the low-molecular-weight cyclic and linear carbonates (e.g. EC, PC, DMC), which arein the most commonly used liquid electrolytes in LIBs. Essentially, polycarbonates are high-molecular weight analogues of linear

alkyl carbonates, and they demonstrated reasonable performance as SPE in Li batteries.[162] Similar to the Li^+ coordinating ether oxygens of polyether electrolyte hosts, polycarbonates can coordinate with Li ions through the carbonyl group oxygen (Figure 2.4), and alkoxy oxygens near the carbonyl group have also been involved in salt solvation. In general, aromatic rigid segments restrict the mobility and conductivity to not satisfactory values ($\sim10^{-8}$ at ambient temperature) for practical cell operation.[136] Thus, aliphatic polycarbonates, including poly(trimethylene carbonate) (PTMC), poly(ethylene carbonate) (PEC), poly(propylene carbonate) (PPC) were preferred because of their amorphous structure, flexible chain segments and high dielectric constant. The main objective was to achieve suitable ionic conductivity, and, especially, high electrochemical, mechanical, and thermal stability.
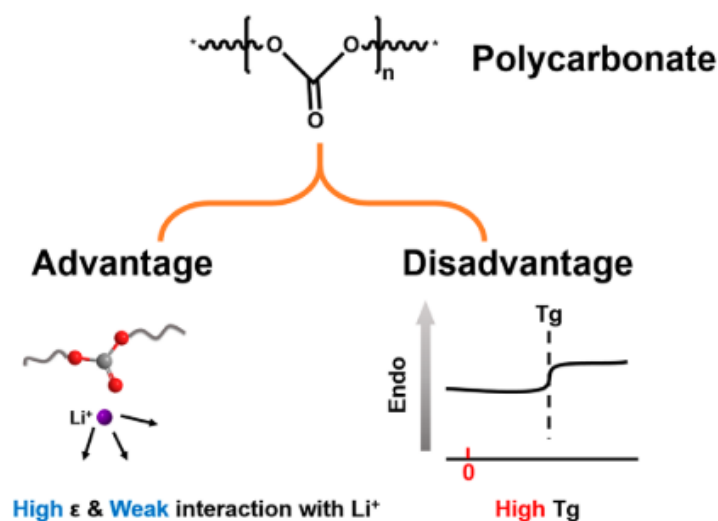
Figure 2.4 Advantages and disadvantages of polycarbonate-based polymer electrolytes. Figure adapted/reprinted from Zhao, Y. et al.[141]

In this scenario, the investigation began with the simplest PEC, characterized by the same number of methylene groups in the main chain of PEO. Well-controlled chain configuration and appreciable molecular weight were obtained by copolymerization of carbon dioxide with ethylene oxide.[163] The resulting polymer was amorphous, and it displayed a relatively low T_g of 9 °C. Tominaga and Okumura et al.[158,164–166] demonstrated remarkable improvement in ionic

conductivity up to $4.7 \cdot 10^{-4}$ S cm^{-1} at 20 °C along with a drastic decrease of T_g close to –60 °C when a high concentration of LiTFSI was used (polymer in salt instead of salt in polymer). Very recently, the unexpected plasticizing effect of lithium salt in PEC and PPC was investigated and explained as partial polymer decomposition into EC and PC catalysed by salt and residual solvents from the casting procedure.[167] As a result, unfortunately, fully dry and not degraded PEC based SPEs were demonstrated to be not suitable for the targeted battery applications. The same approach previously described for PEO-based SPEs was also applied to this polymer category. Several research works in the literature report about the synthesis of grafted PEC, including rigid and bulky phenyl and tert-butyl ethers as well as more flexible glyme-like side groups.[136,168,169] Ionic conductivity values of about $\sim 10^{-5}$ S cm^{-1} and a transference number of 0.6 were obtained at the expenses of mechanical properties, being the resulting material more like a liquid than a solid. Aimed to overcome these issues, many efforts were dedicated to studying the poly(trimethylenecarbonate) (PTMC), which gained even more interest as potential candidates to replace PEO as SPE in LIBs. In contrast to the five-membered analogues, the six-membered cyclic carbonates are more suited for ring-opening polymerization under mild conditions with common [Sn(octoate)$_2$] or in the presence of different organocatalysts[170] with alcohols. Silva and Smith et al.[171–174] deeply investigated the properties of PTMC in combination with different salts (i.e., LiBF$_4$, LiClO$_4$, LiTFSI), and they demonstrated conductivity values slightly lower than those observed in several solvent-free systems based on PEO and electrochemical stability limitations mainly due to the nature of salts. The system PTMC:LiTFSI was further investigated by Sun et al.[175] They reported the conductivity vs temperature trend for several compositions with [Li$^+$]:[carbonate] ratio ranging from 1:13 to 1:8. The best sample PTMC$_8$LiTFSI demonstrated electrochemical stability up to 5.0 V vs Li$^+$/Li^0 and ionic conductivity of the order of 10^{-7} S cm^{-1} at 60 °C. Despite the relatively low ionic conductivity, the elevated Li-ion transference number ($t_{Li}^+ \sim 0.8$)[157] allowed the realization and testing of a Li metal half-cell with LFP able to deliver approximately 150 mAh g^{-1} at low current rates. Compared to conventional polyether-based SPEs, higher lithium transference numbers were obtained for the PTMC-based SPEs. This behaviour might result from favourable dissociation and less stable Li-polymer coordination structures. In addition, simulations and computational modelling demonstrated that the carbonyl ester oxygen atoms are the foremost responsible for the Li-ion coordination, which perfectly agrees with the experimental observations.[157]

Aimed to match the advantages of both ethylene oxide and carbonate units, several polyether/carbonate have been synthesised by combining ether side chains and carbonate main polymer backbone, and thoroughly investigated.[141] Literature report by Takashi M. et al.[176] showed that ionic conductivities of polymer electrolytes increase with the increasing length of the ether groups, confirming that ion transport is coupled with the polymer segmental motion, diverging from the typical Arrhenius plot. The research on this family of copolymers is still in the first stage of investigation, with a limited number of studies about polycarbonates. However, preliminary results showed that almost no crystallization could be observed in the polyether/carbonate copolymers, and the copolymers possess low T_g, which allows improving the conductivity at room temperature. Noteworthy, when the proportion of the –EO– group is increased, the copolymer properties were similar to that of polyether, exhibiting a low t_{Li+}, higher ionic conductivity and limited ESW. On the contrary, when the content of the carbonate groups increases, the conductivity decreases due to the relatively high T_g, and the t_{Li+} increases due to weaker Li ion coordination; in addition, an extended ESW is obtained.

2.1.2 Single ion conducting polymer electrolytes (SICPEs)

Despite the advantages of different SPEs addressed in the previous section, conventional salt in polymers are dual ion conductors, and they present numerous challenges to be overcome. As suggested by the name of this category, both ions (cations and anions) are mobile in the host matrix. In particular, Li^+ cations are generally less mobile than their anionic counterpart and the difference results in the formation of a concentration gradient across the electrolyte when the battery is repeatedly charged and discharged. The anions migrate in the opposite direction of cations, and the accumulation at the electrode surface limits the amount of active material for redox reactions; consequently, the overall operating voltage and energy density of the cell are negatively affected. The transference number can be simply considered as the fraction of the total ionic conductivity that Li^+ ions carry. Doyle et al.[177] demonstrated the importance of the lithium-ion transference number to enhance materials utilization, cell power and energy density, particularly at a high current regime when large ions migration is required in small time fractions. Thus, efficiency, cycle-life and charge transfer of the cell can be increased by maximising the fraction of the ionic charge transferred by the movement of lithium ions between

the two electrodes across the electrolyte. Indeed, several reports in literature state that the homogeneity of lithium plating, which crucially affects dendrite growth, is directly linked to the transport of anions and, through their immobilization/movement limitations, the rate of dendrite formation can be reduced.[178,179] In this scenario, the novel category of single ion conductors (SIC) is one of the best choices to increase the effective current supplied by the cell and remove the problems associated with the concentration of anions at the electrode/electrolyte interface. SIC actually refers to an electrolyte in which the anion is anchored, and only the lithium cation is free to move. Such specific feature can be achieved in different ways: by covalently bonding the anion onto a polymer or inorganic framework or by effectively immobilising to anion by an acceptor species (Figure 2.5). Being the topic of this Thesis work, the category of single ion conducting polyelectrolytes (SICPs or SICPEs) will be thoroughly detailed in the following.
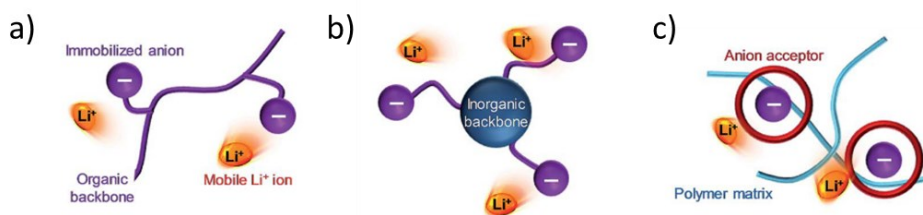
Figure 2.5 Illustration of different methods to achieve single Li⁺ ion transport features: (a) polyanions, (b) organic/inorganic hybrids and (c) anion acceptor-containing polymers. Figure adapted/reprinted from Jeong, K. et al.[180]

SICPEs can be defined as polyanions or polycation, depending on the nature of anchored moieties to the polymer chain. This Ph.D. Thesis focuses on polyanionic systems, composed of a polymer backbone bearing covalently bonded anionic functional groups and a free-to-move lithium counterions responsible for cations mobility. Because of their single-ion nature, the lithium transport number values approach the unity, with remarkable benefits to the electrochemical performance, as Li^+ ions are predominantly engaged in the redox reaction while anions remain relatively inactive. The characteristics of such electrolyte materials in terms of ionic conductivity, Li^+ ion transference number (t_{Li^+}), flexibility and processability are strictly related to the type of polymer backbone, nature and charge delocalization

of anchored anions. Generally, they are obtained through the polymerization of negatively charged ionic monomer precursors bearing counter Li$^+$ cations.[180] Their preparation is carried out principally by two methods: the direct polymerization of functionalized ionic monomers and the chemical modification of the already synthetized polymers. Both methods involve different polymerization techniques, from the most commonly used free radical polymerization to controlled radical polymerizations (e.g., atom transfer radical polymerization - ATRP[181], and reversible addition fragmentation chain transfer - RAFT)[148], and the anionic polymerization.[182]

The first approach toward polymerizable ionic monomers was reported by Ohno et al.[183], who synthetized a variety of ionic liquid monomers (ILMs) by anion exchange reaction of a cationic imidazolium halide type monomer with different counter anions. Since then, the large family of ILMs and polymeric ionic liquids (PILs) was deeply investigated by the research groups of Prof. Mecerreyes, Shaplov and Forsyth/MacFarlane.[184–189] Noteworthy, ILs are generally defined as compounds fully composed of ions with a melting point below 100 °C. However, Mecerreyes et al.[185], during zwitterionic polymers investigation, found that the insertion of anion moieties along the monomer chain led in some cases to solid salt with a high melting point instead of conventional IL. Considering the sizeable interest from the research community and the number of possible technological applications, the category of solid ionic monomers and corresponding polymers were included into the field of ILMs and PILs. Indeed, one of the critical parameters governing the properties of the final SICPE is the nature of the ionic monomer. Anionic lithium monomers (or ILMs) generally have a polymerizable termination, such as (meth)acrylate, styrenic or vynilic end-group. Recently, Mecerreyes group reporteed an ester functionalized diol ILM (with di-hydroxy-terminations) to exploit polycondensation technique, but the control over polymerization was lower in comparison with living polymerization methods.[190] The position of the negative charge and the nature, length, and flexibility of the spacer drastically affect the properties of the monomer and the final polymer electrolyte. Many literature reports demonstrated that anchoring an anion at the end of the monomer chain led to PILs with improved conductivity. By correlation, aimed to enhance the mobility of the coordinating anions, several works have been performed to investigate the effect of the chemical nature and length of the spacer on the performance of the final PILs. A progressive ionic conductivity improvement was noticed, obtained by increasing the spacer and moving from a chain containing ester groups to alkyl and, finally, to

a chain composed of ethylene oxide units. It is likely because the CH_2CH_2O units actively contribute to ions dissociation, thus enhancing the ionic conductivity. Furthermore, the nature of the anchored anion plays a fundamental role in the mobility of Li^+ cations. Because of the large abundance and easy synthesis procedures, carboxylates and sulfonates ILMs were investigated.[191,192] However, these systems were characterized by localized negative charges that strongly coordinate cations, thus resulting in limited Li^+ ion mobility. Sizeable amount of research has been conducted studying SICPEs bearing borate,[193,194] phosphates,[195] oxyaluminate ($[Al(OR)_4]^-$), and thioaluminate ($[Al\text{-}(SR)_4]^-$) anions.[196,197] However, the real breakthrough in terms of ionic conductivity enhancement was achieved after introducing weakly coordinating and highly delocalized sulfonamide anions.[198,199]

The presence of multiple electron-withdrawing groups, such as $-CF_3$ improves the mobility of Li^+ cations and high Li-ion transference number ($t_{Li}^+ = 0.90$). The novel lithium: 1-[3-(methacryloyloxy)propylsulfonyl]-1-(trifluoromethanesulfonyl)imide (LiMTFSI), poly[(4-styrenesulfonyl)-(trifuoromethanesulfonyl)imide] (LiSTFSI) and poly[(4-styrenesulfonyl)(trifuoromethyl(S-trifuoro-methylsulfonylimino)sulfonyl)imide] (LiSSsTFSI) monomers were firstly polymerized to get homopolymers (Figure 2.6 a-c) that were further mixed with PEO to obtain self-standing blend electrolytes with ionic conductivity in the range from ~10^{-7} to ~10^{-5} S cm^{-1} at 70 °C, along with t_{Li+} close to unity.[180] Unfortunately, the high glass transition temperature of ionic homopolymer and the high crystallinity of PEO were still an obstacle to reaching suitable conductivity values for practical LIBs application. Aimed at reducing the T_g and correspondingly enhancing the mobility of ion coordinating chains, copolymers comprising different polymerizable non-ionic monomers were studied. Comb-branched, simple block and triblock copolymers exhibited higher conductivity along with well-defined Li^+ ion transport behaviour. Among a large number of remarkable results, Bouchet et al.[200], Porcarelli et al.[201,202] and Feng et al.[203] were the first to report the practical advantages of the ILMs copolymerization with flexible oligoether chains (such as PEGM), especially in suppressing the crystallinity of PEO and boosting the ion conduction (Figure 2.6 d,f).

The homopolymer deriving from LiSTFSI and LiMTFSI ILMs were characterized by high T_g of 152 and 95 °C, respectively, with limited ionic conductivity in the order of 10^{-12} S cm^{-1} and suitable degradation temperature above

200 °C. The best outcomes in terms of ionic conductivity were stated for the triblock copolymer samples poly(LiSTFSI)-b-PEO-b-poly(LiSTFSI) and poly(LiMTFSI)-b-PEO-b-poly(LiMTFSI), which exhibited values above 10^{-5} and close to 10^{-4} S cm^{-1}, respectively, at 70 °C (Figure 2.6 e,g). Indeed, the novel SICPEs demonstrated relatively high electrochemical stability toward anodic oxidation for stable galvanostatic cycling at 70 and 80 °C with LFP cathode in lab-scale Li-metal cells at different C/n rates ranging from C/20 to 2C, delivering specific capacity values close to the theoretical one and showing great capacity retention. Generally, SICPE block copolymers exhibited a well-defined structure associated with very low ionic conductivity at 25 °C, mainly due to the presence of LiSTFSI/LiMTFSI-rich microphase segregation and crystalline PEO-rich microphase..[204]

An increase in temperature above 60 °C led to a transition from an ordered structure to a homogeneous disordered morphology, where the Li$^+$ ions were released from the clusters, which correspondingly increased the ionic conductivity by five orders of magnitude (up to $10^{-4} \div 10^{-3}$ S cm^{-1} at 60 °C[200–202] A significant increase in conductivity was detected with the transition from lamellar microphase separation to the disordered morphology at temperatures above the melting point of PEO blocks ($T_m > 55$ °C). Furthermore, Jangu et al.[205] demonstrated that preparation of triblock copolymers (C-AB-C) torough insertion of an ionic block by random copolymerization of ILM with di(ethylene glycol) methyl ether methacrylate triblock copolymers, allows a microphase-separated morphology and a combination of excellent mechanical properties and higher ion transport in comparison with previous reports. The authors explained this effective ion transfer not only by an increase in the number of lithium cations, but also by a substantial improvement in microphase segregation and channel connectivity.[205] These results can be explained as follows: the mechanism of Li-ion transfer in PEO-derived materials is based on the hopping of the Li between oxygen atoms in oxy ethylene units; when PEO chains are "frozen" and separated from the ionic block in lamellar morphology, the Li ions are trapped and cannot move. Thus, polymers do not benefit from phase separation, and ionic conductivity increases only when block copolymers become disordered systems. However, when in copolymers the ILM is copolymerized randomly with a monomer having short and flexible side PEO chains, such system allows for lithium ion hopping also at low temperature along with reduction of T_g.
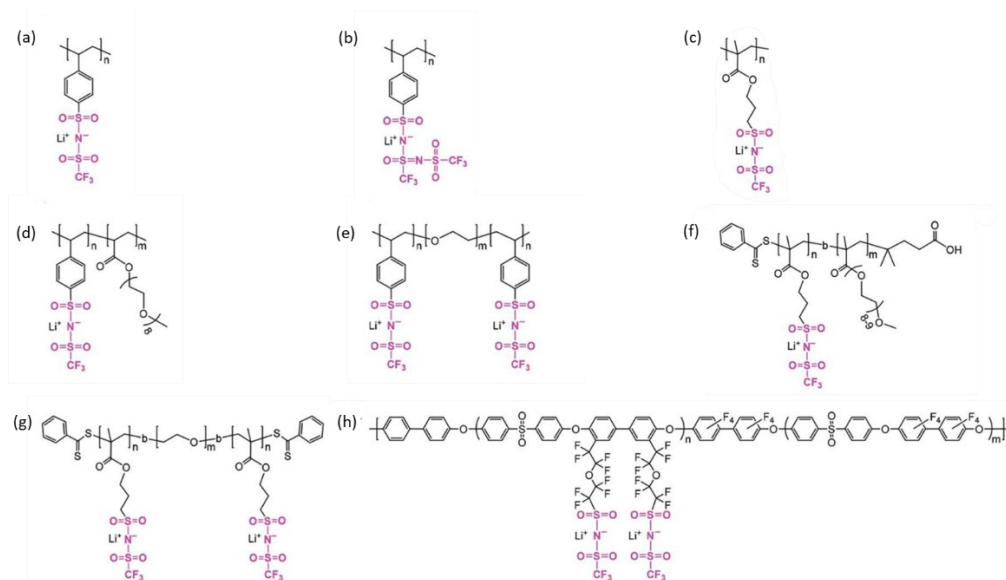
Figure 2.6 Representative polyanions based on sulfonylimide anchored anion groups. Figure adapted/reprinted from Jeong, K. et al.[180]

The copolymerization with PEO and poly(ethylene glycol) methyl ether methacrylate (PEGM) decreased the T_g of the ILMs drastically, resulting in SICPEs with T_g values ranging between –20 and –60 °C and t_{Li+} of about 0.9. Indeed, Porcarelli L. et al.[189] reported the synthesis of novel methacrylic ILMs along with the investigation of the structure and spacer length effect on the final SICPEs performance, highlighting the need for flexible anionic centres, preferentially placed at the end of the comb-like side chains.

The limited ambient temperature ionic conductivity was one of the main bottlenecks for the application of SICPEs in practical batteries. Aimed to overcome this obstacle, many efforts have been spent to design quasi-solid state SICPEs comprising liquid plasticizers, such as EC and PC. Among the considerable number of literature works, it is essential to mention the crosslinked SICPEs prepared by Porcarelli et al.[130], which were based on LiMTFSI, PEGM, PC additive, and cross-linkable monomers like poly(ethylene glycol) methyl ether dimethacrylate (PEGDM) (Figure 2.7a). The self-standing membrane exhibited excellent specific capacity during galvanostatic cycling with LFP at 25 °C and C/10 (Figure 2.7 b,c).

In this scenario, more recently Nguyen et al. reported the preparation of multiblock copolymer (Figure 2.6 h), which was based on an ionophilic block (perfuoroether sulfonylimide) and a hydrophobic block (perfuoroaromatics) swelled in EC.[206] The addition of organic carbonate solvents obviously allowed for higher ionic conductivity (~10^{-3} S cm^{-1} at 30 °C); in addition, materials showed extended anodic stability (~4.9 V), allowing stable cycling with NMC cathode at C/5 and 40 °C (Figure 2.7 d,e). Nevertheless, all the advantages of gel-type SICPEs are mainly triggered by the addition of flammable solvent at the expense of safety if compared with truly solid-state SICPEs. Nonetheless, the gel-type SICPEs based on fluoropolymer backbone or side chains gathered attention because of the excellent ESW and the presence of strong withdrawing fluorine units.
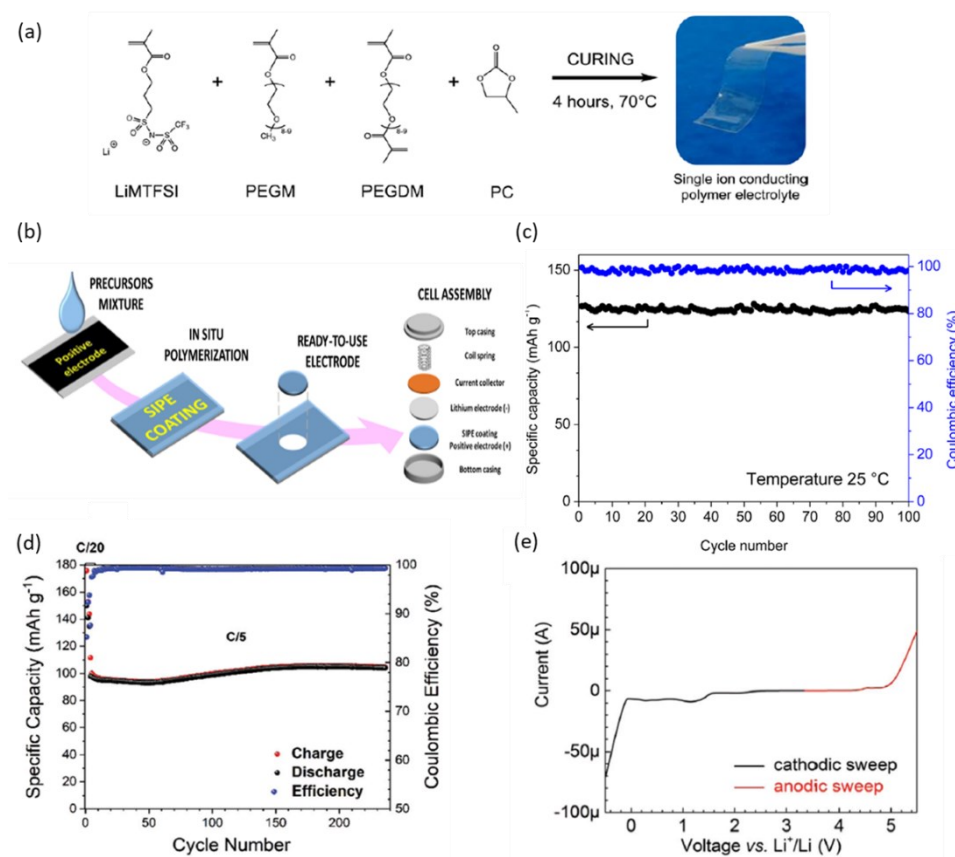
Figure 2.7 Application of gel-type SICPEs in quasi-solid-state Li cell: (a) general pathway for the preparation of SICPE based on LiMTFSI, PEGM, PC additive, (b) schematic representation of the in-situ polymerization process on the electrode sheets and cell assembly, (c) specific capacity of the crosslinked SICPEs in Li metal cell with LiFePO₄. Gel-type multi-block copolymer containing

Another emerging category of SICPEs is the boron-based polymer electrolyte systems, considered of interest for the reduced interaction of Li-ions and boron-centred polyanions.[207] The obtained borate polymer containing –EO– spacer displayed a higher dielectric constant compared to previously reported PEO-based sulfonylimide SICPEs due to strong delocalization of negative charge by perfluorotetraphenyl units attached to the anion center. However, by exploiting the flexible siloxane backbone, the overall conductivities of the polymers (10^{-7} S cm^{-1} at 25 °C)[194] were still low due to their relatively high T_g, which slowed segmental dynamics at ambient temperature.

Following the same trend of SPEs, most recently, the research focus switched to the polycarbonate family of SICPEs, which already collected much attention because of their excellent stability toward high oxidation voltage. As mentioned in paragraph 2.1.1 for SPEs, the total or partial replacement of ethylene oxide units with polycarbonate ones mitigates the interfacial polymer matrix degradation with high voltage cathodes (e.g., NMC), along with achieving enhanced mechanical properties while maintaining sufficient ionic conductivity. However, compared to the large volume of information regarding polycarbonate SPEs,[136,141,154–161] there are just a few investigations about the category of SICPEs; remarkably, preliminary results arepromising for future application in many energy-related fields.

Deng et al.[208] reported an effective way to convert CO_2 into a desirable product, such as a polycarbonate polymer matrix (Figure 2.8a). This polymer electrolyte was synthesized by the terpolymerization of propylene oxide (PO), allyl glycidyl ether (AGE), and CO_2, then the allyl terminations were functionalized by mean thiol-ene click chemistry and, successively, lithiated with LiOH. The combination of predominantly alkyl side chains with carboxylic anion termination resulted in limited Li$^+$ ion mobility (ionic conductivity of 1.61×10^{-4} S cm^{-1} at 80 °C), transference number of 0.86 and ESW up to 4.3 V vs Li$^+$/Li.

(a)

(b)
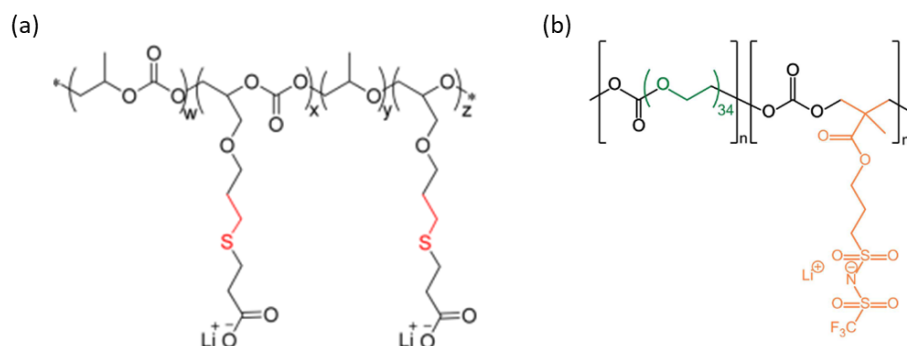
Figure 2.8 Grafted polymer PPCAGE-g-COO⁻ Li⁺ (a) and poly(ethylene oxide carbonate) with single ion conducting features. Figure adapted/reprinted from Deng K. et al. [210] and Meabe L. et al. [211]

Aimed at achieving higher segmental mobility and ionic conductivity, Meabe L. et al.[160,190] reported a SICPE based on poly(ethylene oxide carbonate), obtained by mean polycondensation techniques, which was already investigated by the latter (Figure 2.8b). The incorporation of ethylene oxide units into the main chain and the utilization of efficient sulfonamide anion terminations allowed to get ionic conductivity of above 10^{-4} S cm^{-1} at 80 °C. Unfortunately, the large amount of PEO resulted in high crystallinity and insufficient mechanical integrity above 60 °C. In order to suppress the crystalline behaviour, a semi-interpenetrated cross-linked network was prepared by adding cross-linkable monomers. The resulting SICPE was still characterized by suitable ionic conductivity and enhanced mechanical properties. Indeed, the extended ESW up to 4.9 V was further demonstrated by means of galvanostatic cycling with NMC (111) cathode in a voltage range between 4.2 V and 2.8 V, upon the treatment of lithium metal surface anode with 5μL of 2 M LiFSI in DME (dimethyl ether). Compared with the parent SPE, the novel SICPE exhibited lower overpotential during the plating/stripping process and a distinct plateau, indicating better lithium-ion transfer properties.

Chapter 3

3 Polymerization procedures and experimental techniques

In this Ph.D. work, several polymerization techniques were used to prepare intermediate oligomer/polymer and block or random copolymers, from the simple free radical polymerization to reversible addition−fragmentation chain transfer (RAFT)[209], and ring-opening polymerizations (ROP).[210] As well as, different methods for sample preparation and experimental techniques were exploited in order to obtain a thorough chemical-physical and electrochemical characterization of materials.

3.1 RAFT, ROP and free radical

Free radical polymerization is one of the most useful techniques in the chemistry field because of its capacity to be exploited with different monomers/oligomers bearing different functional groups and performed in a wide range of media. Indeed, the formation of active radicals can be mediated by thermal and ultraviolet (UV) light sources, making this technique suitable for the UV-induced crosslinking process, which is a fast, cost-effective and green procedure for the production of polymer electrolytes. However, the last decade has seen the development of polymerization techniques that can allow control over the polymer molecular weight. In the field of controlled polymerizations, the RAFT process has grown into one of the most versatile and powerful techniques for synthesizing complex polymeric architectures.[211] RAFT is a reversible deactivation radical polymerization (RDRP), which, contrarily to the free radical, belongs to the family of living radical polymerizations. It is one of the most studied and used polymerization techniques because it allows the preparation of polymeric

architectures with predictable molecular weight, low polydispersity, high end-group fidelity and capacity to progressively increase the chain growth. Indeed, in comparison with other living polymerization, such as nitroxide-mediated polymerization (NMP) and atom transfer radical polymerization (ATRP), RAFT limits the number of dead chains by through proper control of the amount of initiator, thus obtaining block copolymers preparation with 100% of monomer conversion. Furthermore, the large number of literature information about RAFT polymerization of (meth)acrylates and styryl derivatives makes it the most suitable technique for the preparation of novel SICPEs starting from ILMs, such as LiMTFSI and LiSTFSI.

As introduced in the previous chapter, we indicated that polycarbonates and polyesters are attracting even more attention in the development of SICPEs because of their attractive electrochemical features. ROP stands out as the leading approach to obtain aliphatic polymers/oligomersstarting from cyclic monomers in this scenario. This technique allows the use of a catalytic amount of metal complexes (e.g., $Sn(Oct)_2$), and a protic source (e.g., alcohol) used in large excess (compared with the metal catalyst), which behaves both as a co-initiator and as a chain transfer agent. Recent advances in the ROP of cyclic carbonates allowed to elaborate a new metal-free green method, which uses various alcohols (benzyl alcohol, glycerol, propane-1,3-diol, etc.) as initiators and highly basic amines (1,8-diazabicyclo(5.4.0)undec-7-ene (DBU), 1,5,7-triazabicyclo[4.4.0]dec-5-ene (TBD), 4-dimethylaminopyridine (DMAP), etc.) as catalysts.[170,212,213]

The ROP starts with the opening of the cyclic monomer ring, obtaining the aliphatic specie, which is active toward further polymerization with another cyclic monomer or repeating unit to create the final polymer. After the cyclic ring is opened, the polymerization proceeds according to one of the three different major reaction mechanisms, namely cationic, anionic, or coordination-insertion mechanisms. Anionic ROP of ε-caprolactone initiated by an alkoxide is a typical example of ROP, where a polarized carbon atom is attacked by nucleophilic activated alcohol (organocatalyst-alcohol complex) to generate the new aliphatic nucleophile, which is active to attack another cyclic monomer.[214] An essential feature of this mechanism is that ROP is typically a living polymerization, and it is possible to control the polymer features as described for the RAFT polymerization.

Recently, there have been great efforts to increase the control over the polymer macromolecular structure, and the combination of ROP and RAFT or ATRP techniques is gathering much attention. This path was further investigated by exploiting RAFT chain transfer agents containing hydroxyl functionality, such as (4-cyano-4-(dodecylsulfanylthiocarbonyl)sulfanylpentanol (CDP) or (S)-2-cyano-5-hydroxypentan-2-yl benzodithioate) as dual initiator, allowing the subsequent realization of ROP and RAFT polymerizations.[213,215] Such an approach was mainly applied to lactides[215,216] and, to a lesser degree, to cyclic carbonates.[213,215]
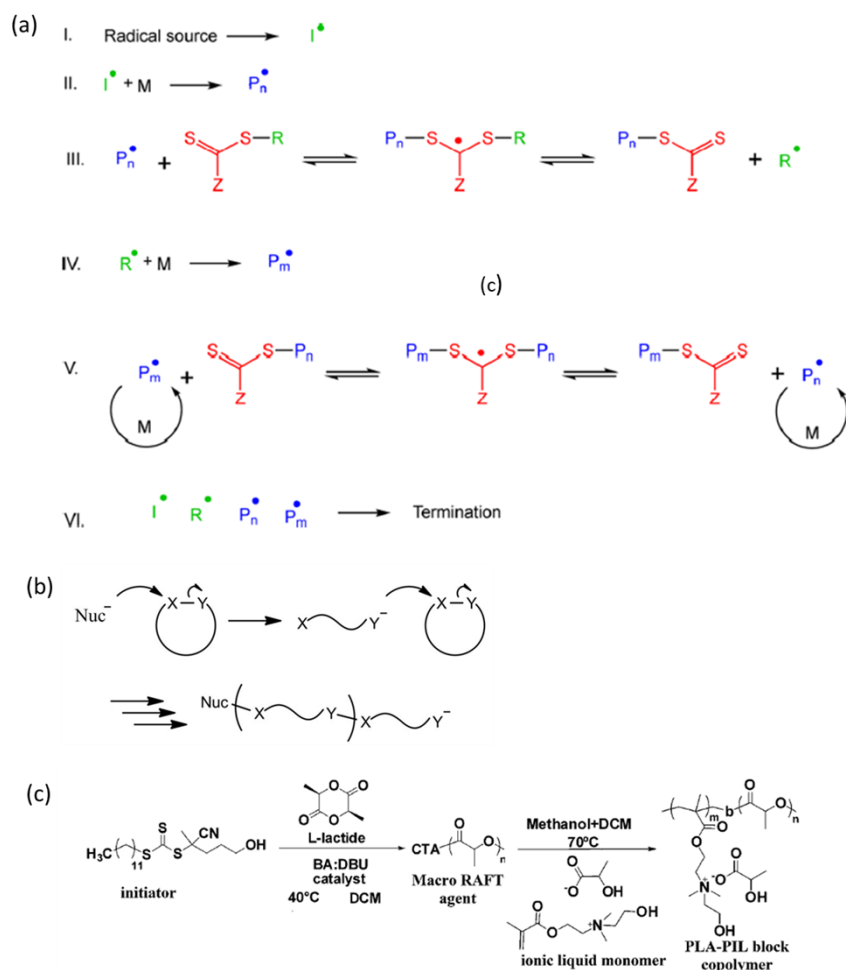
Figure 3.1 Mechanism of Reversible Addition−Fragmentation Chain Transfer Polymerization (RAFT) (a), general reaction pathway of anionic ring opening polymerization (ROP) (b), and preparation of block copolymer by dual ROP-RAFT polymerization technique. Figure adapted/reprinted from Perrier S. [146,] Isik M. [216]

Several literature works report the advantages of combining ROP and RAFT polymerization performed either in one or two synthetic steps.[217–219] The combination allows controlling the number of hydrophobic blocks, generally from cyclic carbonates or carboxylic esters (e.g. TMC, lactide), and hydrophilic blocks from ethylene oxide-based monomers or ILMs. The critical point to performing this kind of polymerization is the presence of dual initiators, such as hydroxyl-terminated chain transfer agents (CTA), which can initiate ROP and RAFT polymerizations, independently and selectively. Furthermore, several studies reported the advantages of using selective and living polymerization techniques to prepare SPE with specific structures and features. Depending on the degree of segregation and polymerization, the volume fraction of different blocks and the chemical nature of monomers, it is possible to control the phase separation design and, thus, the polymer nanostructure, which can include spheres, cylinders, lamellae and gyroid structures.[206] Isik et al.[216] prepared a new poly(lactide)-block-poly(2-cholinium lactate methacrylate) amphiphilic block copolymer by coupling ROP of L-lactide and controlled RAFT polymerization of ILM. The resulting block copolymer exhibited relatively low polydispersity and intriguing self-assembling behaviour, leading to phase separation in spherical nanostructures.

3.2 Experimental setup

3.2.1 NMR and IR spectroscopy

NMR spectra were recorded using an Avance III HD 600 MHz spectrometer (Bruker) at 25 °C in the indicated deuterated solvents and reported in ppm. The signal corresponding to the residual protons of the deuterated solvent was used as an internal standard for ^{1}H and ^{13}C NMR, while the C_6F_6 and $LiBF_4$ were utilized as external standards for ^{19}F and ^{7}Li, respectively.

IR spectra were acquired on a Nicolet Magna-750 Fourier IR-spectrometer using KBr pellets or on Brucker Tensor 27 Fourier IR-spectrometer using ATR technology (128 scans at the resolution of 2 cm^{-1}) and Spectragryph optical spectroscopy software.

3.2.2 Transference number and plating/stripping measurements

The lithium-ion transference number (t_{Li}^+) was determined at 70 °C in symmetric lithium metal/copolymer/lithium metal cells, subjected to different polarization biases (ΔV), depending on preliminary tests, to evaluate electrolyte bulk resistance, thus determining the initial (I_o) and the steady-state (I_{ss}) currents. EIS was performed on VMP3 multipotentiostat (20 V, ±400 mA, Bio-Logic Science Instruments) by applying a polarization bias between 300 kHz and 0.5 mHz at OCV conditions to obtain the resistance of the passivation layer before ($R_{SEI+CT,o}$) and after ($R_{SEI+CT,ss}$) polarization. The t_{Li}^+ was calculated using the Evans/Vincent/Bruce[220] and Abraham et al.[221] (Equation 3 and Equation 4, respectively):

$$t_{Li+} = \frac{I_{ss} \cdot (\Delta V - I_o \cdot R_{SEI+CT,o})}{I_o \cdot (\Delta V - I_{ss} \cdot R_{SEI+CT,ss})} \qquad \text{Equation 3}$$

$$t_{Li+} = \frac{I_{ss} \cdot R_{b,ss} \cdot (\Delta V - I_o \cdot R_{SEI+CT,o})}{I_o \cdot R_{b,o} \cdot (\Delta V - I_{ss} \cdot R_{SEI+CT,ss})} \qquad \text{Equation 4}$$

where t_{Li}^+ is the Li transference number, ΔV is the potential applied across the cell, $R_{SEI+CT,o}$ and $R_{SEI+CT,ss}$ are the initial and steady-state resistances of the passivating layer, I_o and I_{ss} are the initial and steady-state currents, $R_{b,o}$ and $R_{b,ss}$ are the variation of bulk electrolyte resistance.

The stability/compatibility at the interface with the lithium metal electrode was tested at 70 °C in symmetric lithium metal/copolymer/lithium metal cells at a constant current (galvanostatic). The reversible plating/stripping tests were performed at 70 °C at various current density values (mA cm^{-2}) and different time steps.

3.2.3 Size Exclusion Gel Permeation Chromatography (SEC-GPC)

For the determination of M_n, M_w and M_w/M_n (PDI) of non-ionic polymers (without anchored ionic moieties), a 1260 Infinity II gel permeation chromatography (Agilent Technologies) was used. The chromatograph was equipped with an integrated multi-detector composed of IR, UV, viscometer and light scattering. The separation was conducted using in series a PLgel guard

column, PLgel 5 mm MIXED-D column, and PLgel 5 mm MIXED-C column (Agilent Technologies). The eluent was THF, and the flow rate was 1.0 mL·min^{-1} at 40 ºC. Instead, for the characterization of polyanions (polymer bearing charges), a 1200 Infinity gel permeation chromatography (GPC, Agilent Technologies) was applied. The chromatograph was equipped with an integrated IR detector, a PL PolarGel-M column and a PL PolarGel-M guard column (Agilent Technologies). 0.1 M solution of Li(CF$_3$SO$_2$)$_2$N in DMF was used as an eluent, the flow rate was maintained at 1.0 mL·min^{-1} and the measurements were performed at 50 °C. For all polymers, the polymethylmethacrylate standards (EasiVial PM, Agilent Technologies, M$_p$ = 550 – 1558×10^3) were used to perform calibration.

The degree of polymerization (DP) was determined using the following Equation:

$$DP = \frac{M_n GPC}{M_{monomer}}$$ Equation 5,

where M$_n$ GPC is the molar mass of the polymer determined by GPC, while M$_{monomer}$ is the molar mass of the monomer.

The $M_{n(NMR)}$ for random poly[LiM$_n$-r-PEGM$_m$] copolymers was defined using simplified Equation 6:

$$M_{n(NMR)} = \overline{M}_{unit} \cdot q \cdot \frac{[LiM]_0 + [PEGM]_0}{[CPAD]_0} + M_{CPAD}$$ Equation 6,

where q is the total conversion of PEGM and LiM monomers (determined by ^{1}H NMR); M_{CPAD} is the molar mass of CPAD; [PEGM]$_o$, [LiM]$_o$ and [CPAD]$_o$ are the initial amount of monomers and CPAD in moles; $\overline{M}_{unit}$ is the average molecular weight of the monomer repeating unit, which is calculated following the Equation 7:

$$\overline{M}_{unit} = \frac{n}{n+m} \cdot M_{LiM} + \frac{m}{n+m} \cdot M_{PEGM}$$ Equation 7,

where

The M$_{n(NMR)}$ for block poly[(LiM$_n$-r-PEGM$_m$)-b-PhEtM$_k$] copolymers reported in chapter 5 are calculated by simplified $Mn(NMR) = M_{PhEtM} \cdot q \cdot \frac{[PhEtM]_0}{[macro-CTA]_0} + M_{macro-CTA}$ Equation **8**:

$$M_{n(NMR)} = M_{PhEtM} \cdot q \cdot \frac{[PhEtM]_0}{[macro-CTA]_0} + M_{macro-CTA} \qquad \text{Equation 8,}$$

where q is the conversion of PhEtM monomer (determined by ^{1}H NMR); $M_{macro-CTA}$ is the molecular weight of respective macro-CTA poly[LiM$_n$-r-PEGM$_m$] determined by ^{1}H NMR; M_{PhEtM} is the molar mass of PhEtM; [PhEtM]$_0$ and [macro-CTA]$_0$ are the initial amounts of monomer and macro-CTA, respectively. The number of monomer units k in poly[(LiM$_n$-r-PEGM$_m$)-b-PhEtM$_k$] was calculated as follows: k= q·[PhEtM]$_0$.

3.2.4 Thermal gravimetric analysis (TGA), Differential Scanning Calorimetry (DSC) and Thermal mechanical analysis (TMA)

Thermal gravimetric analysis (TGA) was carried out in air on a TGA2 STARe System (Mettler Toledo), applying a heating rate of 5 °C·min^{-1}. For Differential Scanning Calorimetry (DSC) measurements, all polymer samples were preliminary dried at 60 °C/1 mm Hg for 12 h in the B-585 oven (Buchi Glass Drying Oven, Switzerland) filled with P_2O_5 and transferred under vacuum inside an argon-filled glovebox (MBRAUN MB-Labstar, H_2O and O_2 content <0.5 ppm), where they were hermetically sealed in Al pans. The calorimeter was calibrated before measurements using the indium calibration standard (Mettler-Toledo, purity > 99.999 %). DSC of polymer samples was performed on a DSC3+ STARe System (Mettler Toledo) with a heating rate of 5 °C min^{-1} (1st cycle) and 10 °C ·min^{-1} (2nd cycle) in the fixed range of temperature. The glass transition temperature (T_g) was determined during the second heating cycle as the first one was used to eliminate the thermal history of the sample.

Thermal mechanical analysis (TMA) was performed for copolymers, illustrated in chapter 5. Measurements were carried out under an inert atmosphere (He) using a DIL 402 select Expedis dilatometer (NETZSCH, Selb, Germany) at a heating rate of 5 °C min^{-1} and a constant load of 0.3 N. Heat distortion temperature (THDT) was determined as a temperature at which a noticeable deformation under applied load and scanning/heating rate was observed.

3.2.5 Rheology

Rheological measurements were performed using an Anton Paar Physica MCR 302 rheometer equipped with a CTD 450 temperature control device with a

disposable aluminium parallel plate. Polymer samples were loaded directly onto the rheometer aluminium plate, and special care was taken to avoid bubbles. Measurements were recorded in the oscillation mode at an imposed 1% strain amplitude (γ), ensuring that both moduli G′ and G″ were obtained in the linear viscoelastic regime. All measurements were carried out at 25 and 70 °C. Tests were repeated at least twice to ensure good repeatability of the results.

3.2.6 Atomic Force Microscopy (AFM)

Atomic Force Microscopy (AFM) images were recorded with MFP-3D infinity microscope (Asylum Instruments/Oxford Instruments) in the tapping mode (-20 °C, in air). AC160TS-R3 (Olympus) cantilevers were applied with a stiffness of 26 N m^{-1} and resonance frequency of 300 KHz. The domains periodicity was evaluated from 3 different 1×1 μm^2 images. Two profiles were taken on each image, and the distance was recorded over 10 consecutive periods. The images were recorded in the so-called 'soft tapping mode', to avoid deformation and indentation of the polymer surface by the tip. All the images were collected with the maximum available number of pixels (512) in each direction. The general procedure for preparing the samples for AFM was as follows: films were cast from 10 wt% solution of the respective block copolymer in DMF on a microscope glass and allowed to evaporate at 80 °C slowly. The obtained thin films were dried at 80 °C / 1 mm Hg for 24 h. Before AFM analysis, samples were soaked in anhydrous ethanol for a few seconds and then dried under nitrogen flux.

3.2.7 Electrochemical impedance spectroscopy (EIS)

Ionic conductivity (σ) was determined by electrochemical impedance spectroscopy (EIS) with a VSP potentiostat/galvanostat (Bio-Logic Science Instruments). The latter were preliminary dried at 60 °C/1 mm Hg for 12 h in the B-585 oven (Buchi Glass Drying Oven, Switzerland) filled with P_2O_5 and were transferred under vacuum inside an argon-filled glovebox (MBRAUN MB-Labstar, H_2O and O_2 content <0.5 ppm), to avoid any influence of moisture/humidity on the conductivity of polymer electrolytes. A symmetrical stainless steel/copolymer/stainless steel configuration was used in combination with ECC-Std test cells (EL-Cell GmbH, Germany) and after the assembly, it was taken out from the glovebox. Cell impedance was measured at the open circuit potential (OCV) by applying a perturbation voltage of 20 mV in the frequency range from

10^{-2} to 2×10^{5} Hz and in different ranges of temperatures. The temperature was controlled using the programmed M-53 oven (Binder, Germany), where cells were allowed to reach thermal equilibrium for at least 1h before each test. The ohmic resistance (R, Ω) of the polymer electrolyte sample, obtained from the Nyquist plot at the low frequency end of the semicircle, was used to calculate the ionic conductivity using the following Equation:

$$s = \frac{d}{A \cdot R}$$ Equation 9

3.2.8 Cyclic voltammetry (CV)

CV was used to determine the electrochemical stability window (ESW) of solid polymer electrolytes at 70 °C. VMP3 multipotentiostat (20 V, ±400 mA, Bio-Logic Science Instruments) and ECC-Std test cells (EL-Cell GmbH, Germany) were used to carry out the electrochemical characterization. Moisture contaminations were avoided by assembling the cells inside the Ar-filled glove-box (MBraun UNILab, H_2O and O_2 content <0.1 ppm). The two-electrode cells were assembled by sandwiching copolymers between the working electrode and a lithium metal foil, which simultaneously served as the reference and the counter electrode. Separate tests were performed to determine the cathodic and anodic electrochemical stability. Carbon-coated aluminium and copper disks were used as working electrodes during anodic and cathodic scans, respectively, and a scan rate of 0.1 mV s^{-1} was applied in both cases.

3.2.9 LiFePO₄ (LFP) based cathode preparation

The LiFePO$_4$ (LFP)-based electrode was obtained in the form of a catholyte using the respective polymer electrolyte as the active binder. The aim is to provide an ionically conducting interface between the SICPE and the active material particles, to enhance the "wettability" of the active material particles through the whole electrode thickness and in the bulk of the electrode, thusdecreasing the ion diffusion resistance at the electrode/electrolyte interface.[201]

A composition of 60 wt.% of carbon coated LiFePO$_4$ 10 wt.% of C65 carbon black and 30 wt.% of the respective copolymer was used for the catholyte preparation. In details, LFP active material powder and C65 carbon black were first gently mixed in a hand mortar and, successively, added to the ca. 5 wt.% solution

of the copolymer in 1-methyl-2-pyrrolidinone (NMP) upon stirring. The stirring was continued at ambient temperature for 1 h, after which the resultant suspension was additionally homogenized using an Ultra-Turrax® mixer (IKA-Werke GmbH & Co. KG) for 10 min. The obtained dense slurry was cast onto a carbon coated aluminium current collector using a doctor-blade with a blade height of 300 μm. NMP solvent was removed by evaporation at ambient temperature for 12 h and further drying at 60 °C/1 mm Hg for 24 h in the B-585 oven (Buchi Glass Drying Oven) filled with P_2O_5. The cathode tape was further transferred under vacuum inside an argon-filled glovebox (MBRAUN MB-Labstar, H_2O and O_2 content <0.5 ppm). The same procedure was applied for all composite cathodes based on $LiFePO_4$ used in this thesis work. The obtained composite cathodes were characterized by film thickness after drying of approximately 60±3 μm, and active mass loadings of 4.17 mg cm^{-2}, 3.91 mg cm^{-2}, 3.44 mg cm^{-2}, respectively, for different samples reported in chapters 4, 5 and 6.

3.2.10 LiNiMnCoO$_2$ (NMC) based cathode preparation

LiNiMnCoO$_2$ (NMC) based cathode film was prepared following the same procedure described above for LFP catholyte, with a slight different composition, namely: 75 wt.% of LiNiMnCoO$_2$ active material, 10 wt % of C65 carbon black and 15 wt.% of copoly8 reported in chapter 4. The obtained composite cathode was characterized by film thickness after drying of 65±2 μm and active mass loading of 4.32 mg cm^{-2}.[219]

3.2.11 Laboratory-scale Li-metal cell assembly and testing

Lab-scale LFP/copolymer/Li and NMC/copoly8/Li battery prototypes assembly was performed inside the Ar-filled glovebox using the ECC-Std test cells (EL-Cell GmbH). A 100 μm thick polyethylene terephthalate (Mylar®) round spacer with a 10 mm internal diameter was laid on top of the composite cathode tape (250 μm separator was used only in chapter 6). Afterwards, a layer of copolymer electrolyte was applied manually directly on the composite cathode surface within the internal diameter of the spacer. The assembly was completed with a lithium metal disk anode.

Lab-scale LFP/copolymer/Li cells were galvanostatically cycled on a VMP3 multipotentiostat (20 V, ±400 mA, BioLogic Science Instruments) at 70 °C between

2.5 and 3.8 or 4 V vs Li$^+$/Li at different charge/discharge current regime (C/n) considering the theoretical cathode capacity of 170 mAh g^{-1} while, lab-scale NMC/copoly8/Li cells were cycled at 70 °C between 3 and 4.3 V vs Li$^+$/Li considering the theoretical cathode capacity of 185 mAh g^{-1}.

Cycling tests were also conducted at different current rates, where the rate is denoted as C/n, corresponding to a full discharge or full charge of the theoretical cathode capacity (C) in n hours (e.g. for LFP cathode: C/20 corresponds to a full discharge or full charge of the theoretical cathode capacity of 170 mAh g^{-1} in 20 hours).

Chapter 4

4 Unique carbonate-based single ion conducting block copolymers enabling high-voltage, all-solid-state lithium metal batteries

4.1 Introduction

As introduced in the previous section, among SPEs, a new class of polyelectrolytes, namely "single ion-conducting polymer electrolytes or polyelectrolytes" (SICPEs or SICPs), deserves considerable attention.[130,189,207,222–226] Apart from ionic conductivity and Li^+ transference number, other fundamental features of SICPEs include wide electrochemical stability and compatibility with active materials, such as lithium metal anode and high-voltage cathodes. Several examples of solid-state SICPE electrolytes delivering excellent results at the anode side were already reported to date;[223] however, the long-term stability with high-voltage cathodes (e.g., lithium nickel manganese cobalt oxide - NMC, and, Li-rich NMC at low Co content) without using liquid additives to enhance the performances is still challenging. A considerable amount of studies have already investigated and confirmed that the presence of ethylene oxide units tends to decrease the glass transition of SICPEs, and consequently, increase the ionic conductivity, at the expenses of restricting the electrochemical stability of such polyelectrolytes in the range of $4.0 \div 4.5$ V vs Li^+/Li.[189,201,227,228] Actually, it was already demonstrated that introducing carbonate groups in typical salt-in-polymer electrolytes improves the resistance to high oxidation voltage compared to PEO/Li salts material.[159,160,164] As an example, Meabe et al.[190] reported a polyelectrolyte based on poly(ethylene oxide carbonate) main chain,[190] which exhibited good

performances in NMC-based half cells at C/20 rate and 70 °C in the 2.8-4.2 V range. Notwithstanding, the promising cycling results in NMC-based half cells required the lithium pretreatment with a 2M solution of lithium bis(fluorosulfonyl)imide (LiFSI) in dimethoxyethane. The SICPE electrolyte's failure to form a highly conductive SEI layer under the defined cycling conditions requires pretreatment. Such limitation could be overcome by designing a SICPE macromolecular architecture that leads to the formation of stable interfaces between the polymer electrolyte and both electrodes.

In this respect, this chapter is focused on the development of novel solid-state SICPEs, namely poly[(ionic liquid)-*b*-(carbonate)] block copolymers Scheme 4.1). The addition of the polycarbonate block to poly(ionic liquid) significantly enhanced the final SICPE chemical-physical and electrochemical properties. The combination of ROP and RAFT polymerization techniques, [213,215] exploited by RAFT-agent having hydroxyl terminal group as dual initiator, allowed the realization of ring-opening polymerization (ROP) of trimethylene carbonate (TMC) monomer and reversible addition-fragmentation chain transfer (RAFT) polymerization of methacrylic monomers (Scheme 4.1). The resultant block copolymer electrolytes showed significantly improved mechanical properties compared to random copolymer based on LiMTFSI and PEGM and high oxidative stability ($\geq$4.8 V vs Li$^+$/Li at 70 °C), enhanced compatibility with composite cathodes (both NMC and LFP) as well as with lithium metal anode, high Li-ion transport enabling high power and excellent plating/stripping ability with resistance to dendrite growth.
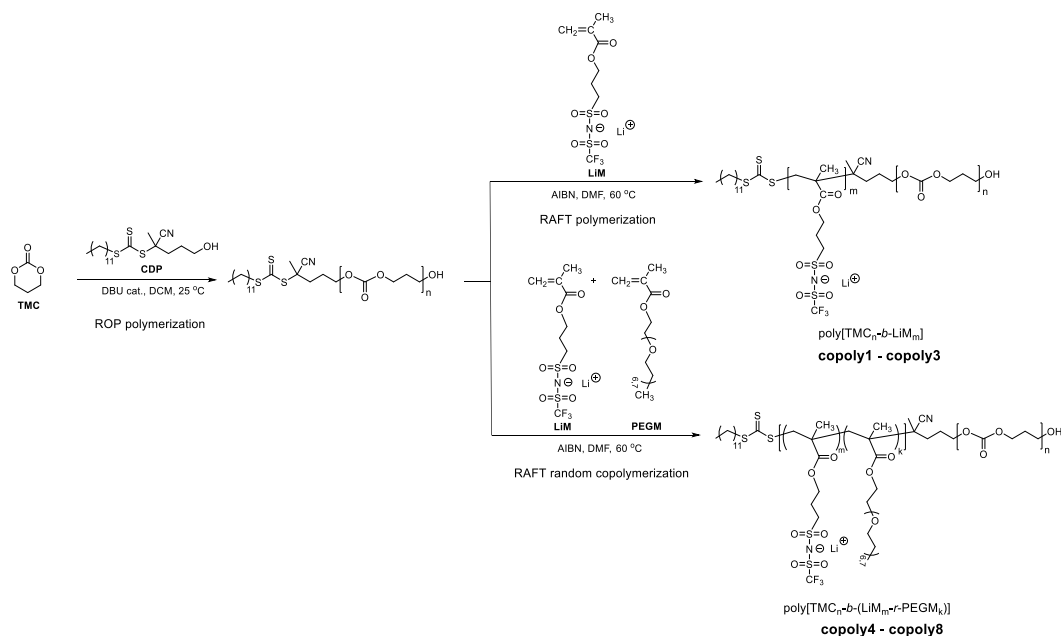
Scheme 4.1 Scheme of the synthetic route for the preparation of poly[TMC$_n$-b-LiM$_m$] and poly[TMC$_n$-b-(LiM$_m$-r-PEGM$_k$)] block copolymers via the subsequent combination of ROP and RAFT polymerizations.

4.2 Results and discussion

4.2.1 Ring opening polymerization (ROP) of trimethylene carbonate (TMC) and synthesis of lithium 1-[3-(methacryloyloxy)propylsulfonyl]-1-(trifluoromethanesulfonyl)imide (LiM)

The ionic monomer was synthesized following the procedure published previously.[201] The resultant crystalline powder was dried at 25 °C/1 mm Hg overnight and stored under an inert atmosphere in an argon-filled glove box (MBRAUN MB-Labstar, H$_2$O and O$_2$ content < 0.5 ppm). Spectroscopic data of the target compound agree with those reported in the literature.[201] As previously stated in Chapter 3, ROP stands out as one of the leading approaches among living polymerization techniques for accessing polycarbonates with desired molar mass and well-defined end groups.[212] Thus, the present work started with a thorough

investigation of TMC polymerization using CDP as the initiator and DBU as the catalyst (Scheme 4.1, Table 4.1). At first, the targeted degree of polymerization was fixed to 200 (see Equation 5), while the initiator to catalyst (CDP:DBU) molar ratio was varied from 0.05:1 to 1:1 (Table 4.1, samples ROP1 to ROP6). The maximum molar mass for poly(TMC) was found to be 16400 g mol^{-1}, observed at 0.20:1 CDP:DBU molar ratio (Table 4.1, ROP3). Even in the best run, the M_n determined experimentally was lower than the targeted one (20420 g mol^{-1}). Except for 0.05:1, all other CDP:DBU ratios could perform ROP of TMC with a sufficiently low polydispersity index (M_w/M_n) varying from 1.17 to 1.40 (Table 4.1, ROP1 – ROP6). Further on, different degrees of TMC polymerization were attempted at a fixed CDP:DBU ratio equal to 0.2:1.0 (Table 4.1, ROP7 – ROP10 and ROP3). All the experiments were conducted to high monomer conversion (85-90%) and/or reaction completion. The experimental vs targeted M_n dependence was found to be close to the linear theoretical one only until the degree of polymerization reached 150. In contrast, for M_n above 15000 g mol^{-1} the experimental values significantly deviated from the straight line, as further evidence of extreme character polymerization. The M_w/M_n values gradually decreased with increasing molecular weight up to M_n = 20000 g mol^{-1}, which indicates an absence of molecular scrambling.[213] It should be mentioned that, for all obtained poly(TMC) samples, the GPC-SEC chromatograms from a refractive index (RI) detector showed a small shoulder in the high molar mass region, likely accounting for the loss of polymerization control due to the high activity of DBU catalyst.[213]

Table 4.1 Ring opening polymerization (ROP) of trymethylene carbonate (TMC) using CDP RAFT-agent and DBU catalyst ([TMC] = 2M, temperature - 22 °C, duration - 40 h).

Sample	[TMC] [Initiator] molar ratio	[Initiator] [Catalyst] molar ratio	Solvent	M_n (target) (g mol^{-1})	M_n (SEC) (g mol^{-1}) [a]	M_w/M_n SEC [a]	Yield (%)
ROP1	200:1	0.05:1	DCM	20420	11300	1.68	84
ROP2	200:1	0.10:1	DCM	20420	13500	1.39	90
ROP3	200:1	0.20:1	DCM	20420	16400	1.27	82
ROP4	200:1	0.25:1	DCM	20420	15300	1.40	84
ROP5	200:1	0.30:1	DCM	20420	12300	1.29	90
ROP6	200:1	1:1	DCM	20420	9600	1.17	80
ROP7	50:1	0.20:1	DCM	5105	8000	1.34	97
ROP 8	100:1	0.20:1	DCM	10210	12200	1.32	78
ROP9	150:1	0.20:1	DCM	15315	16000	1.31	82
ROP10	300:1	0.20:1	DCM	30630	14300	1.40	84
ROP11	150:1	0.20:1	THF	15315	10200	1.23	50
ROP12	150:1	0.20:1	Toluene	15315	17900	1.55	15

[a] By GPC in THF at 40°C with PMMA standards calibration.

The influence of the solvent on ROP of TMC was evaluated by synthesizing poly(TMC) in dichloromethane, THF and toluene (Table 4.1, ROP9, ROP11, andROP12, respectively). While in DCM and THF the reaction occurred in solution, the nascent poly(TMC) started to precipitate in toluene after 5 hours of reaction, thus reducing the isolated yield to 15% (Table 4.1, ROP12). Comparing ROP in THF and DCM, it was concluded that the experimental mass of poly(TMC)

obtained in DCM was closer to the targeted one ($M_{n\,DCM}$ = 16000, $M_{n\,THF}$ = 10200, $M_{n\,target}$ = 15315 g mol^{-1}), while the yield of the reaction was higher (50 and 82%, respectively).

The following reaction parameters were found to be optimal to synthesize poly(TMC) with the highest molecular weight and low polydispersity: 22 °C, 40 h, 0.2:1.0, and 0.25 g ml^{-1}, in temperature, duration of reaction, CDP:DBU molar ratio and TMC concentration, respectively, and DCM as a solvent (Table 4.1, ROP9). Once the optimal conditions were established, the synthesis of poly(TMC) was scaled up, and the macro-chain transfer agent was obtained with a molecular weight of 18300 g mol^{-1} (GPC in THF) or 20100 g mol^{-1} (GPC in 0.1M LiTFSI in DMF). The poly(TMC) structure was confirmed by ^{1}H, ^{13}C NMR and IR spectra.[219] H^{1} NMR (Figure 4.1a) showed the desired end-groups and no indication of competitive side reactions. 4-cyano-4-[(dodecylsulfanylthiocarbonyl)sulfanyl]pentan carbonate was clearly observed at the end-chain position, while the peaks related to the main chain were slightly shifted upfield relatively to the TMC monomer. Complete assignments for H^{1} NMR are the following: 4.23 ppm (TMC repeating unit: C$\underline{H}_2$CH$_2$C$\underline{H}_2$), 2.04 ppm (TMC repeating unit: CH$_2$C$\underline{H}_2$CH$_2$), 3.7 ppm (terminal TMC unit: C$\underline{H}_2$OH) and 3.31, 1.92, 1.87, 1.64, 1.38, 1.25, 0.87 ppm (CDP moiety). The molar mass of poly(TMC) determined by NMR ($M_{n\,NMR}$ = 16999 g mol^{-1}) was in line with GPC observations.
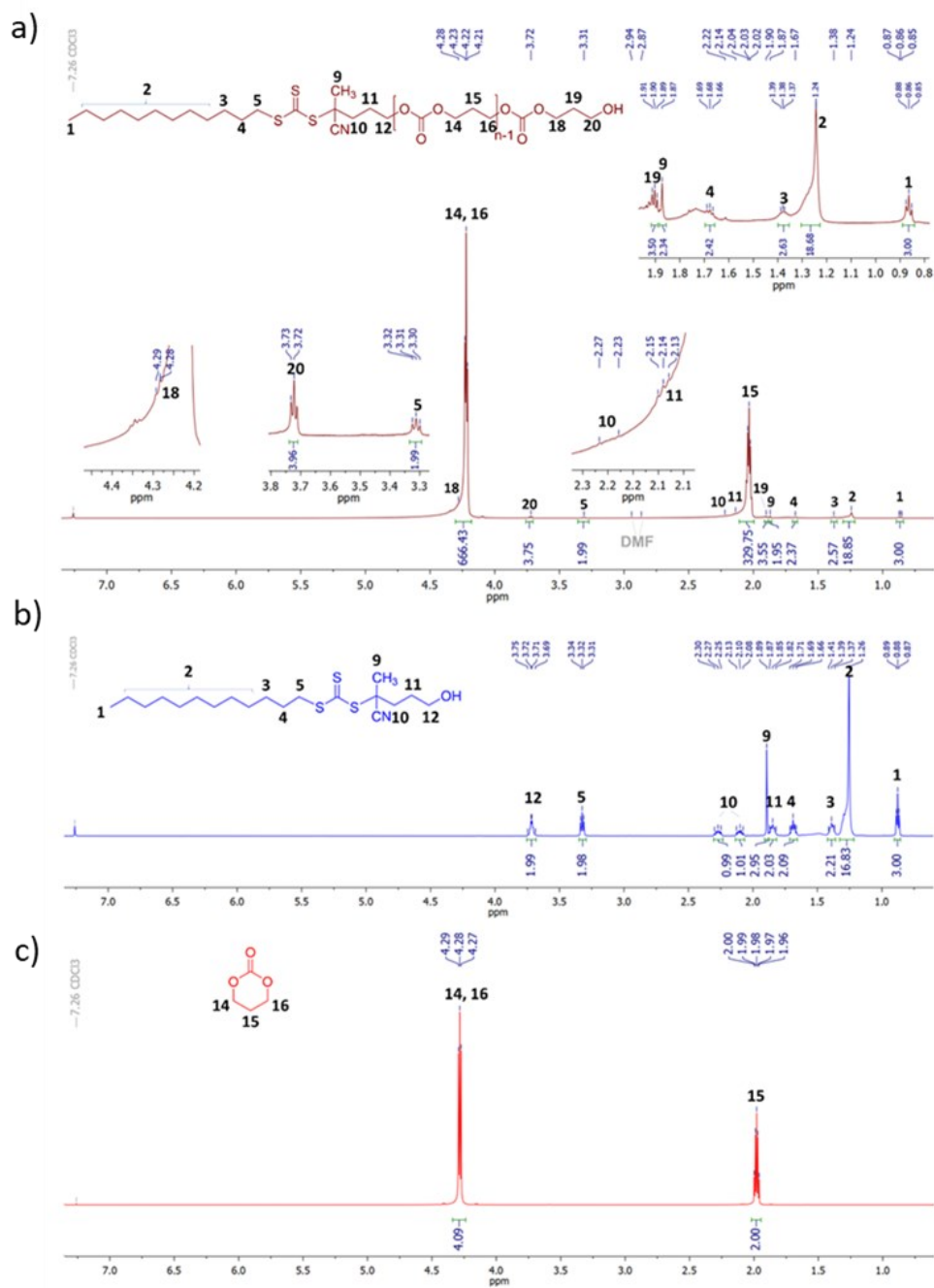
Figure 4.1 ¹H NMR of poly(TMC) (ROP9) (a), CDP RAFT agent (b) and TMC monomer (c).

4.2.2 RAFT synthesis of poly[TMC$_n$-b-LiM$_m$] and poly[TMC$_n$-b-(LiM$_m$-r-PEGM$_k$)] block copolymers

The investigation of block copolymers synthesis started with the RAFT polymerization of LiM monomer using poly(TMC) precursor as macro-RAFT transfer agent and AIBN as initiator. DMF was chosen as a solvent due to its ability to dissolve both poly(TMC) and LiM, as well as because its utilization in (co)polymerization of LiM monomer guarantees high yields and high molecular weights of the resultant polyelectrolytes.[189,201,229–231] Using the optimal reaction conditions determined previously for RAFT polymerization of LiM,[201] namely ([AIBN]:[macro-RAFT]=1:5 by mol, [DMF]:[poly(TMC)+LiM]=3:1 by weight), a set of poly[TMC$_n$-b-LiM$_m$] block copolymers, (Table 4.2, copoly 1-3) targeting different degrees of polymerization, was successfully prepared.

Table 4.2 Selected properties of poly(TMC) macroRAFT agent and poly[TMC$_n$-b-LiM$_m$] copolymers obtained by RAFT polymerization.

Polymer	poly(TMC) (A-block)	poly[TMC$_n$-b-LiM$_m$] (A-b-B copolymer)							
		B-block	A-b-B copolymer						
	M_n (SEC)^a (g mol^{-1})	M_n (target)	M_n (SEC) (g mol^{-1})	M_w/M_n (SEC)	σ (S cm^{-1})		T_{g1} (°C)^c	T_{g2} (°C)^c	T_{onset} (°C)^d
					25 °C	70 °C			
poly(TMC)	-	-	-	-	-	-	-15	-	175
copoly1	20100	5000	21100	1.31	9.5 x 10^{-10}	1.3 x 10^{-7}	-14	-	190
copoly2		9000	23050	1.32	2.2 x 10^{-11}	2.0 x 10^{-8}	-14	140	190
copoly3		18000	24700	1.36	8.4 x 10^{-11}	5.6 x 10^{-8}	-14	140	205

^{a} By GPC in 0.1 M solution of LiTFSI in DMF at 50 °C, Mw/Mn = 1.29 (Mn= 18400 g mol-1, Mw/Mn = 1.19 by GPC in THF at 40 °C). ^{b} Molar ratio calculated considering the experimentally determined molar masses. ^{c} By DSC. ^{d} By TGA in air.

The obtained ionic block copolymers were firm and densely packed yellowish rubber-like materials. The GPC-SEC analysis of poly[TMC$_n$-b-LiM$_m$] block copolymers in 0.1M LiTFSI solution in DMF revealed the increase of M_n values in comparison with the initial poly(TMC), while the M_w/M_n ratios, ranging between

1.32 and 1.36, were found to be satisfactory (Table 4.2, copoly 1-3). SEC traces show the shifting of molecular weights to a higher region under preservation of the distribution. The GPC-SEC chromatograms of all investigated block polymers exhibit single symmetrical peaks. Despite a relatively good yield of copolymers (67-69%), the determined M_n values were less than the theoretical ones (Table 4.2, copoly 1-3). This result correlates with the previously observed trend of underestimating molecular weights for LiM based copolymers via the GPC method.[201,202] One should note that molecular weights were calculated via conventional calibration and referred to PMMA standards. Indeed, the high electrostatic repulsion between monomer units in the formed polymer can slow down the homopolymerization of LiM. The long duration of the reaction (48 h) and polymer yields below 85-90% likely account for the above mentioned second explanation.

The structure and purity of poly[TMC$_n$-b-LiM$_m$] block copolymers were supported by ^{1}H, ^{13}C, ^{7}Li NMR and IR spectroscopies.[219] As demonstrated previously,[201,202,230] the highest ionic conductivity for linear methacrylate-based SICs could be achieved by copolymerizing lithium ion containing monomers with poly(ethylene glycol) methyl ether methacrylate (PEGM). The presence of oxyethylene fragments in the side chain of poly(PEGM), by analogy to PEO,[232] significantly improves the solubility of ionic species, thus facilitating their dissociation and, correspondingly, enhancing the ionic conductivity of the resulting copolymers. The study was further focused on the synthesis of poly[TMC$_n$-b-(LiM$_m$-r-PEGM$_k$)] using the same conditions of poly[TMC$_n$-b-LiM$_m$] synthesis (see Scheme 4.1). Random RAFT copolymerization was used to prepare a set of block copolymers with the fixed length of poly(TMC) block and variable size of poly(LiM$_m$-r-PEGM$_k$) extension at different LiM:PEGM molar ratios (Table 4.3, copoly4-copoly8). The resulting poly[TMC$_n$-b-(LiM$_m$-r-PEGM$_k$)] ionic block copolymers are yellow rubber-like materials (Figure 4.2a), with bit softer consistency than poly[TMC$_n$-b-LiM$_m$] and harder than poly(LiM$_m$-r-PEGM$_k$), as shown in Figure 4.2b.
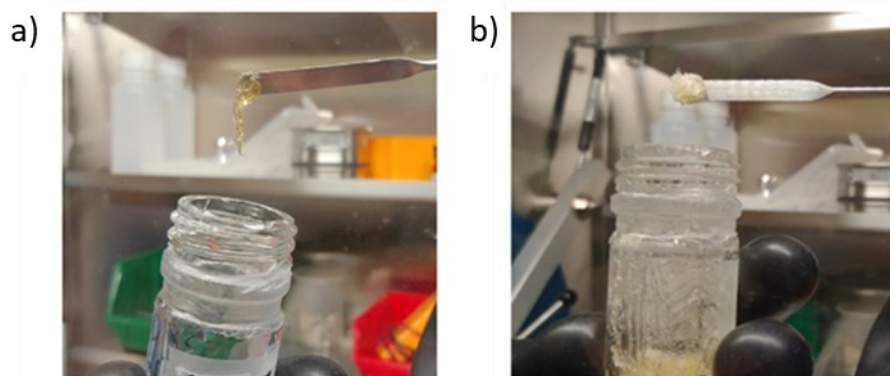
Figure 4.2 Digital photographs showing the appearance of poly[LiM$_m$-r-PEGM$_k$] (a) and poly[TMC$_n$-b-(LiM$_m$-r-PEGM$_k$)] copoly8 (b) inside argon filled glove box.

GPC-SEC traces of poly[TMC$_n$-b-(LiM$_m$-r-PEGM$_k$)] exhibit single symmetrical peaks and clearly demonstrate the shift of molecular weights to a higher region.[219] As in the case of poly[TMC$_n$-b-LiM$_m$], the M_n values determined for poly[TMC$_n$-b-(LiM$_m$-r-PEGM$_k$)] were lower than the theoretical ones (Table 4.3), while the M_w/M_n ratios remained satisfactorily low in the range of 1.22 – 1.39, demonstrating the control over polymerization (Table 4.3, copoly4-copoly8). The LiM:PEGM molar ratios determined by NMR were higher in comparison with the theoretical ones, showing higher reactivity of PEGM monomer (Table 4.3).

Table 4.3 Selected properties of poly[TMCn-b-(LiMm-r-PEGMk)] copolymers obtained by random RAFT copolymerization also compared with different polymeric systems.

Polymer	poly(TMC) (A-block)		poly[TMCn-*b*-(LiMm-*r*-PEGMk)] (A-b-B copolymer)										
			B-block		A-b-B copolymer							
	M_n (SEC)^a (g mol^{-1})	M_w/M_n (SEC)^a	LiM/PEGM mol. ratio (target)	M_n (target)	LiM/PEGM mol. ratio (NMR)^b	M_n (SEC)^c (g mol^{-1})	M_w/M_n (SEC)^c	σ (S cm^{-1}) 25°C	σ (S cm^{-1}) 70°C	T_{g1} (°C)^d	T_{g2} (°C)^d	T_{onset} (°C)^e
copoly 4			01:02	20000	1 : 3.3	29730	1.24	$1.4×10^{-7}$	$3.6×10^{-6}$	-35	-16	-
copoly 5			01:02	30000	1 : 2.9	34120	1.33	$1.0×10^{-7}$	$2.8×10^{-6}$	-36	-16	-
copoly 6	20100^f	1.29^f	01:05	15000	1 : 9.0	25450	1.26	$1.1×10^{-7}$	$1.9×10^{-6}$	-50	-16	-
copoly 7			01:05	20000	1 : 8.3	30480	1.22	$2.9×10^{-7}$	$3.7×10^{-6}$	-49	-16	165
copoly 8			01:05	30000	1 : 8.1	34600	1.39	$1.1×10^{-7}$	$2.9×10^{-6}$	-51	-16	155
poly(PEGM)^g	23600	1.16	-	-	-	-	-	-	-	-62	-	160
poly(LiM)^g	52700	1.20	-	-	-	-	-	$1.1×10^{-12}$	-	105	-	250
poly(LiMm-*r*-PEGMk)	30600	1.14	01:05	-	1 : 6.8	-	-	$2.3×10^{-7}$	-	-31	-	170

^{a}By GPC in 0.1M LiTFSI in DMF at 50 °C. ^{b}By NMR in DMSO-d$_6$ at 25 °C. ^{c}By GPC in 0.1M LiTFSI in DMF at 50 °C. ^{d}By DSC. ^{e}By TGA in air. $^f M_n$= 18400 g mol-1 and M_w/M_n = 1.19 by GPC in THF at 40 °C. ^{g}For comparison from ref. [201]

The structure and purity of poly[TMCn-*b*-(LiMm-*r*-PEGMk)] were confirmed by ^{1}H, ^{13}C, ^{19}F and ^{7}Li NMR, as well as IR spectroscopy and elemental analysis[219] (^{1}H NMR shown in Figure 4.3). Apart from signals attributed to poly(TMC) block, end-groups from CDP RAFT agent and poly(LiM), the ^{1}H NMR of poly[TMCn-*b*-(LiMm-*r*-PEGMk)] contains signals at 3.52 and 3.24 ppm, assigned to OCH$_2$CH$_2$O and CH$_3$O fragments of PEGM, respectively.
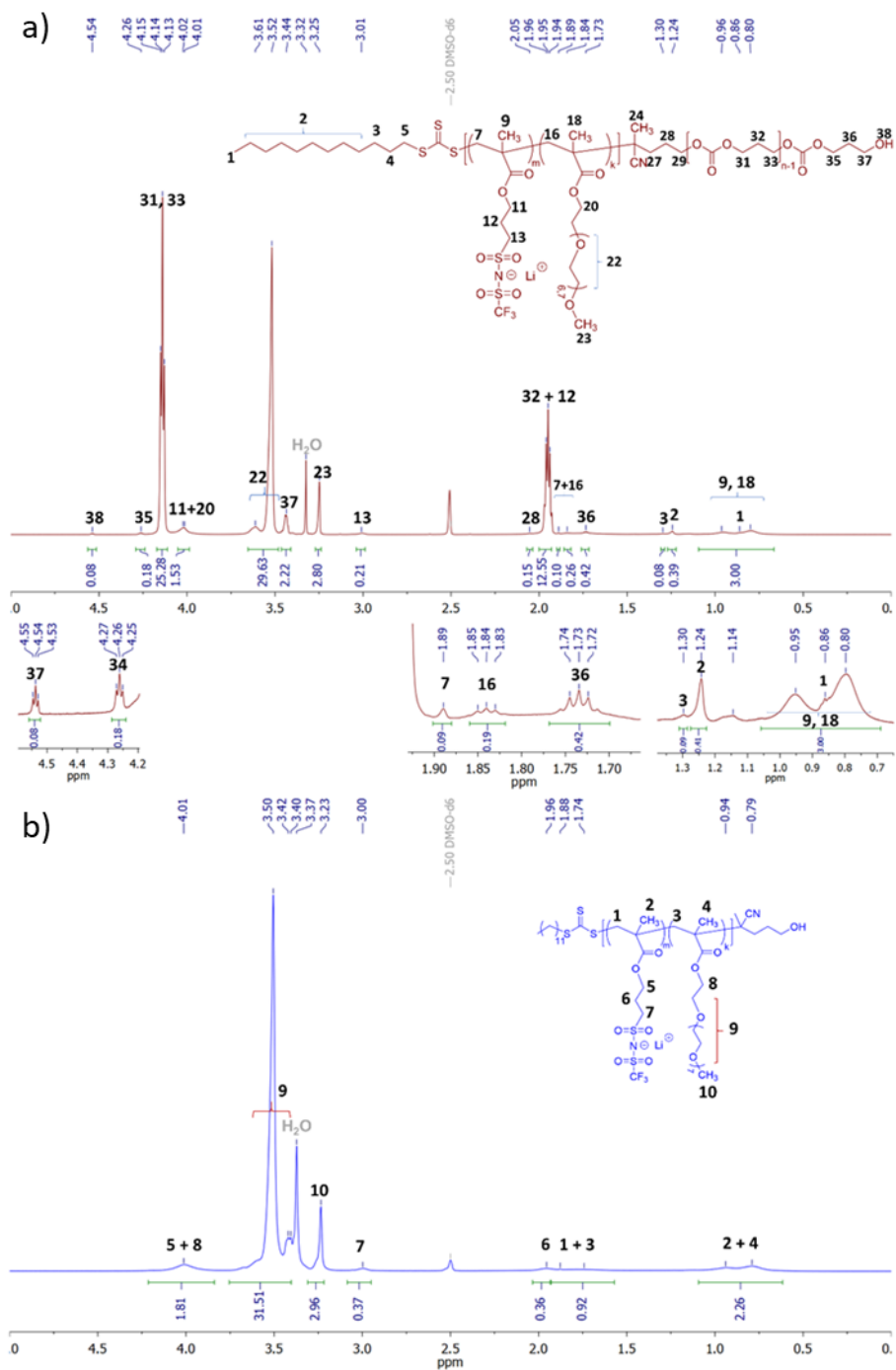
Figure 4.3 ^{1}H NMR of poly[TMC$_n$-b-(LiM$_m$-r-PEGM$_k$)] (copoly8) (a) and poly(LiM$_m$-r-PEGM$_k$) (b) (25 °C, DMSO-d6).

4.2.3 Chemical-physical and electrochemical characterization

Thermal properties

The determination of the temperature operation limits for ionic block copolymers was assessed by thermo-gravimetric analysis. Indeed, as detailed in the introductory section, the electrolyte thermal stability is fundamental to guarantee the safety of practical LIBs.[12] According to TGA (Figure 4.4a), the onset mass loss temperature (T_{onset}) for poly(TMC) was found to be 175 °C, while it exceeded 250 °C for poly(LiM).[201] The T_{onset} values of poly[TMC$_n$-b-LiM$_m$] decreased accordingly to the following order with respect to the ionic part content (Table 4.2):

$$T_{onset} \text{ in } °C: copoly3\ (205) > copoly2\ (190) \approx copoly1\ (190)$$

The thermal stability of poly[TMC$_n$-b-(LiM$_m$-r-PEGM$_k$)] block copolymers was mainly controlled by the degradation of TMC and PEGM parts, characterized by the lowest thermal stability limit (T_{onset} = 175 and 160 °C, respectively). As a result, all poly[TMC$_n$-b-(LiM$_m$-r-PEGM$_k$)] block copolymers, independently of their composition, possessed similar onset loss temperatures in the range of ~155-165 °C (Figure 4.4a and Table 4.3). Overall, these values are attractive for application in practical Li-based batteries accounting for remarkably safer characteristics compared to conventional liquid electrolyte based devices, which become thermally unstable already above 80 °C.[233]

The glass transition temperatures of copolymers were determined by DSC (Figure 4.4b). The starting block poly(TMC) macroRAFT agent with M_n = 20100 g mol^{-1} showed a T_g of −15 °C (Figure 4.4b). The copoly 1, having a PC:LiM units ratio equal to 197:3 (measured by GPC), is characterized by a single T_g of −14 °C. A second T_{g2} at around 140 °C is present in copoly2, which corresponds to the transition temperature of neat poly(LiM) observed at 105 °C (Figure 4.4b and Table 4.3).[201]
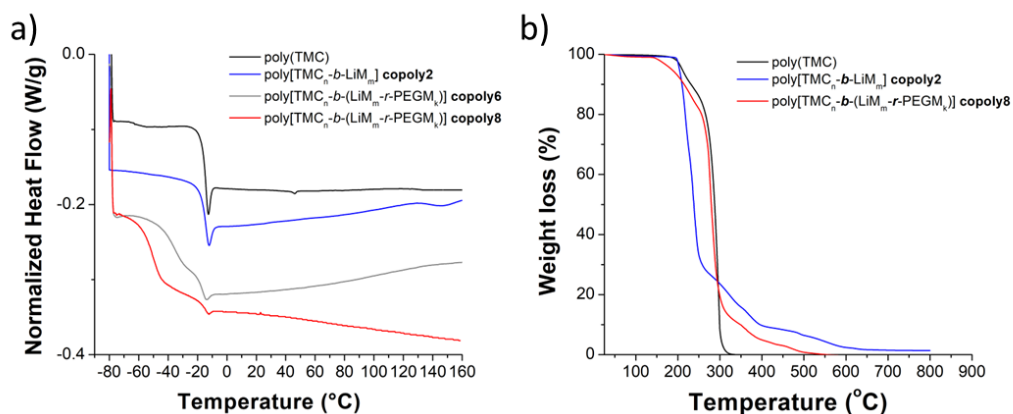
Figure 4.4 DSC (a) and TGA (b) traces of poly(TMC), copoly2, copoly6 and copoly8.

The RAFT random copolymerization of PEGM and LiM in different ratios led to the significant decrease in T_g of the obtained poly[TMC$_n$-b-(LiM$_m$-r-PEGM$_k$)] block copolymers (Figure 4.4b and Table 4.3). It is worth noticing the presence of the two distinct glass transition temperatures for the copoly4 - copoly8 samples (Table 4.3). The poly(TMC) block related T_{g2}, was constantly observed at –16 °C, while the T_{g1} values ranged from –36 to –51 °C in the following order:

T_{g1} in °C: copoly8 (-51) ≤ copoly6 (-50) ≤ copoly7 (-49) << copoly5 (-36) ≤

copoly4 (-35)

As for the above detailed data and considering the low glass transition temperature of the neat poly(PEGM) (–62 °C)[201], it can be assumed that the T_{g1} of poly[TMC$_n$-b-(LiM$_m$-r-PEGM$_k$)] block copolymers is governed mainly by the PEGM:LiM molar ratio and is practically independent on the molar mass of copolymer (Table 4.3).

Ionic conductivity

Ionic conductivity (σ) values of polyelectrolytes as a function of the temperature were recorded by electrochemical impedance spectroscopy (EIS) and applying Equation 9 (Table 4.2 and Table 4.3). Before EIS measurements, samples

were heated at 60 °C (1h) and, subsequently, equilibrated at 20 °C for 4h to ensure optimal interfacial contact with the electrodes. First, ionic conductivities were determined for poly[TMCn-b-LiMm] block copolymers (Table 4.2). At 25 °C, σ values increased from 8.4×10^{-11} to 9.5×10^{-10} S cm^{-1} depending on the size of LiM block, arranged as follows in descending order:

σ in S cm^{-1}: copoly1 (9.5×10^{-10}) >> copoly2 (2.2×10^{-11}) > copoly3 (8.4×10^{-11})

Thus, for higher block copolymer M_n and LiM block size, the ionic conductivity of polyelectrolyte decreases. At 70 °C, σ values largely increased up to 2×10^{-7} S cm^{-1}, while maintaining the same trend as above. The rather low ionic conductivity values are likely ascribed to the limited chain mobility of the ionic block having high glass transition temperatures (T_{g1} = –16, T_{g2} = 140 °C).

Representative plots of ionic conductivity vs temperature for poly[TMC$_n$-*b*-(LiM$_m$-*r*-PEGM$_k$)] block copolymers are shown in Figure 4.5. The random copolymerization of LiM with PEGM during the growth of the second block allowed for significant ionic conductivity enhancement compared to the poly[TMC$_n$-*b*-LiM$_m$] polyelectrolyte samples. Indeed, all poly[TMC$_n$-*b*-(LiM$_m$-*r*-PEGM$_k$)] block copolymers provided σ values exceeding 10^{-7} S cm^{-1} already at 25 °C. Ionic conductivity values were found to be similar, in the range of 1.0 to 2.9×10^{-7} S cm^{-1}:

σ in S cm^{-1}: copoly7 (2.9×10^{-7}) > copoly4 (1.4×10^{-7}) > copoly6 (1.1×10^{-7}) ≈

copoly8 (1.1×10^{-7}) ≥ copoly5 (1.0×10^{-7})
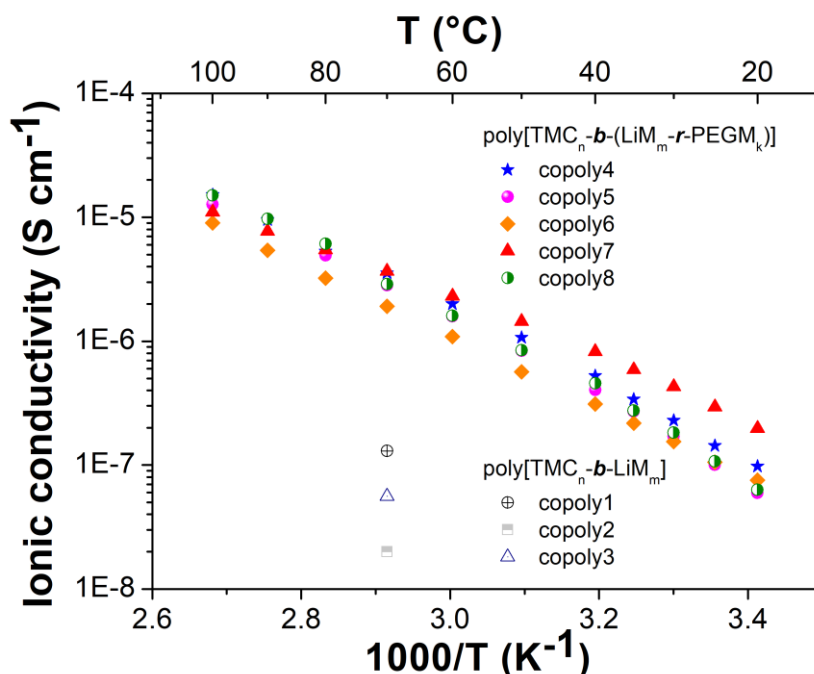
Figure 4.5 Arrhenius plot of ionic conductivity vs. inverse temperature determined by EIS in the range 20−100 °C for ionic block copolymers.

For all copolymers, ionic conductivity increased by increasing the temperature to about 10^{-6} S cm^{-1} already at 60 °C. Slight deviations from the linear Arrhenius behaviour were observed (Figure 4.5), particularly for copoly7, indicating that diffusion of lithium ions occurs through isolated hopping on the pendant sulfonamide groups and results from the local segmental motion of the coordination sites in the polymer main chain. At 70 °C, the ionic conductivity values of the poly[TMC$_n$-b-(LiM$_m$-r-PEGM$_k$)] block copolymers were found to be close in the 1.9 to 3.7×10^{-6} S cm^{-1} range (Table 4.3). Thus, the optimal copolymer composition choice for further electrochemical tests was made based on mechanical properties. As for its efficient film forming ability, copoly8 was selected as the representative sample for scale up and further studies.

Morphology

Ionic (multi)block copolymers show the spontaneous formation of ordered micro- and nanosized structures, which contribute to enhancing both their ionic conductivity and mechanical properties.[234–239] In poly[TMCn-b-(LiMm-r-PEGMk)] block copolymers (Table 4.3, copoly4-copoly8), two distinct phase transition temperatures were observed (Fig. 3b); thus, the morphology of the representative copoly8 was investigated by atomic force microscopy (AFM) technique. AFM images of phase shift revealed a native nanophase separation at the surface of the drop cast film (Figure 4.6). Quasi-hexagonally-packed cylinders arrangement perpendicular to the surface can be clearly observed. The phase shift can be qualitatively linked to the stiffness of the surface, where the higher surface stiffness creates a higher repulsive contact force; this, in turn, increases the resonance frequency/diminishes the phase shift. A nanophase attribution can be made on the cylinders, having 22.5 ± 2.5 nm diameter and representing the poly(TMC) phase, regularly distributed inside the poly(LiMm-r-PEGMk) matrix with a 35.7 ± 4.5 nm pitch. The observed copoly8 strong nanophase separation can explain the same ionic conductivity level of random poly(LiMm-r-PEGMk) despite having less free ion-conducting species (Table 4.3).
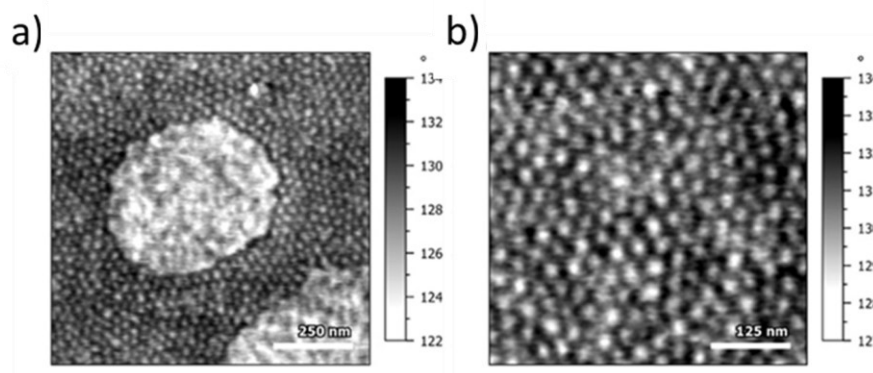
Figure 4.6 AFM images of poly[TMC$_n$-b-(LiM$_m$-r-PEGM$_k$)] copoly8 film at different resolutions (a, b).

Rheology

The viscoelastic properties of the newly synthesized poly[TMC$_n$-b-(LiM$_m$-r-PEGM$_k$)] (namely, copoly8) and previously reported poly(LiM$_m$-*r*-PEGM$_k$)[201] were compared by carrying out rheological measurements in a small-amplitude oscillatory flow mode. The temperature dependence of complex viscosity at a constant frequency of 1 Hz is shown in **Errore. L'origine riferimento non è stata trovata.**a. Both copolymers demonstrated a neat decrease in their complex viscosity with an increase in temperature from 25 to 70 °C.
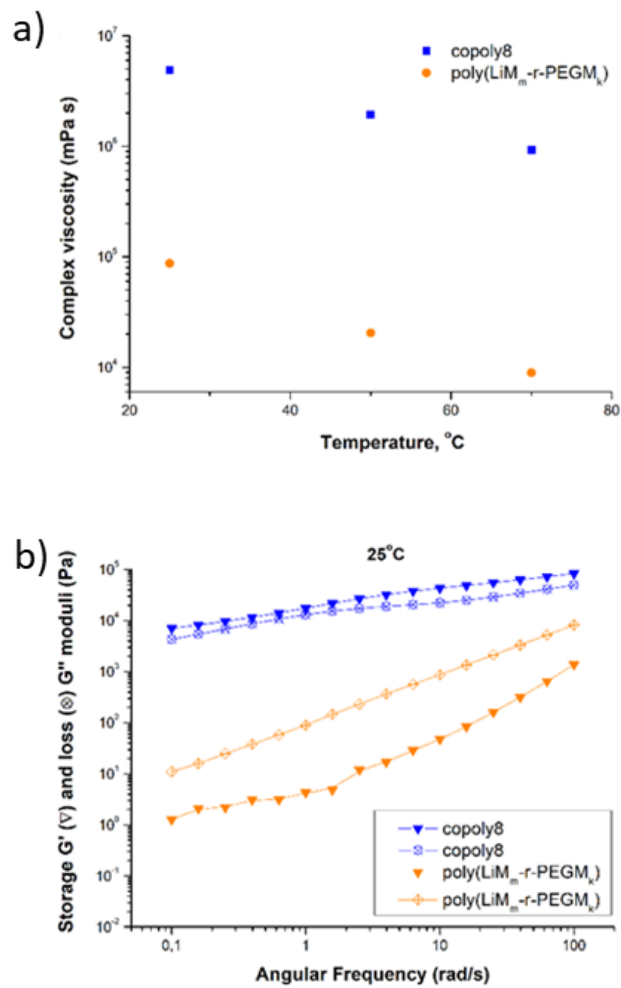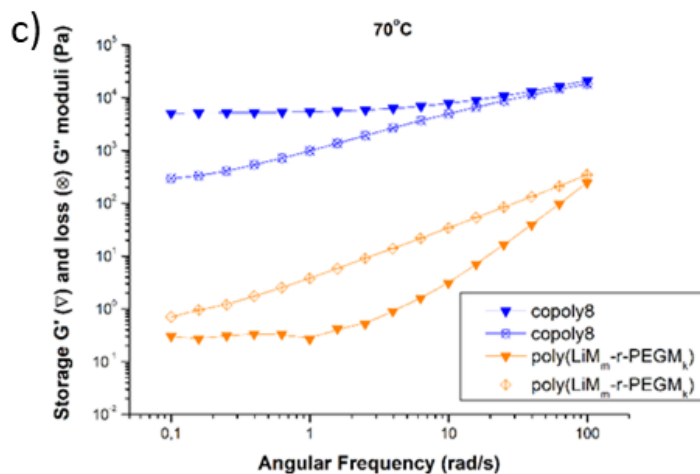
Figure 4.7 Temperature dependence of the complex viscosity (a) and frequency dependence of the storage modulus G' (full symbols) and the loss modulus G" (open symbols) obtained at 25 °C (b) and 70 °C (c) for poly[TMC$_n$-b-(LiM$_m$-r-PEGM$_k$)] copoly8 and poly(LiM$_m$-r-PEGM$_k$).

However, copoly8 exhibited a much higher complex viscosity compared to poly(LiM$_m$-r-PEGM$_k$) in the whole range of testing temperatures. The storage (G') and loss (G") moduli frequency dependence was also investigated (**Errore. L'origine riferimento non è stata trovata.** b,c).

While poly(LiM$_m$-r-PEGM$_k$) showed higher liquid-like character (G" > G'), the poly[TMC$_n$-b-(LiM$_m$-r-PEGM$_k$)] demonstrated enhanced solid-like character (G' > G") at both 25 and 70 °C. In addition, the absolute values of G' in the case of copoly8 were several orders of magnitude higher than those of poly(LiM$_m$-r-PEGM$_k$) under the same measurement conditions. These outcomes are relevant considering that the increase of solid polymer electrolyte modulus is reported to suppress/limit lithium dendrite's formation and growth.[240,241] As the compared copolymers are both linear and of similar molecular weight (Table 4.3), the observed change in viscoelastic properties can only be attributed to the presence of the poly(TMC) block in copoly8. The stiffer poly(TMC) block improves the

viscoelastic properties of poly[TMC_n-b-(LiM_m-r-$PEGM_k$)] copolymer in comparison with poly(LiM_m-*r*-$PEGM_k$).

Electrochemical stability

The electrochemical stability window (ESW) of the representative copoly8 sample was investigated by separate cathodic/anodic cyclic voltammetric (CV) scans at 70 °C (Figure 4.8). A slow scan rate (0.1 mV s^{-1}) allowed faint reduction process detection, which correlated with a small current flow above 1 V vs Li$^+$/Li. In contrast, the peak at about 1.5 V was likely ascribed to the decomposition of some electrolyte components, thus forming a passivating layer towards the lithium metal electrode and reducing some traces of side products from synthesis. Well-defined and highly reversible lithium plating/stripping processes are clearly detectable, as for the highly reversible couple of reduction/oxidation peaks between −0.5 and 0.5 V vs Li$^+$/Li, which confirms the efficient transfer of lithium ions through the polymer network and at the polymer/electrode interface. In the following anodic scan towards higher potential values, the possible oxidation of the electrolyte was ruled out, as for the absence of any detrimental oxidative processes below 4.2 V vs Li$^+$/Li. The oxidation peak starting at above 4.2 V and closing at about 5 V vs Li$^+$/Li in the first anodic scan was likely associated with the partial decomposition of ethylene oxide containing moieties in the polymer electrolyte. During the successive cycles, the intensity of the peaks largely decreased, which makes, making it difficult to identify any appreciable oxidative currents up to 5.5 V vs Li$^+$/Li. In general, the anodic decomposition of an electrolyte is mainly associated with the oxidation of anions[130], but in the single-ion conducting polymer electrolyte under study, anions are chemically bonded to the polymer network. [130]Strongly anchored perfluorinated sulfonimide anions, covalently bonded to the polymer network, support this assumption; they can be oxidized only at the electrolyte/electrode interface, accounting for the wide ESW (up to 5.5 V vs Li$^+$/Li at 70 °C). The obtained ESW represents an excellent result for a single-ion polymer electrolyte, particularly at high temperatures, where side reactions are more prone to occur.[242] It makes copoly8 one of the polyelectrolytes with the highest electrochemical stability amongst the literature reports[223,243], and guarantees its safe, practical use with high voltage cathodes.[242]
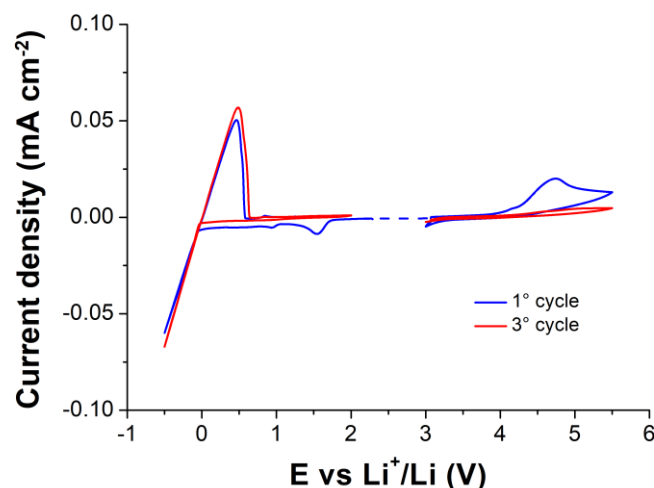
Figure 4.8 Electrochemical stability window for poly[TMC$_n$-b-(LiM$_m$-r-PEGM$_k$)] copoly8 obtained by CV at 70 °C (stainless steel as working electrode and Li foil as counter and reference electrodes, scan rate 0.1 mV s^{-1}).

Lithium-ion transference number and compatibility with lithium metal electrode

The stability/compatibility at the interface with the lithium metal electrode was confirmed by constant current (galvanostatic) reversible plating/stripping tests performed at 70 °C and increasingly higher current density values ranging from 0.025 and 0.5 mA cm^{-2} (30 min per step, see Figure 4.9 a,b). The study of the novel single-ion conducting polymer electrolyte demonstrated excellent continuous reversible cycling, without any detectable short circuit issues, even at a high current of 0.5 mA cm^{-2}. A prolonged plating/stripping test was performed at a fixed current density regime of 0.1 mA cm^{-2} for 100 h, followed by an additional 100 h doubling the current to 0.2 mA cm^{-2}. The test did not evidence a significant overpotential increase over time with respect to the initial value or any abrupt or unexpected current spikes/drifts, which can be related to irregular dendrite growth. A deep understanding of the interfacial properties between the lithium metal and the polymer electrolyte is fundamental to guaranteeing lithium metal based cell operation. For this purpose, symmetrical Li/copoly8/Li cells were assembled, and the electrolyte/Li metal electrode interfacial resistance as a function of the storage time was monitored at 70 °C. Remarkably stable interfacial resistance was obtained

after few days, revealing the interfacial compatibility between the lithium metal electrode and the single-ion conducting polymer electrolyte under study.

Furthermore, the promising prospects of the newly developed single-ion conducting polymer electrolyte were corroborated by testing copoly8 for its lithium-ion transference number (t_{Li}^+), determined by the methods of Evans/Vincent/Bruce[220] and Abraham et al.[221] (Equation 3 and Equation 4 respectively in Chapter 3). The resulting values from EIS experiments of a Li/copoly 8/Li cell at 70 °C revealed that cell impedance did not change significantly during the experiment, and the limited initial resistance value of 670 Ω only decreased to 509 Ω, thus proving that a stable interfacial layer was readily formed at the interface with the lithium metal electrode (Figure 4.9d).

Concurrently, the plot of the current response to the applied bias as a function of time resulted in a drop of less than one order of magnitude (from 7.66 to 7.08 μA, Figure 4.9c) before the steady-state was reached. It resulted in a calculated t_{Li}^+ value of 0.91 (or 0.90 considering the changes in the bulk resistance and applying Equation 4). It is worth noticing that both t_{Li}^+ values are noticeably close to unity and significantly higher compared to standard liquid electrolyte containing salts, or RTIL-based electrolytes, or cationic PILs/Li salts and/or salt in polymers (e.g., PEO/Li) and/or composite electrolytes reported previously.[244,157] The deviation of t_{Li}^+ value from unity can be attributed to the non-zero mobility of anchored anions, chiefly due to: the presence of flexible, long spacer between anchored anions and the main chain, and the overall inherent motion of polyanionic block since the test was conducted at temperature far above T_g value. Overall, t_{Li}^+ values for copoly8 are high enough to allow homogeneous lithium plating and stripping, thus preventing the formation and growth of inhomogeneous lithium dendritic structures; this, in turn, guarantees safe and stable long-term operation, chiefly in lithium metal batteries.[240,245]
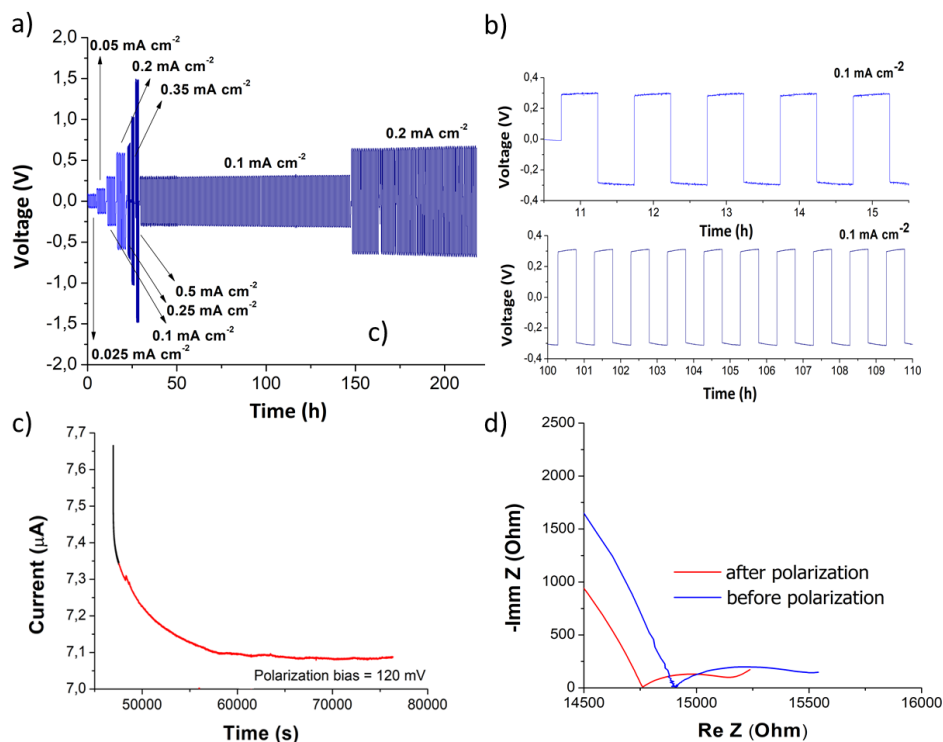
Figure 4.9 Electrochemical characterization performed with symmetrical cell with Li/copoly8/Li configuration at 70 °C: (a) galvanostatic plating and stripping test at different current densities (0.025, 0.05, 0.1, 0.2, 0.25, 0.35, 0.5 mA cm^{-2}); (b) characteristics of the voltage profiles at 0.1 mA cm^{-2} and different testing time; (c) EIS and (d) polarization current variation results from lithium-ion transference number measurement.

Electrochemical behavior in Li metal cell

The newly prepared copoly8 polyelectrolyte was tested in a lab-scale lithium test cell with a lithium metal negative electrode (anode) and commercial LiFePO$_4$ (LFP) as the positive electrode (cathode) in a Li/copoly8/LFP configuration. The LFP-based electrode was obtained in the form of a catholyte using the same copoly8 as the active binder. The catholyte preparation process and the electrode active material loading are detailed in chapter 3. The cell was assembled using the neat copoly8 as the electrolyte without further treatment of the electrodes or addition of any plasticisers/enhancers (e.g., solvents, salts). The electrochemical behaviour of the laboratory-scale solid-state cell at 70 °C and C/20 rate, based on the theoretical specific capacity of the LFP active material, is shown in Figure 4.10a. It delivered

stable and efficient charge/discharge cycling (> 145 mAh g^{-1}) at the first cycle, which corresponds to > 91 % of the practical specific capacity output (158 mAh g^{-1} at C/20) achieved by the commercial LFP used as active material when cycled with standard LP30 liquid electrolyte. During prolonged cycling, excellent cycling stability and capacity retention were demonstrated with a very limited (≤ 2 %) capacity decay after more than 50 cycles and an outstanding Coulombic efficiency (CE) approaching 100% during the whole cycling test. This result is remarkable, particularly considering the active material loading, which is high for a lab-scale polymer electrolyte cell[67] and not so far from standard commercial cells.[246] The excellent CE confirms the reversibility of the Li$^+$ ion intercalation process and the stability of the obtained single-ion block polyelectrolyte. Very interestingly, no loss and even no gradual decrease of specific capacity during initial cycling was observed, which also accounts for the purity of the sample, its stability towards oxidation/reduction, compatibility with both electrode materials, and the formation of a stable passivation layer at the electrode/electrolyte interface.

The remarkable electrochemical performance in terms of high capacity output and capacity retention after more than 50 consecutive charge/discharge cycles at C/20 rate is likely ascribed to the efficient ion conduction in the polymer separator and the favourable charge transport at the electrode/electrolyte interface in the cell. Figure 4.10b shows highly reversible and stable constant current potential versus specific capacity profiles, corresponding to the typical flat plateaus of Li$^+$ ion de-insertion (charge) and insertion (discharge) from/in the LiFePO$_4$/FePO$_4$.[247] Clean and flat profiles with a sharp voltage drop at the end of the redox reaction related to Li$^+$ de-insertion/insertion mechanism suggest that polarization behaviour during ion insertion/diffusion at the cathode/SIC interface was actually limited. The voltage difference between the charge and discharge potential plateaus of about 0.4 V is not negligible. The fundamental cause of voltage drop (overpotential) can be associated with the relatively low ionic conductivity and the intrinsic high bulk resistance of polyelectrolyte. It is worth noticing that the thickness of the electrolyte used in this proof-of-concept cell (100 μm) might have negatively affected the ion diffusion between cathode and anode throughout the electrolyte; moreover, the commercial LFP used in this work is optimized to deliver high energy density rather than high power output. The increase of the conductive carbon loading in the electrode may mitigate the overpotential issue; however, the optimization of the electrode formulation was beyond the scope of this research, which was intended

to show a proof-of-concept. Nonetheless, the voltage drop decreased while cycling (< 0.3 V after 5 cycles), which accounts for a sort of activation of materials and amelioration of the interface upon cycling.
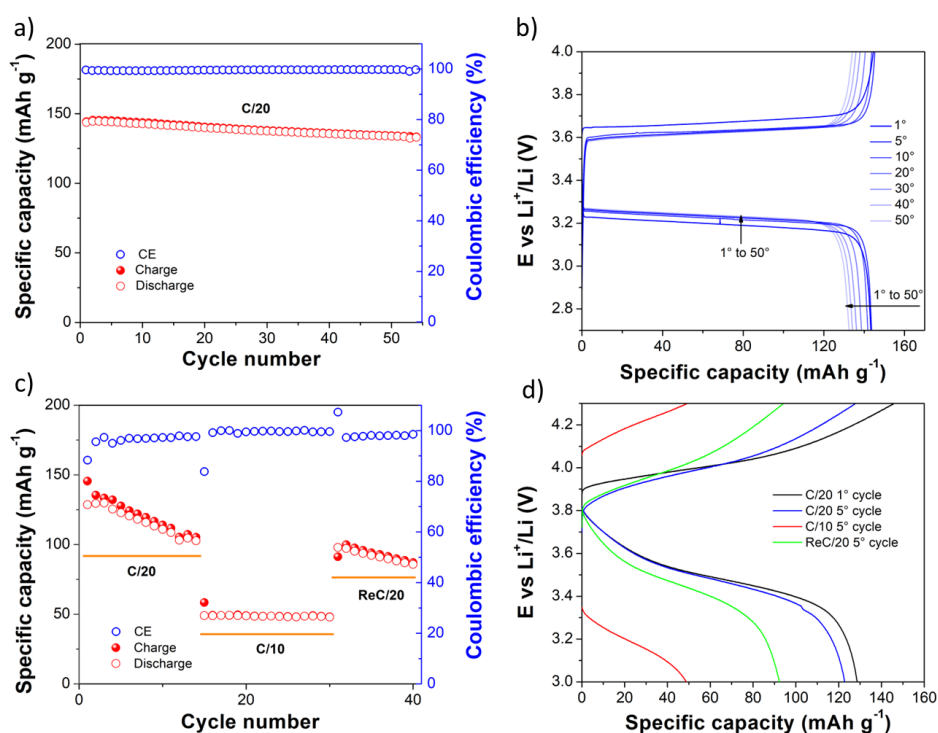
Figure 4.10 Galvanostatic cycling behaviour of Li/copoly8/LFP (a, b) and Li/copoly8/NMC (c, d) solid-state cells at 70 °C. Specific capacity vs cycle number dependence (a) and corresponding charge/discharge voltage vs specific capacity profiles at constant C/20 rate (b) of Li/copoly8/LFP cell. Specific capacity vs. cycle number dependence at C/20 and C/10 rates (c) and corresponding charge/discharge voltage vs specific capacity profiles at C/20 and C/10 rate (d) of Li/copoly8/NMC cell.

In consideration of the excellent electrochemical stability at anodic potential, exceeding 4.5 V vs Li$^+$/Li, copoly8 was further tested in a lab-scale lithium cell with a lithium metal negative electrode (anode) and a commercial LiNiMnCoO$_2$ (NMC) as the active material at the positive electrode in a Li/copoly8/NMC configuration. The NMC-based cathode was also obtained in the form of a catholyte, as reported in chapter 3. The electrochemical behaviour of the solid-state

lab-scale cell was first studied in the voltage range between 3 and 4.3 V vs Li^+/Li (70 °C, C/20 and C/10 constant current rates, based on the theoretical specific capacity of the NMC active material). The solid-state NMC-based cell delivered initial specific charge capacity values of 145 and 124 mAh g^{-1} after 1 and 6 cycles at C/20 rate, respectively (Figure 4.10c). Thus, no drastic capacity fade during initial cycling was observed, with a CE improving cycle-by-cycle (exceeding 95% after 5 cycles). While doubling the current rate to C/10, the specific discharge capacity delivered by the cell was still close to 50 mAh g^{-1} with only a slight overpotential increase compared to the potential vs specific capacity profile obtained at a lower rate (Figure 4.10d). This behaviour was ascribed to the limitations associated with the internal resistance of the cell, as already observed for the LFP-based cell, mainly affected by the relatively high intrinsic resistance of polyelectrolyte and the not engineered interface between the binder and the active material.

It is important to remark that this proof-of-concept cell is, to the best of my knowledge, the first example of neat polycarbonate-based SICPE operating in a truly solid-state Li-metal cell with high energy 4V-class NMC electrode, and assembled without any performance enhancers, additives like plasticisers and/or surface electrode treatment. An additional and more demanding test was performed on the Li/copoly8/NMC cell up to 4.8 V vs Li^+/Li (70 °C, C/20 rate), increasing the anodic voltage limit from 4.3 to 4.8 V vs Li^+/Li by 0.1 V steps every 2 cycles (Figure 4.11a). A clear charge profile typical of lithium-ion extraction was detected up to 4.8 V vs Li^+/Li, thus confirming the very high voltage stability and cycling performance of the newly developed SIC. As already demonstrated in a previous report,[130] the crosslinking technique allows the synthesis of SPE with embedded plasticizer components, such as solvents and/or oligomers, enhancing the cycling performance without detrimentally compromising the polymer thermal stability thus, in turn, the safety of the final device.[130] Following the same route, but without drastically altering the identity of this work, a new Li/copoly8-PC/LFP lab-scale cell was assembled (the amount of PC was fixed at 5-8 wt.% with respect to the total mass of polyelectrolyte in the cell). The result of the constant-current cycling test is shown in Figure 4.11b.
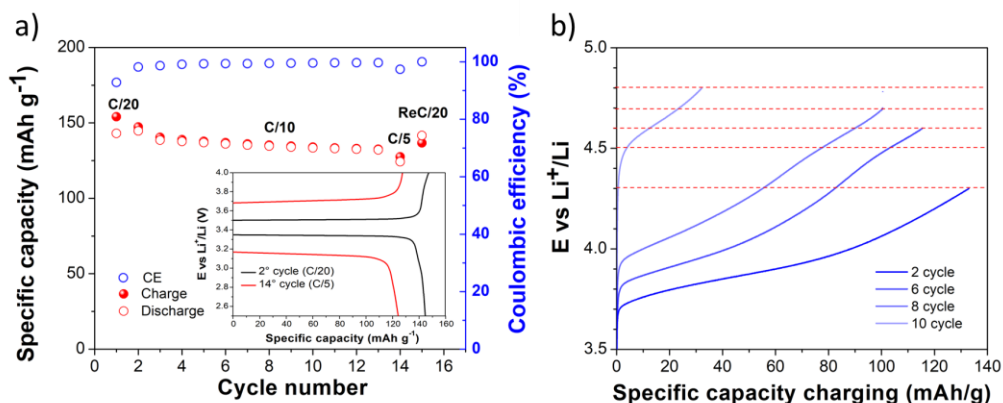
Figure 4.11 (a) Galvanostatic cycling behaviour at C/20, C/10 and C/5 rates upon charge and discharge at 70 °C of the Li/copoly8-PC/LFP lab-scale cell: specific capacity vs cycle number plot, including Coulombic efficiency values. The inset shows the charge/discharge profiles at C/20 and C/5; (b) charge/discharge potential vs specific capacity profiles at C/20 constant current rate from 4.3 to 4.8 V vs. Li$^+$/Li with constant increment of 0.1 V each 2 cycles for Li/copoly8/NMC cell.

It is well evident that the new cell showed a substantial reduction of capacity drop compared to the previous LFP-based truly solid-state cell, while doubling the current regime to C/10 and even up to C/5 without any remarkable drop in the specific capacity. Moreover, the voltage profiles remained flat and stable with very limited overpotential at C/20 rate, which accounts for a greatly reduced electrode/electrolyte resistance, as shown in the inset of Figure 4.11b. The overpotential increased at C/5, however, with a flat profile and no sign of enhanced sloping of the curve and very limited polarization. It accounts for the largely enhanced ion conduction in the polymer electrolyte separator and the more favourable charge transport between the electrodes and the electrolyte in the new cell even with a minimal amount of added plasticizer. The CE exceeded 99 % during initial and prolonged cycling at low and at high rates, thus confirming the reversibility of the lithium-ion intercalation process and the electrochemical and interfacial stabilities of obtained single-ion conducting block copolymer electrolytes.

4.3 Conclusions

In this chapter, we reported the synthesis of novel solid-state polyelectrolytes based on poly(carbonate)-b-poly(ionic liquid) with single Li^+ ion conducting features. The single-ion conducting polyelectrolytes were purposely modified by designing novel block copolymers that combine one block responsible for high ionic conductivity and the second block for improved mechanical properties and outstanding electrochemical stability. Such ionic block copolymers were obtained by subsequent ring opening polymerization (ROP) and reversible addition-fragment chain-transfer (RAFT) polymerization techniques. The proof-of-concept lab-scale truly solid-state Li-metal cells assembled with such novel ionic block copolymers using both standard LFP and high voltage NMC-based composite electrodes at relatively high active material loading provided excellent performances in terms of high specific capacity output, stability, and reversible cycling even up to 4.6-4.8 V vs Li^+/Li.

Chapter 5

5 Self-assembly of single Li-ion conducting block copolymers for improved ionic conductivity and viscoelastic properties

5.1 Introduction

The ideal SICPE electrolyte for a solid-state battery should have the ionic conductivity of a liquid, the mechanical properties of a solid, and the formability of a thermoplastic.[248] However, the link between high bulk ionic conductivity and low T_g limits the realization of highly mechanically stable flexible single-component linear SICPE with sufficiently good electrochemical performance for practical Li-metal cell operation.[249] One of the approaches to overcome this problem was demonstrated by Elabd, Winey and co-workers [236,250–253] and consisted in the synthesis of cationic block copolymers, where the partial incompatibility between ionic and neutral blocks resulted in a microphase-separated morphology. Block copolymers with strong microphase separation exhibited ~1.5-2 orders of magnitude higher ionic conductivity than block copolymers with weak microphase separation.[251] Such effect was explained by the existence of a correlation between the morphology and ionic conductivity of SICPEs. As a result of microphase segregation, the nanoscale domains were formed, thus playing the role of ion-conducting channels with elevated concentrations of mobile ions and enhanced conductivity.[251] In addition, the efficiency of charge transport in cationic PILs increased with the transition from hexagonally packed cylinders (1-D conducting pathway), lamellae (2-D conducting pathway) to 3-D network structures (continuous conducting microdomain).[251]

Despite the publications dedicated to the phase separation in cationic block copolymers, only a few reports examined the relationship between morphological behaviour and ion transport in anionic SICPEs with lithium counter ion.[204,205,227,238,254,255] As mentioned in paragraph 2.1.2, the presence of PEO in the middle of block copolymers drastically limits the ionic conductivity at ambient temperature, and suitable Li-ion mobility is achieved only above the melting temperature of PEO. When PEO chains are "frozen" and separated from the ionic block in lamellar morphology, Li$^+$ ions are trapped and cannot move. Thus, polymers **1**, **2** and **3** (Scheme 5.1) do not benefit from the phase separation, and ionic conductivity starts to increase only when block copolymers become a disordered system. However, when in the triblock copolymer, the LiSTFSI or LiMTFSI is copolymerized randomly in the middle block with a monomer having short and flexible side PEO chains (Scheme 5.1, **4**), such a system still allows for Li hopping, while profiting from an improved mechanical performance from lamellar microphase separation.
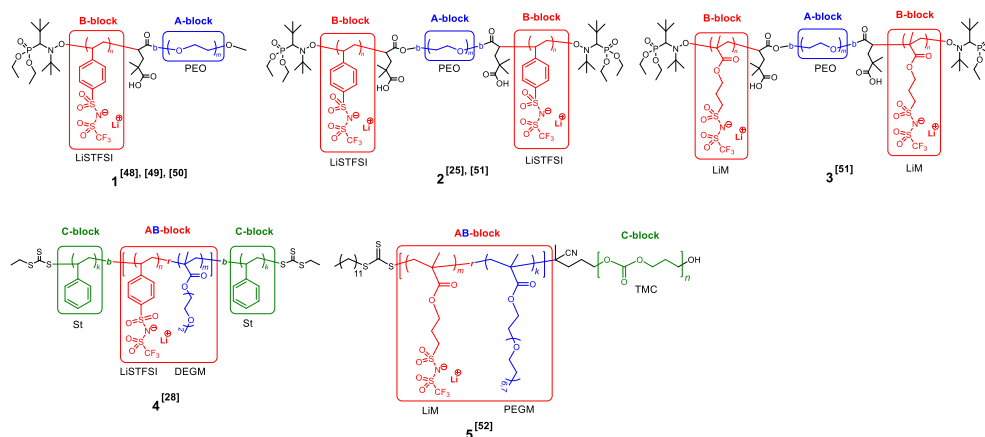
Scheme 5.1 An overview of the anionic single ion conducting block copolymers reported in literature (1 to 5, including references to the related articles).

Based on the literature knowledge[204,206] and the interesting features of poly[TMC$_n$-*b*-(LiM$_m$-*r*-PEGM)$_k$] block copolymers (Scheme 5.1) deriving from the partial immiscibility of different polymer blocks, previously described in chapter 4; This

Chapter focuses on the investigation of microphase segregation impact on the ionic conductivity to allow proper cycling of lab-scale Li-metal cells; in addition, the mechanical properties of the polyelectrolytes are reported, Specifically, the target is to overcome the previous results, demonstrating the synthesis of novel A-B block copolymers with single Li-ion conducting features, where A block represents a random copolymer of LiMTFSI (LiM) and PEGM (as reported in Chapter 4), while B block consists of poly(2-phenylethyl methacrylate) (poly(PhEtM) by means of controlled RAFT polymerization. In addition, the tuning of LiM:PEGM ratio and molecular weights of both blocks allows proper control over the microphase separation. The best block copolymers, namely poly[(LiM$_{17}$-r-PEGM$_{86}$)-b-PhEtM$_{131}$] and poly[(LiM$_{17}$-r-PEGM$_{86}$)-b-PhEtM$_{194}$], are characterized by lamellar microphase separation and demonstrated significantly improved viscoelastic properties (3 to 5 orders of magnitude increase in storage moduli, at both 25 and 70°C) at a similar level of ionic conductivity in comparison with random poly[LiM$_{17}$-r-PEGM$_{86}$]. Finally, poly[(LiM$_{17}$-r-PEGM$_{86}$)-b-PhEtM$_{131}$], having a high lithium-ion transference number and high oxidative stability, was used for the assembly of lab-scale Li-metal cell prototypes, which showed reversible cycling near theoretical capacity, thus demonstrating the promising prospects of the new single-ion conductors for the development of truly solid-state lithium polymer batteries.[256]

5.2 Results and discussion

5.2.1 Synthesis of lithium 1-[3-(methacryloyloxy)propylsulfonyl]-1-(trifluoromethanesulfonyl)imide (LiM) and poly[LiMn-r-PEGMm]copolymers

The ionic monomer was synthesized in full accordance with the procedure published previously.[201,219] Poly[LiM$_n$-r-PEGM$_m$] random copolymers were prepared via RAFT copolymerization, varying the LiM:PEGM molar ratio and using 4-cyano-4-(phenylcarbonothioylthio)pentanoic acid (CPAD, >97%, Aldrich) as RAFT agent, 2,2'-azobisisobutyronitrile (AIBN, 98%, Aldrich) as initiator and dimethylformamide (DMF, HPLC grade 99.5%, Acros) as solvent. The resulting transparent and viscous copolymer solution was diluted with milli-Q water and

dialyzed against water for two days. The 4-methoxyphenol (polymerization inhibitor, 40 mg, 0.04 wt%) was added to the obtained aqueous solution, and the copolymer was isolated by freeze-drying. Finally, the copolymer representing soft and sticky pink material was thoroughly dried at 50 $^\circ$C/1 mm Hg for 24 h and stored in the argon-filled glove box (MBRAUN MB-Labstar, H_2O and O_2 content < 0.5 ppm) for five days prior to further investigation. The random RAFT copolymerization of LiM and PEGM was performed because all copolymers previously synthesized from ionic monomers and PEGM were amorphous, and none of them tended to crystallize.[189,201,203,205,219,230] Indeed, incorporating PEGM monomers into such copolymers led to a significant decrease in their T_g, positively affecting their ionic conductivity. Once the optimal reaction conditions were established, a set of poly[LiM$_n$-r-PEGM$_m$] copolymers with molecular weights in the range of 31.9 - 55.0 kDa and different LiM:PEGM ratios (from 1:1 to 1:10) were obtained via RAFT copolymerization (Table 5.1).

Table 5.1 Synthesis of poly[(LiM$_n$-r-PEGM$_m$) copolymers.

№	Polymer	PEGM:LiM[a]	$M_{n \text{ (NMR)}}$ (kDa)[b]	$M_{n \text{ (SEC)}}$ (kDa)[c]	M_w/M_n[c] (SEC)	T_g, (°C)[d]	σ, (S/cm) 25°C
1	poly[LiM$_{35}$-r-PEGM$_{35}$]	1	30.0	33.3	1.32	15	1.3×10^{-8}
2	poly[LiM$_{17}$-r-PEGM$_{50}$]	3	30.7	38.3	1.15	-21	4.3×10^{-7}
3	poly[LiM$_{11}$-r-PEGM$_{54}$]	5	30.8	35.5	1.13	-29	4.1×10^{-7}
4	poly[LiM$_{17}$-r-PEGM$_{86}$]	5	49.1	55.0	1.16	-25	4.1×10^{-7}
5	poly[LiM$_{10}$-r-PEGM$_{55}$]	6	31.3	32.3	1.14	-26	3.1×10^{-7}
6	poly[LiM$_8$-r-PEGM$_{56}$]	7	30.6	35.0	1.14	-31	2.3×10^{-7}
7	poly[LiM$_6$-r-PEGM$_{60}$]	10	32.4	31.9	1.27	-47	2.7×10^{-7}
8	poly(PEGM)$_{71}$	1/0	35.5	26.2	1.13	-57	-

[a] By ^{1}H NMR (CDCl$_3$). [b] Calculated by Equation 6. [c] By GPC in 0.1 M solution of LiTFSI in DMF at 50°C with PMMA standards. [d] By TMA, 5°C/min.

All samples demonstrated only one glass transition temperature in between the transitions attributed to neat poly(PEGM) (T_g = –57 °C) and poly(LiM) (T_g = 105 °C) [219], thus proving the formation of random copolymers. The results reported here fully agree with those published previously for random copolymers based on LiSTFSI and poly(ethylene glycol)methyl ether acrylate monomers.[203] Ionic

conductivity measured for random poly[LiM$_n$-r-PEGM$_m$] copolymers revealed that at PEGM:LiM = 1:5 mole ratio, the polymer electrolyte conductivity is about 4.1×10^{-7} S cm^{-1} at 25 °C and T$_g$ about –25 °C.

5.2.2 Synthesis of poly[(LiM$_n$-r-PEGM$_m$)-b-PhEtM$_k$] copolymers

The synthesized random poly[LiM$_n$-*r*-PEGM$_m$] copolymers were further applied as macro-chain-transfer agents (macro-CTAs) in the synthesis of poly[(LiM$_n$-*r*-PEGM$_m$)-*b*-PhEtM$_k$] block copolymers as showed in Scheme 5.2. The 2-phenylethyl methacrylate (PhEtM) was chosen for the preparation of the B-block for the following reasons: i) the monomer contains methacrylic functional group similar to LiM and PEGM that will ensure the successful realization of the block copolymers synthesis with the same CPAD RAFT agent, and ii) PhEtM possesses the aromatic moiety, which makes the block incompatible with polar LiM and PEGM copolymers.
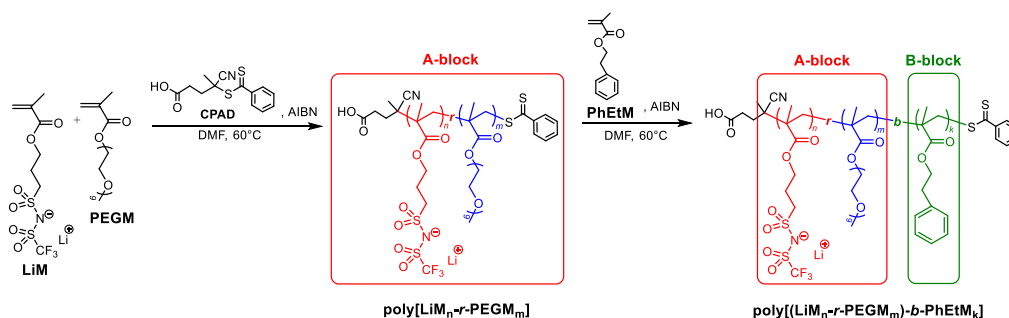
Scheme 5.2 Poly[(LiM$_n$-r-PEGM$_m$)-b-PhEtM$_k$] block copolymers prepared via RAFT copolymerization.

After determination of the optimal conditions for PhEtM RAFT polymerization by studying the polymerization kinetics with CPAD RAFT agent, a set of poly[(LiM$_n$-*r*-PEGM$_m$)-*b*-PhEtM$_k$] block copolymers was synthesized using the macro-CTA (Table 5.2). The block copolymer was purified by precipitation into the excess of diethyl ether, thoroughly washed with diethyl ether and then dried at 50 °C/1 mm Hg for 24 h. The resulting block copolymer appeared as a slightly pink rubber-like material and it was stored in the argon-filled glove box. The n:m ratio

controls the ionic content in synthesized macro-CTAs (poly[LiM$_n$-r-PEGM$_m$])
copolymers, while the control over the ratio between molecular weights of the
blocks (M_A/M_B) was gained by varying the PhEtM loading. The obtained
poly[(LiM$_n$-r-PEGM$_m$)-b-PhEtM$_k$] block copolymers with M$_{n(NMR)}$ < 40 kDa
appeared as wax like materials, while copolymers with M$_{n(NMR)}$ > 40 kDa exhibited
rubber-like properties.

Table 5.2 Synthesis of poly[(LiM$_n$-r-PEGM$_m$)-b-PhEtM$_k$] block copolymers.

N	poly[(LiM$_n$-r-PEGM$_m$)-b-PhEtM$_k$] (A-b-B block copolymer)				
	Block copolymer	$M_{n\,(SEC)}$ (kDa)^a	$M_w/M_n{}^a$ (SEC)	$M_{n\,(NMR)}$ (kDa)^b	$M_A/M_B{}^b$
1	poly[(LiM$_6$-r-PEGM$_{27}$)-b-PhEtM$_{53}$]	24.3	1.12	25.8	1.6:1
2	poly[(LiM$_{17}$-r-PEGM$_{50}$)-b-PhEtM$_{82}$]	43.2	1.19	46.3	2.0:1
3	poly[(LiM$_{11}$-r-PEGM$_{54}$)-b-PhEtM$_{40}$]	39.2	1.15	38.5	4.0:1
4	poly[(LiM$_{11}$-r-PEGM$_{54}$)-b-PhEtM$_{74}$]	43.3	1.13	44.8	2.2:1
5	poly[(LiM$_8$-r-PEGM$_{56}$)-b-PhEtM$_{82}$]	42.4	1.17	46.2	2.0:1
6	poly[(LiM$_{17}$-r-PEGM$_{86}$)-b-PhEtM$_{49}$]	57.7	1.21	58.4	5.3:1
7	poly[(LiM$_{17}$-r-PEGM$_{86}$)-b-PhEtM$_{75}$]	61.6	1.19	63.4	3.4:1
8	poly[(LiM$_{17}$-r-PEGM$_{86}$)-b-PhEtM$_{131}$]	67.7	1.17	74.1	2.0:1
9	poly[(LiM$_{17}$-r-PEGM$_{86}$)-b-PhEtM$_{194}$]	74.7	1.19	85.9	1.3:1

^{a} By GPC in 0.1 M solution of LiTFSI in DMF at 50°C with PMMA standards.

^{b} By Equation 8 and ratio between M_n of different blocks.
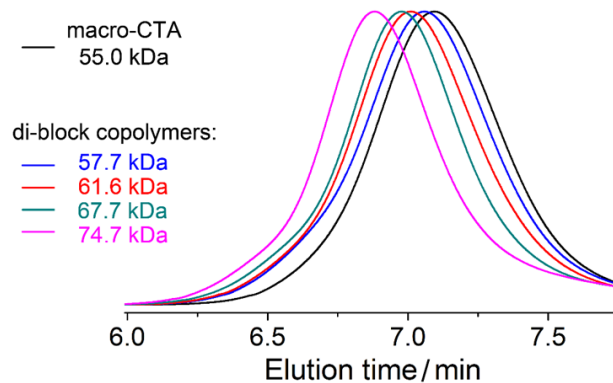
Figure 5.1 SEC traces of poly[(LiM$_{17}$-r-PEGM$_{86}$)-b-PhEtM$_k$] block copolymers obtained from poly[LiM$_{17}$-r-PEGM$_{86}$] macro-CTA.

Figure 5.1 shows the SEC chromatograms of the parent poly[LiM$_{17}$-*r*-PEGM$_{86}$] with $M_{n(SEC)}$ = 55.0 kDa and the subsequent increase in the molecular weight of the growing block copolymers poly[(LiM$_{17}$-*r*-PEGM$_{86}$)-*b*-PhEtM$_k$] with k = 49, 75, 131 or 194 (Table 2, lines 6-9). A clear shift of the SEC traces toward a higher molecular range with M_w/M_n remaining < 1.21 confirms the efficient polymerization initiation and demonstrates the formation of the second block. At the same time, the large difference between $M_{n(NMR)}$ and $M_{n(SEC)}$ can be explained by the structural difference between the comb-like poly(PhEtM) with aromatic substituents and poly(methyl methacrylate) (PMMA) calibration standards. The chemical structure, composition and purity of poly[(LiM$_{17}$-r-PEGM$_{86}$)-b-PhEtM$_{131}$] block copolymers were confirmed by NMR (Figure 5.2) and IR spectroscopy.
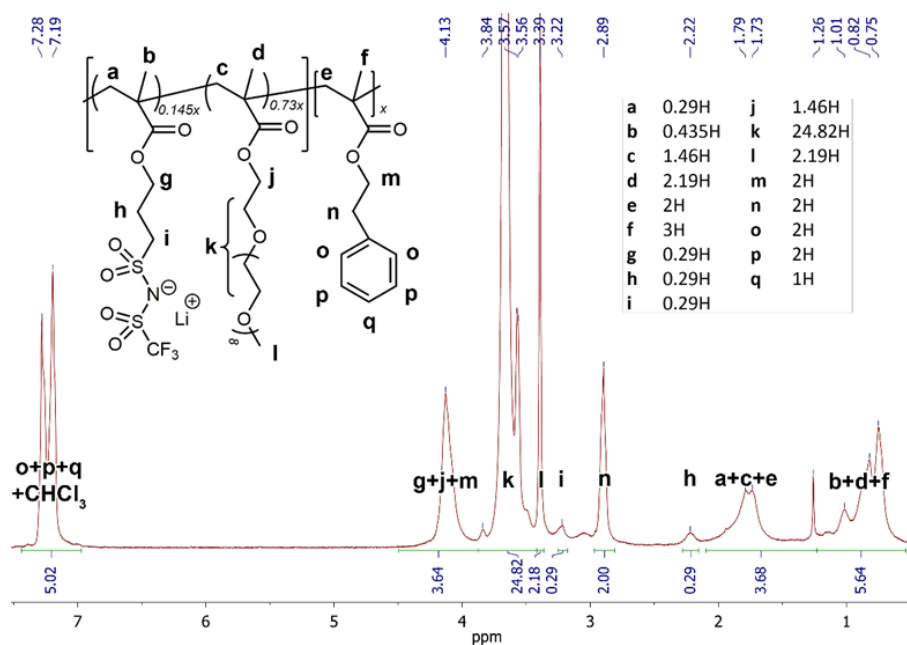
Figure 5.2 ^{1}H NMR of poly[(LiM$_{17}$-r-PEGM$_{86}$)-b-PhEtM$_{131}$] in CDCl$_3$.

5.2.3 Chemical-physical and electrochemical characterization

Thermomechanical analysis

Thermal properties of poly[(LiM$_n$-*r*-PEGM$_m$)-*b*-PhEtM$_k$] block copolymers were studied by thermal-mechanical analysis (TMA). Most of the samples demonstrated three transition temperatures (Table 5.3).

Table 5.3 Selected properties of Poly[(LiM_n-r-PEGM_m)-b-PhEtM_k] block copolymers.

N	poly[(LiM_n-r-PEGM_m)-b-PhEtM_k]	$M_A/M_B{}^a$	T_{g1}, (°C)^b	T_{g2}, (°C)^b	T_{HDT}, (°C)^b	σ_{DC}, (S/cm) at 25°C	Type of morphology^c	Domain length (nm)	Cylinders diameter (nm)
1	poly[(LiM$_6$-r-PEGM$_{27}$)-b-PhEtM$_{53}$]	1.6:1	-39	35	67	2.6×10^{-8}	disordered	-	-
2	poly[(LiM$_{17}$-r-PEGM$_{50}$)-b-PhEtM$_{82}$]	2.0:1	-47	34	93	3.0×10^{-8}	HPC^d	25.4±0.9	16.6±4.4
3	poly[(LiM$_{11}$-r-PEGM$_{54}$)-b-PhEtM$_{40}$]	4.0:1	-48	23	-	7.8×10^{-8}	HPC	16.3±0.1	10.6±3.6
4	poly[(LiM$_{11}$-r-PEGM$_{54}$)-b-PhEtM$_{74}$]	2.2:1	-51	26	69	9.5×10^{-8}	HPC	22.8±1.8	13.7±3.1
5	poly[(LiM$_8$-r-PEGM$_{56}$)-b-PhEtM$_{82}$]	2.0:1	-51	21	75	5.0×10^{-8}	HPC	18.6±3.4	11.9±2.4
6	poly[(LiM$_{17}$-r-PEGM$_{86}$)-b-PhEtM$_{49}$]	5.3:1	-48	25	-	2.8×10^{-7}	HPC	18.9±1.6	12.8±2.7
7	poly[(LiM$_{17}$-r-PEGM$_{86}$)-b-PhEtM$_{75}$]	3.4:1	-49	31	76	2.3×10^{-7}	HPC	29.7±1.4	18±4.1
8	poly[(LiM$_{17}$-r-PEGM$_{86}$)-b-PhEtM$_{131}$]	2.0:1	-48	42	83	3.8×10^{-7}	lamellar	34.1±1.2	-
9	poly[(LiM$_{17}$-r-PEGM$_{86}$)-b-PhEtM$_{194}$]	1.3:1	-49	51	120	3.4×10^{-7}	lamellar	38.7±0.8	-

^{a} Defined by Equation 8. ^{b} By TMA. ^{c} By AFM on block copolymer coatings. ^{d} Hexagonally packed cylinders.

These transitions were attributed as follows: i) the first low-temperature transition corresponded to the glass transition (T_{g1}) of the parent poly[LiM$_n$-r-PEGM$_m$] ionic block, ii) the second transition was assigned to the glass transition (T_{g2}) of the poly(PhEtM) block, and iii) the final transition related to heat distortion temperature (T_{HDT}) at which a noticeable deformation was observed under applied load and scanning/heating rate. These three transition temperatures were found to be strongly dependent on the number of LiM units in the ionic poly[LiM$_n$-r-PEGM$_m$] block, the molecular weight of the poly(PhEtM) block, the total molar mass of the block copolymer and the ratio of ionic and non-ionic blocks (M_A/M_B). These observations can be summarized as follows: i) the decrease in LiM content and increase in PEGM:LiM ratio from 3 to 7 led to the decrease in T_{g1} (Table 5.3, entries 1-5), and ii) the increase in PhEtM units number resulted in the increase in T_{g2} and T$_{HDT}$ (Table 5.3, entries 6-9).

Ionic conductivity

Ionic conductivity (σ) of poly[(LiM$_n$-r-PEGM$_m$)-b-PhEtM$_k$] block copolymers was investigated by dielectric spectroscopy applying Equation 9 (vedi chapter 3), and related results are listed in Table 5.3. The ionic conductivity was dependent on

different parameters, such as the PEGM/LiM ratio, the total molecular weight of the block copolymer and the ratio of ionic and nonionic blocks M_A/M_B.

a) The PEGM/LiM ratio affects the ionic conductivity of block copolymers, similarly to parent poly[LiM$_n$-r-PEGM$_m$] random copolymers (Table 5.3). Considering the series of samples, namely poly[(LiM$_{17}$-r-PEGM$_{50}$)-b-PhEtM$_{82}$], poly[(LiM$_{11}$-r-PEGM$_{54}$)-b-PhEtM$_{74}$] and poly[(LiM$_8$-r-PEGM$_{56}$)-b-PhEtM$_{82}$] (Table 5.3) with similar values of $M_{n(NMR)}$ = 44.8÷46.3 kDa and M_A/M_B = 2.0÷2.2, the highest ionic conductivity (σ = 9.5×10^{-8} S cm^{-1}, 25 °C) was obtained for the block copolymer with PEGM/LiM = 5. A different trend was observed for block copolymers having closed PEGM/LiM = 4.4÷5.0 and M_A/M_B = 1.6÷2.2 ratios but different molecular weights, $M_{n(NMR)}$ = 25.8, 44.8 and 74.1 kDa (Table 5.3). An almost three times increase in the $M_{n(NMR)}$ was accompanied by a nearly 14 times increase in ionic conductivity (from 2.6×10^{-8} to 3.8×10^{-7} S cm^{-1} at 25 °C). Thus, in terms of charge transfer efficiency, the poly[(LiM$_{17}$-r-PEGM$_{86}$)-b-PhEtM$_{131}$] block copolymer was almost equal to the parent poly[LiM$_{17}$-r-PEGM$_{86}$], despite the decrease in the concentration of Li cations (3.8×10^{-7} and 4.1×10^{-7} S cm^{-1} at 25 °C, respectively).

b) The molecular weight of poly(PhEtM) block and the M_A/M_B ratio also affected the ionic conductivity of block copolymers (Table 5.3). In poly[LiM$_{11}$-r-PEGM$_{54}$] based block copolymers, the increase in PhEtM unit content led to increased ionic conductivity from 7.8×10^{-8} to 9.5×10^{-8} S cm^{-1} at 25 °C (Table 5.3). In the series of poly[(LiM$_{17}$-r-PEGM$_{86}$)-b-PhEtM$_k$] block copolymers, the increase in ionic conductivity with the increase of PhEtM units from 49 to 194 was less pronounced (Table 5.3 and Figure 5.3). However, it still doubled from 2×10^{-7} to 4×10^{-7} S cm^{-1} at 25 °C.
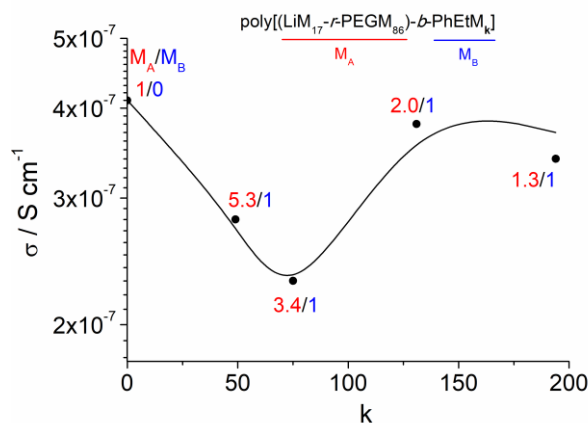
Figure 5.3 Ionic conductivity at 25 °C vs. number of PhEtM units (k) in poly[(LiM$_{17}$-r-PEGM$_{86}$)-b-PhEtM$_k$] block copolymers.

The observations above reported are in contradiction with the concentration of the mobile charges in the copolymer. The increase in non-coordinating monomer content should result in an overall decrease in ionic conductivity because of the reduction of conducting species. However, as proposed at the beginning of this chapter, the synthesis of the block copolymers with two immiscible blocks is supposed to lead to the microphase segregation, which can explain the conductivity results.

The temperature dependence of ionic conductivity for the best poly[(LiM$_{17}$-r-PEGM$_{86}$)-b-PhEtM$_{131}$] block copolymer is shown in Figure 5.4. EIS analysis was carried out between 25 and 120 °C. The Arrhenius plot shows the ionic conductivity increase with the temperature rise, reaching practical values of 10^{-6} and 10^{-5} S cm^{-1} levels at 40 and 80 °C, respectively. The plot slightly deviates from the ideal linear Arrhenius behaviour, especially at temperatures below 40 °C (T_{g2} of the copolymer), indicating an inter-relation between the conductivity and segmental relaxation of polymer segments. On the contrary, the deviation from the linear dependence at elevated temperatures is less pronounced, suggesting that in the range of 50-90 °C, the lithium-ion diffusion occurred prevalently through hopping on anionic sites. The curve gradient change above 90 °C could be probably associated with the third phase transition (T_{HDT}) and the formation of a disordered system.
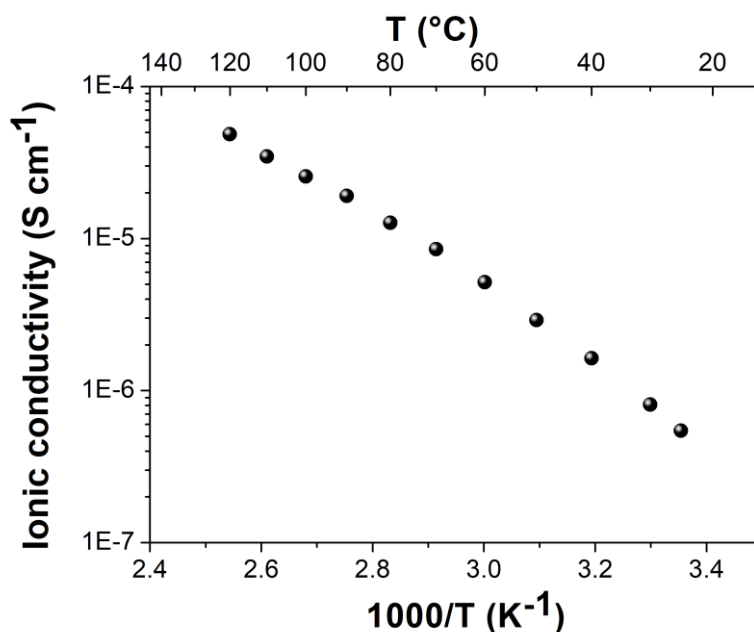
Figure 5.4 Ionic conductivity vs temperature (from 20 to 120 °C) for the sample [(LiM₁₇-r-PEGM₈₆)-b-PhEtM₁₃₁] block copolymer.

Morphological phase behavior

The presence of the two distinct glass transitions temperatures of all poly[(LiM$_n$-*r*-PEGM$_m$)-*b*-PhEtM$_k$] block copolymers demonstrated the presence of two segregated microphases. Thin coatings of block copolymers were studied by atomic force microscopy to prove this assumption and determine the type of morphology (Figure 5.5 and Table 5.3). AFM images of phase shift revealed that the bulk block copolymers mesoscopic self-assembly fits into two categories: perpendicular hexagonally packed cylinders (HPC) and perpendicular lamellas (Figure 5.5). The only exception was found for sample poly[(LiM$_6$-*r*-PEGM$_{27}$)-*b*-PhEtM$_{53}$], not exhibiting any visible phase separation on AFM images. This result can be explained by the low molecular weight of copolymer blocks, resulting in a low incompatibility of the polymer blocks allowing disorder in chains arrangement. With the increase in molecular weight of blocks, the incompatibility of the chains increased, and a mesoscopic phase separation occurred under the HPC perpendicular to the bulk surface (Table 5.3, Figure 5.5 a-d). The subsequent increase in both the number of PhEtM units and the total molecular weight of block

copolymers ended up in a new arrangement of the chains leading to a lamellar type nanophase separation perpendicular to the surface (Table 5.3, Figure 5.5 e-h).[257]
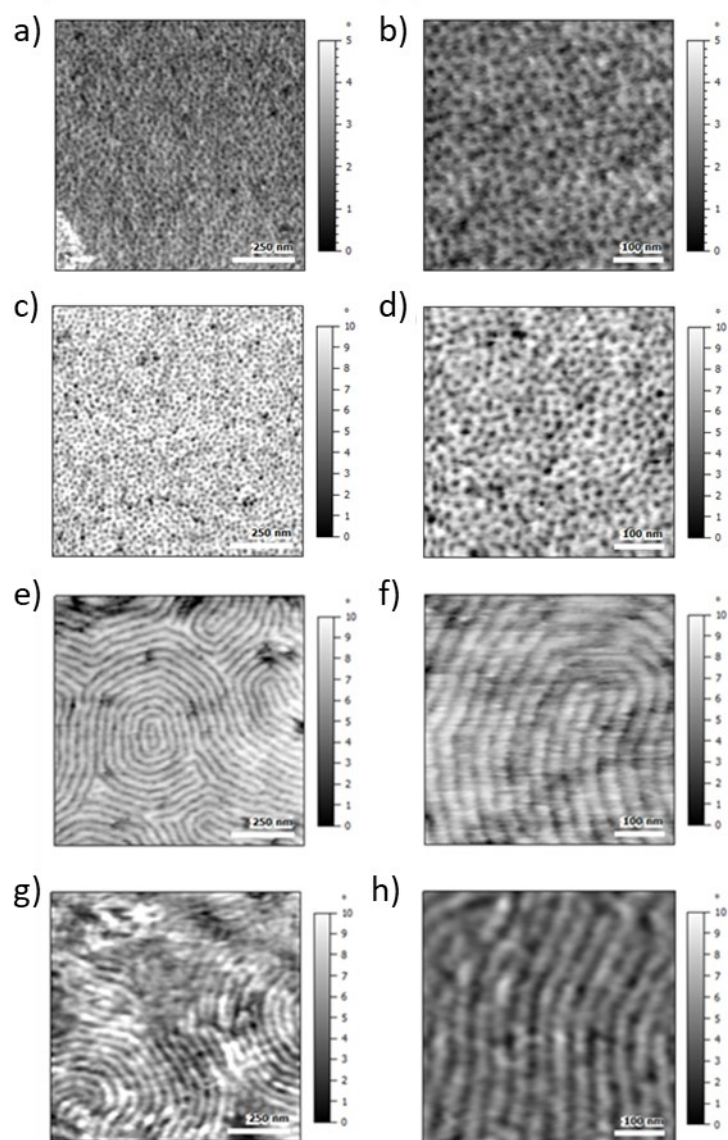
Figure 5.5 AFM images of poly[(LiM$_{11}$-r-PEGM$_{54}$)-b-PhEtM$_{74}$] (a, b), poly[(LiM$_8$-r-PEGM$_{56}$)-b-PhEtM$_{82}$] (c, d), poly[(LiM$_{17}$-r-PEGM$_{86}$)-b-PhEtM$_{131}$] (e ,f), and poly[(LiM$_{17}$-r-PEGM$_{86}$)-b-PhEtM$_{194}$] (g, h) films at different resolutions.

The domain size was found to be dependent on the following factors:

1. *PEGM/LiM ratio.* In block copolymers with molecular weight $M_{n(NMR)} = 44.8 \div 46.3$ kDa and M_A/M_B ratio = 2:1, the diameter of the cylinders and the distance between them were found to be dependent on the composition of the ionic block (Table 5.3). As the number of PEGM units increased (PEGM/LiM ratio increased from 3 to 7), the distance between the cylinders and their diameter gradually decreased (from 25.4 to 18.6 nm and from 16.6 to 11.9 nm, respectively).

2. *M_A/M_B ratio and poly(PhEtM) content (k).* The influence of the M_A/M_B ratio on the size and type of the domains can be traced by the example of low and high molecular weight block copolymers having a fixed PEGM/LiM ratio equal to 5 (Table 3). In both series, with the increase in poly(PhEtM) content (k), the size of the domains increased from 16.3 to 25.4 nm and from 18.9 to 38.7 nm, respectively. Upon reaching a certain value of M_A/M_B value ≤ 2.0 for high molecular weight block copolymers, the type of microphase changed: the hexagonally packed cylinders were transforming into the lamellar morphology (Table 5.3 and Figure 5.5 e-h). The same trend was observed for cylinders diameters, which increased from 10.6 to 13.7 and from 12.8 to 18.0 nm when k raised from 40 to 74 and from 75 to 131, suggesting that poly(PhEtM) chains occupy the centre of the cylinders.

3. *Overall molecular weight of block copolymer.* With the growth in the molecular weight of the block copolymers with constant PEGM/LiM and M_A/M_B ratios (5:1 and ~2.0, correspondingly), the probability of microphase separation increased (Table 5.3). The sample with low molecular weight ($M_{n(NMR)} = 25.8$ kDa) showed only a disordered structure. The increase in $M_{n(NMR)}$ up to 44.8 kDa led to the formation of hexagonally packed cylinders, while a further increase of $M_{n(NMR)}$ to 74.1 kDa was accompanied by a transition to lamellar morphology.

As mentioned above, the ionic conductivity in poly[(LiM$_{17}$-r-PEGM$_{86}$)-b-PhEtMk] block copolymers unexpectedly increased with molecular weight. After morphological investigation, it is possible to conclude that the increase in ionic conductivity benefits from the formation of the long-range-ordered lamellas in comparison with cylindrical phase separation (Table 5.3)[234]. In contrast, when the microphase segregation yields the lamellar structures, the continuous ion-conducting pathways with a high concentration of Li$^+$ cations and ethylene oxide solvating groups are formed, which facilitates the ion transport and increases the

overall ionic conductivity. These results perfectly correlate with those observed for cationic block copolymers reported previously [234,251,258].

Rheological properties

The dynamic rheological properties of poly[(LiM$_{17}$-r-PEGM$_{86}$)-b-PhEtM$_{131}$] block copolymer with the highest ionic conductivity and lamellar microphase segregation were measured by carrying out rheological measurements in a small amplitude oscillatory flow mode at 25 and 70 °C (Figure 5.6). They were further compared to those demonstrated by parent poly[LiM$_{17}$-r-PEGM$_{86}$] random copolymer. Figure 5.6a shows the temperature dependence of complex viscosity at a constant frequency of 1 Hz. The curves of both copolymers exhibited a smooth decrease with the increase in temperature, having nearly the same slope. For all investigated temperatures poly[(LiM$_{17}$-r-PEGM$_{86}$)-b-PhEtM$_{131}$] possessed significantly higher complex viscosity than the parent poly[LiM$_{17}$-r-PEGM$_{86}$].
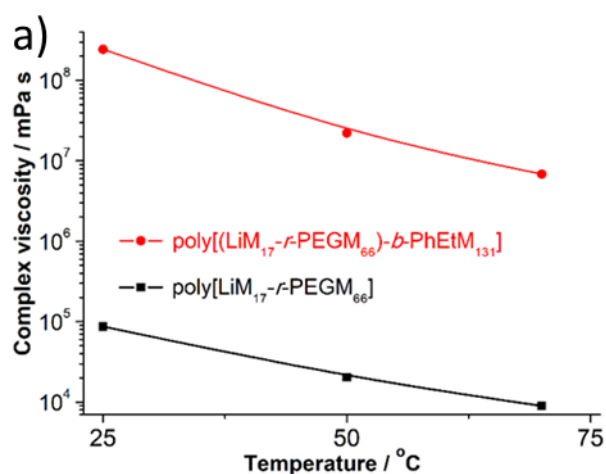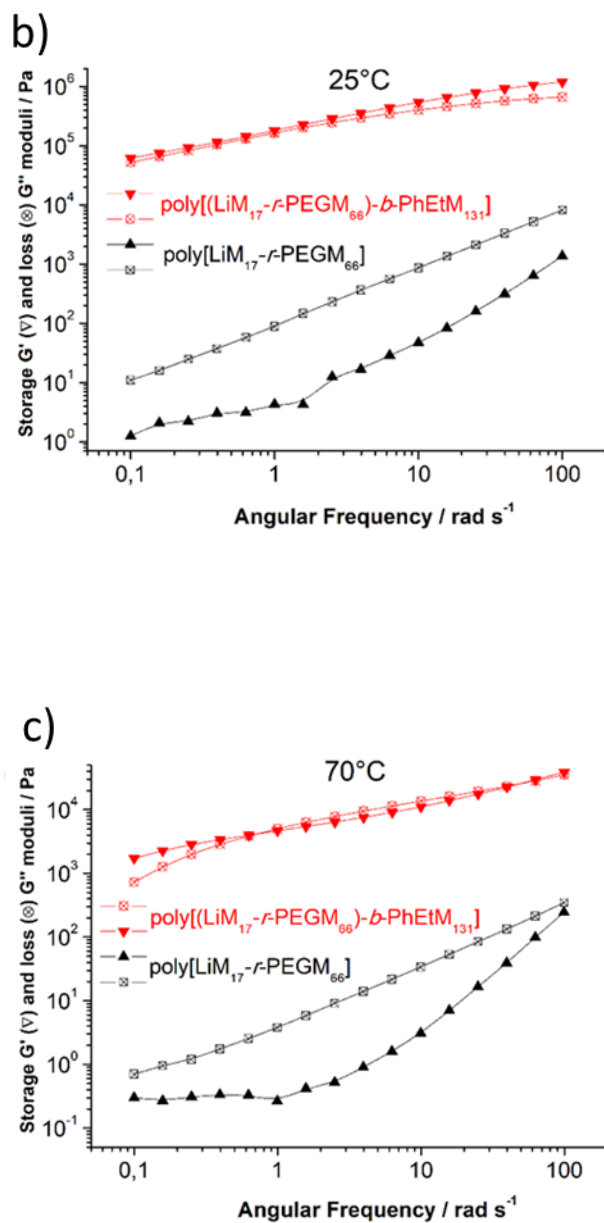
Figure 5.6 Temperature dependence of the complex viscosity (a); frequency dependence of the storage modulus G' (full symbols) and the loss modulus G" (open symbols) obtained at 25 (b) and 70 °C (c) for poly[(LiM$_{17}$-r-PEGM$_{86}$)-b-PhEtM$_{131}$] and poly[LiM$_{17}$-r-PEGM$_{86}$].

The observed enhancement in viscoelastic behaviour increased up to four orders of magnitude. Figure 5.6b and Figure 5.6c show the storage and loss moduli versus angular frequency dependence performed at 25 and 70 °C. For poly[LiM$_{17}$-r-PEGM$_{86}$], the imaginary part (G'') exceeded the real part (G') of the complex modulus over the entire frequency range and at all temperatures. Both moduli exhibited a high degree of frequency dependence. Such behaviour of poly[LiM$_{17}$-r-PEGM$_{86}$] can be ascribed as the one closed to a liquid-like or molten state. In contrast, for poly[(LiM$_{17}$-r-PEGM$_{86}$)-b-PhEtM$_{131}$] the G' was higher than G'' or nearly coincided with it at both temperatures. Moreover, both G' and G'' were less frequency dependent for the block copolymer than for the parent random copolymer over the entire measured range. This behaviour of poly[(LiM$_{17}$-r-PEGM$_{86}$)-b-PhEtM$_{131}$] can be attributed to the one with a solid-like character. Finally, block copolymer demonstrated the improvement in both moduli, up to five orders of magnitude. The presence of a stiff PhEtM block can explain the observed improvement in viscoelastic behaviour as both compared copolymers are linear and have the ionic poly[LiM$_{17}$-r-PEGM$_{86}$] block of the same molecular weight. These results are of high importance as solid polymer electrolytes with increased stiffness were previously reported to suppress/limit the growth of lithium dendrites effectively.[240,241] While poly[LiMn-r-PEGMm] copolymers appeared as a very soft and sticky pink material, the poly[(LiM$_n$-r-PEGM$_m$)-b-PhEtM$_k$] block copolymers looked to be pink rubber-like elastomers that can hold the weight load (Figure 5.7).
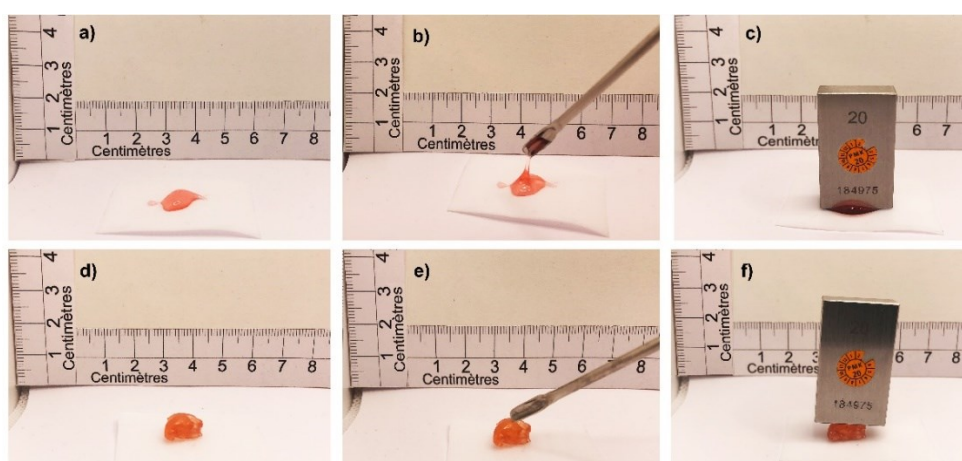
Figure 5.7 Appearance of poly[LiM$_{17}$-r-PEGM$_{86}$] (a-c) and poly[(LiM$_{17}$-r-PEGM$_{86}$)-b-PhEtM$_{131}$] (d-f).

Li^+ ion transference number and electrochemical stability

The promising prospects of the newly developed single-ion conducting polymer electrolyte were further confirmed by testing poly[(LiM$_{17}$-r-PEGM$_{86}$)-b-PhEtM$_{131}$] block copolymer in terms of lithium-ion transference number (t_{Li}^+) and anodic stability window (ASW). The t_{Li}^+ was determined by the method of Abraham et al. [220,221], as detailed in chapter 3 (Equation 4). The typical Nyquist plots of a.c. impedance of a Li/poly[(LiM$_{17}$-r-PEGM$_{86}$)-b-PhEtM$_{131}$]/Li symmetrical cell at 70 °C is shown in Figure 5.8a. The cell Nyquist plot did not change significantly during the experiment, and the initial bulk resistance (R_b) value of 2958 Ω only decreased to 2928 Ω, while the charge transfer resistance (R_{ct}) showed only a limited drop from 250 Ω to 238 Ω, thus proving a stable interfacial contact with the lithium metal electrode. The plot of the current response to the applied bias as a function of time is shown in Figure 5.8b. The current drop from 23.46 to 22.74 μA before the steady-state condition results in a t_{Li}^+ value of 0.96; the high value is fundamental to reduce electrolyte concentration polarisation during charge-discharge steps, thus producing higher power density. The obtained value fully agrees with previous Li transference numbers published for similar SICPEs.[223,259,260] Clearly, such value is noticeably higher than values reported for "standard" liquid electrolytes containing dissolved Li salts, including IL-based electrolytes, cationic PILs/Li salts and/or salt in polymers (e.g., PEO/Li) [223,261–264].
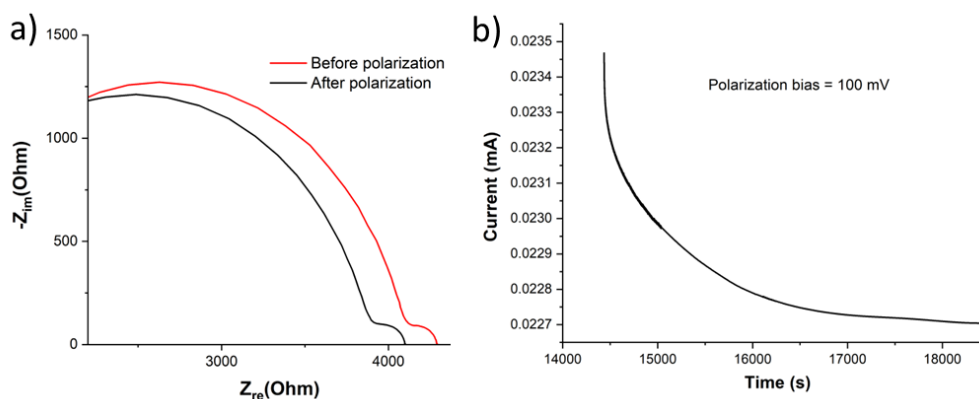
Figure 5.8 . Li-ion transference number analysis: a) Nyquist plots of the a.c. impedance and, b) current variation with time during polarization for symmetrical Li/poly[(LiM$_{17}$-r-PEGM$_{86}$)-b-PhEtM$_{131}$]/Li cell at 70 ºC.

The ESW of the single-ion poly[(LiM$_{17}$-r-PEGM$_{86}$)-b-PhEtM$_{131}$] block copolymer was investigated by cyclic voltammetry at 70 °C. The results are shown in Figure 5.9. The anodic breakdown potential of the sample was close to 4.3 V vs Li$^+$/Li. At such value, the current increase was likely associated with the partial decomposition of ethylene oxide containing moieties and TFSI functional groups in the polymer electrolyte.[265] The peaks intensity largely decreased during the second cycle, along with an anodic limit shifting to about 4.5 V vs Li$^+$/Li, most likely originating from a passivation layer growth at the electrode/electrolyte interface. On the other hand, the first cathodic reduction presents almost undetectable current peaks likely associated to the reduction/decomposition process of residual solvent traces from the synthesis. Indeed, a highly reversible couple of peaks were observed between −0.5 and 0.5 V versus Li$^+$/Li, which are associated with the lithium plating/stripping process, confirming the efficient transfer of lithium ions through the polyelectrolyte. The value of ESW obtained for the newly synthesized block copolymer accounts for stable and safe operation with cathodes operating at medium-high voltage (< 4.5 V versus Li$^+$/Li), such as commercially available LiFePO$_4$, mixed phosphates and LiCoO$_2$.
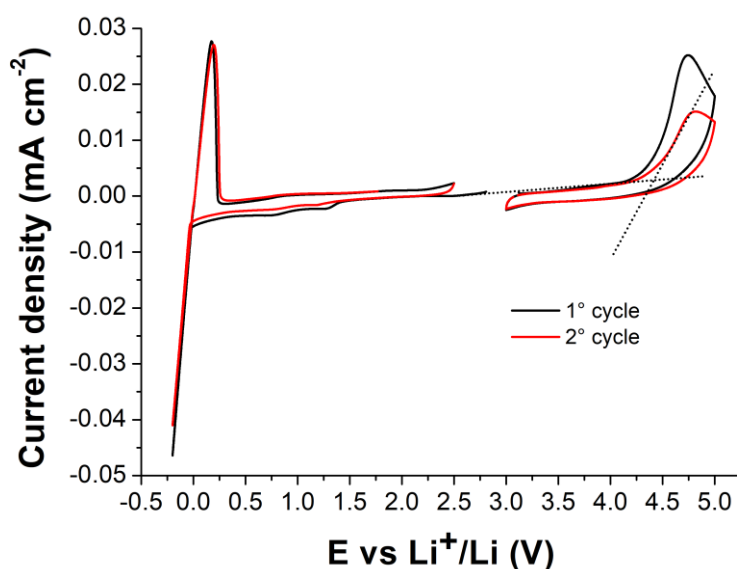
Figure 5.9 Anodic and cathodic stability window for poly[(LiM$_{17}$-r-PEGM$_{86}$)-b-PhEtM$_{131}$] obtained by CV at 70 °C (carbon coated Al and Cu as the working electrode and Li foil as counter and reference electrodes, scan rate 0.1 mV s^{-1}).

Laboratory scale Li-metal cell testing

The electrochemical stability of poly[(LiM$_{17}$-r-PEGM$_{86}$)-b-PhEtM$_{131}$] block copolymer was further confirmed by galvanostatic cycling (Figure 5.10 and Figure 5.11) in the lab-scale cell with a composite LiFePO$_4$-based cathode in the voltage range between 2.5 V and 4 V vs Li$^+$/Li. The LFP-based electrode was prepared in the form of a catholyte using poly[(LiM$_{17}$-r-PEGM$_{86}$)-b-PhEtM$_{131}$] block copolymer as the ion conductive binder (preparation procedure and electrode active material loading are reported in chapter 3). The electrochemical behaviour of the all-solid-state lab-scale cell was investigated by galvanostatic cycling at 70 °C at increasingly high C rates (C/n, n = 20, 10, 5) calculated from the theoretical specific capacity of LFP active material (170 mAh g^{-1}). The rate capability test performed at different C rates (Figure 5.10a) resulted in specific capacity retention above 95 % while moving from C/20 to C/5.
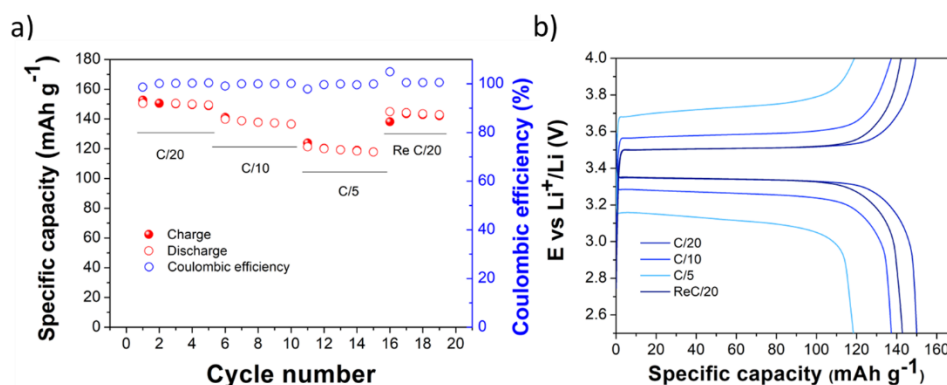
Figure 5.10 Galvanostatic cycling behaviour of Li/poly[(LiM$_{17}$-r-PEGM$_{86}$)-b-PhEtM$_{131}$]/LFP solid-state cells at 70 °C. Specific capacity vs cycle number dependence (a), and corresponding charge/discharge voltage vs specific capacity profiles at a constant current rate (b) of C/20, C/10 and C/5.

Figure 5.10b shows clean potential versus specific capacity profiles and typical flat plateaus even upon increasing the current regime, indicating a highly reversible and stable single-phase de-/insertion (charge/discharge) mechanism from/in the LiFePO$_4$/FePO$_4$. The slight overpotential increase (up to ~0.2 V at C/5) was likely ascribed to the relatively high complex viscosity of the polyelectrolyte, which limits the mobility of the side chains and the overall Li$^+$ conduction. The excellent Coulombic efficiency and capacity retention at C/20 current rate and after several

cycles at higher C rates clearly point out the remarkable electrolyte compatibility with both Li metal and LFP with no electrolyte degradation and/or severe passivation reactions (Figure 5.10a). Improved mechanical properties of poly[(LiM$_{17}$-r-PEGM$_{86}$)-b-PhEtM$_{131}$] in comparison with poly[LiM$_{17}$-r-PEGM$_{86}$] along with suitable ionic conductivity allowed stable and efficient charge/discharge cycling (> 150 mAh g^{-1}) at the first cycle, which corresponds to >94% of the practical specific capacity (158 mAh g^{-1} at C/20) provided by the commercial LFP used as the active material when cycled with a standard LP30 liquid electrolyte (Figure 5.10a). Excellent cycling stability and capacity retention were demonstrated even upon prolonged cycling, with coulombic efficiency values approaching 100 % during the whole cycling test, in which the lab-scale Li metal polymer cell was able to deliver 131 mAh g^{-1} after more than 75 cycles with a capacity retention of 87 % (Figure 5.11).
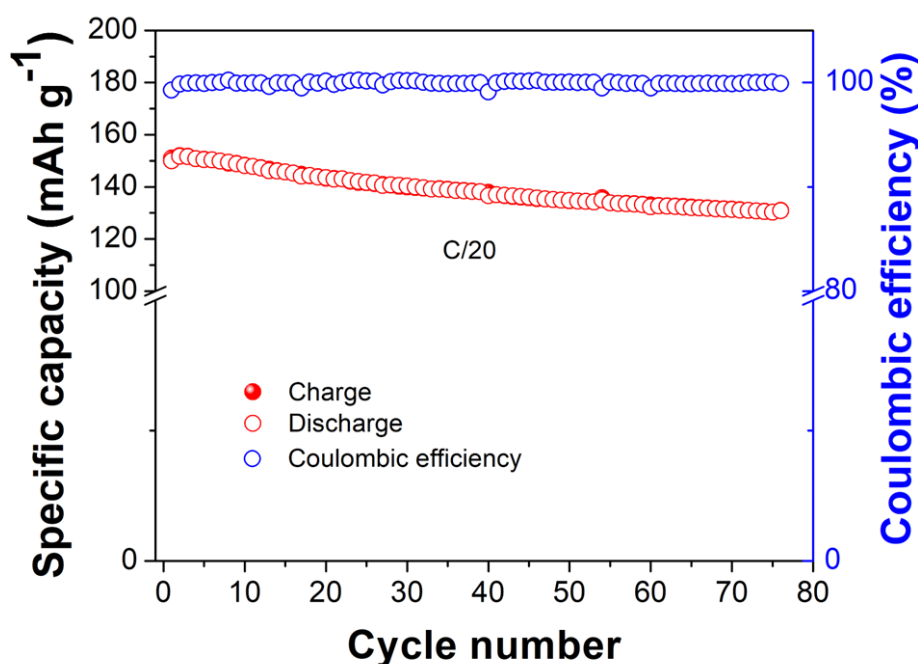
Figure 5.11 Galvanostatic cycling behaviour of Li/poly[(LiM$_{17}$-r-PEGM$_{86}$)-b-PhEtM$_{131}$]/LFP solid-state cells at C/20 and 70 °C.

Overall, this is an excellent result, especially considering the active material loading (3.89 mg cm^{-2}), which is sufficiently high for a truly solid lab-scale polymer

electrolyte cell [266] and can be considered relevant to gain information for practical application devices.[267] The remarkable electrochemical performance in terms of high-capacity output and capacity retention after more than 75 consecutive charge/discharge cycles at C/20 rate is likely ascribed to the efficient ion transport in the solid polymer electrolyte and the favourable charge transport thanks to the optimal electrode/electrolyte interface in the cell.

5.3 Conclusions

In this chapter, we described the synthesis, thermo-mechanical, chemico-physical and electrochemical properties of novel single-ion conducting block co-polymers (A-b-B), possessing randomly distributed Li-conducting and ion-solvating segments in the first block (A), which is accompanied by incompatible poly(2-phenylethyl methacrylate) block (B) providing mechanical strength and initiating phase segregation. Such poly[(LiMn-r-PEGMm)-b-PhEtMk] copolymers were synthesized by segmental RAFT copolymerization, allowing to control the length of both blocks. The comprehensive study carried out on novel materials and synthetic approaches enlightened the promising prospects on the use of safe, electrochemically stable singe-ion conducting electrolytes in advanced solid-state Li-metal based battery technologies.

Chapter 6

6 Novel ionic liquid monomer for high performing solid-state single ion conducting polymer electrolytes

6.1 Introduction

As previously stated in chapter 2 (paragraph 2.1.2), the mobility of the SICPEs side chains carrying the anion moiety (polyanions) has a fundamental role in the Li$^+$ ion transport and conductivity. The first example of single-ion conducting homopolymer derived from LiSTFSI and LiMTFSI ILMs were characterized by high T_g of 152 and 95 °C, respectively, and limited ionic conductivity. Later, the copolymerization with polyethylene oxide (PEO) and poly(ethylene glycol) methyl ether methacrylate (PEGM) allowed to drastically enhance the mobility of anchored coordinating anionic group, resulting in SICPEs with T$_g$ values ranging between –20 and –60 °C and t$_{Li}^+$ of about 0.9.[180,201,203,227] Thus, the beneficial effect of having several ethylene oxide units in the structure of the SICPE, promoting the Li$^+$ ion hopping between anion centres, was confirmed.[189] However, despite the significant upgrades, the limited ambient temperature ionic conductivity and specific capacity, especially at elevated current rates (C/n), were and still are one of the main bottlenecks for the application of SICPEs in practical batteries. The significant decrease in conductivity moving from salt-in-polymer to SICPEs is attributed to the role that anion motion plays in the conduction mechanism in these polymer electrolytes.[177] The main limiting factor for achieving higher ionic conductivity lies in the poor mobility of coordinating anions.

Based on the literature knowledge and the results shown previously, carried out in collaboration with Prof. Alexander S. Shaplov at the LIST institute of Luxemburg, this chapter details the synthesis procedure of a novel ILM characterized by elongated ethylene oxide in comparison to the well know LiMTFSI and the preparation of related copolymer with PEGM. The free-radical polymerization technique was exploited to prepare a set of copolymers with different ILM:PEGM molar ratios. The best sample showed ionic conductivity values of 3.0×10^{-6} and 3.8×10^{-5} S cm^{-1}, respectively, at 25 and 70 °C, and it was further characterized from the chemical-physical and electrochemical viewpoints to get a full comparison with the similar copolymer based on PEGM and LiMTFSI monomers previously prepared. The complete miscibility between the new monomer (ILM53) and PEGM, along with the enhanced -EO- units number, allowed to boost the side-chain mobility, responsible for Li$^+$ hopping through the polymer electrolyte and consequently reach high ionic conductivity values in a wide range of temperature, despite the limited amount of PEGM. The synergic effect of -EO- units in the ILM main chain and the limited amount of non-ionic monomer (PEGM) allowed to prepare copolymers characterized by superior mechanical and electrochemical properties, especially in terms of enhanced performance at high current rates. In addition, a truly solid-state Li-metal lab-scale cell with the novel copolymer demonstrated remarkable capacity output and capacity retention after more than 200 consecutive charge/discharge cycles at C/5 rate at 70 °C, actually outperforming the copolymer based on PEGM and LiMTFSI monomers.

6.2 Results and discussion

6.2.1 Synthesis of α-methacryloyl-ω-3-(trifluoromethylsulfonylaminosulfonyl)propyl-poly(ethylene glycol) lithium ionic monomer (ILM53)

The new ILM synthesis was carried out by the Department of Macromolecular Chemistry research group (Saint-Petersburg State University, Russia) following the procedure reported in Scheme 6.1.
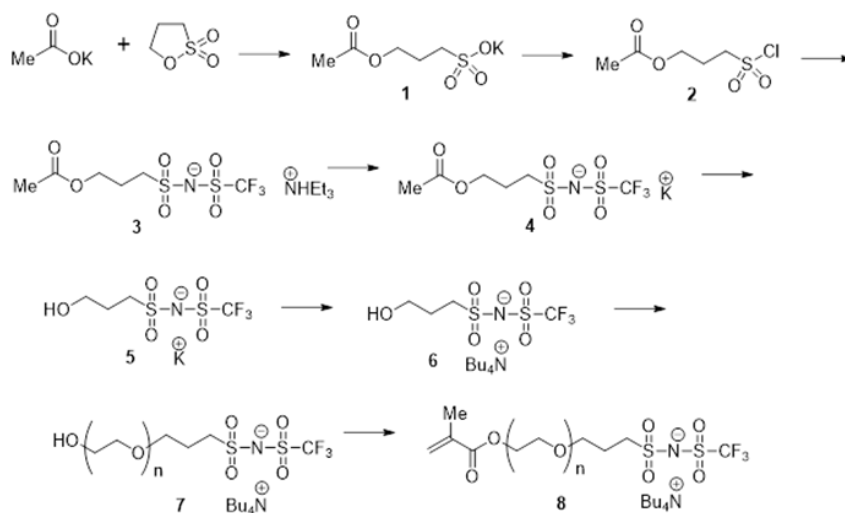
Scheme 6.1 Synthetic route followed for the preparation of the monomer ILM53.

1. *Potassium 3-acetoxypropane-1-sulfonate*

Potassium acetate (9.814 g, 0.1 mol) and propanesultone (12.244 g, 0.1002 mol) were refluxed in acetonitrile (45 mL) for 4.5 h. Diethyl ether (45 mL) was added after cooling. The product was filtered, washed with ether, and dried under vacuum. White powder product was obtained. Yield: 94.4%. NMR (D_2O) 4.16 (t, 2H) 2.96 (m, 2H), 2.05 (m, 2H), 2.03 (s, 3H).

2. *3-(chlorosulfonyl)propyl acetate*

Thionylchloride (98.5, 0.8279 mol) was gradually added to 1 (20.70 g, 93.97 mmol) in DMF (1 mL). After stirring for 24 h, the mixture was poured into an ice bath (500 mL) to quench the thionylchloride, followed by extraction with DCM (50 ml for 3 times). The extract was washed with brine (100 mL for 6 times), dried with anhydrous sodium sulfate and passed through a silica column. DCM was rotary evaporated, and the product was stirred under vacuum for 12 h to remove all traces of solvent. A colourless oil product was obtained. Yield: 90.8%. NMR (CDCl$_3$): ^{1}H NMR (400 MHz, CDCl$_3$) δ 4.21 (t, 2H, J = 6.0 Hz, CH$_2$O), 3.76 (m, 2H, CH$_2$SO$_2$), 2.35 (m, 2H, CH$_2$CH$_2$SO$_2$), 2.06 (s, 3H, CH$_3$). ^{13}C NMR (101 MHz, CDCl$_3$) δ 170.49, 62.15, 60.92, 24.01, 20.63.

3.   *AP-TFSI   TEA   triethylammonium   (3-acetoxypropylsulfonyl) (trifluoromethylsulfonyl) imide*

Triethylamine (24.38 g, 0.241 mol) was added under argon atmosphere to the precooled solution of trifluoromethanesulfonamide (16.34 g, 0.1096 mol) in THF (100 mL) at 0 °C. 2 (21.99 g, 0.11 mol) was dissolved in THF (30 mL) and added dropwise in one hour. The mixture was left under stirring for 1 hour at 0 °C and 4 hours at 20 °C; then filtration and solvent evaporation were performed. The residue was dissolved in DCM (150 mL), washed with water (3 times × 15 mL), and stirred overnight with anhydrous magnesium sulfate and charcoal. The product obtained after filtration and solvent evaporation under vacuum was likely light brown oil. Yield: 95.2%. ^{1}H NMR (400 MHz, DMSO) δ 8.83 (br. s, 1H, NH), 4.08 (t, 2H, J = 6.5 Hz, CH$_2$O), 3.11 (q, 6H, J = 7.3 Hz, Et-1), 3.03 (m, 2H, CH$_2$SO$_2$), 2.00 (s, 3H, CH$_3$), 1.97 (m, 2H, CH$_2$CH$_2$SO$_2$), 1.18 (q, 9H, J = 7.3 Hz, Et-2). ^{13}C NMR (101 MHz, DMSO) δ 170.30 (COO), 120.12 (q, J = 324.4 Hz, CF$_3$) 62.26 (CH$_2$O), 51.28 (CH$_2$SO$_2$), 45.84 (Et-1), 23.49 (CH$_2$CH$_2$SO$_2$), 20.59 (CH$_3$), 8.59 (Et-2). ^{19}F NMR (376 MHz, DMSO) δ -77.28.

4. *AP-TFSI K potassium (3-acetoxypropylsulfonyl) (trifluoromethylsulfonyl) imide*

Product 3 (63.731 g, 0.15376 mol) and potassium carbonate (49.527 g, 0.2583 mol) were refluxed in acetonitrile (150 mL) for 1.5 h. The mixture was diluted with acetonitrile (100 mL), the excessive potassium carbonate was separated by decantation. After mixing with MTBE (150 mL) the product was allowed to

crystallize overnight. Yield: 91.3%; crystallization from propanol-2 (500 mL) gave white crystals, yield 77.5%, m.p. 133-136°C ^{1}H NMR (400 MHz, DMSO) δ 4.08 (t, 2H, J = 6.5 Hz, CH$_2$O), 3.03 (m, 2H, CH$_2$SO$_2$), 2.01 (s, 3H, CH$_3$), 1.97 (m, 2H, CH$_2$CH$_2$SO$_2$).

5.   *HP-TFSI   K   potassium   (3-hydroxypropylsulfonyl)(trifluoromethylsulfonyl)imide*

Product 4 (41.024 g, 0.11675 mol) and anhydrous potassium carbonate (1.15 g, 0.00832 mol) were stirred at 35 °C for 6 h. The solution was filtered, the solvent evaporated under vacuum, and the residue redissolved in 1,4-dioxane. The solvent was removed in vacuum, MTBE (100 mL) was added, and the mixture stirred overnight. The product was filtered and dried under vacuum. Yield 97.9 % ^{1}H NMR (400 MHz, DMSO) δ 3.45 (t, 2H, J = 6.3 Hz, CH$_2$OH), 2.99 (m, 2H, CH$_2$SO$_2$), 1.80 (m, 2H, CH$_2$CH$_2$SO$_2$).

6.   *HP-TFSI   TBA   tetrabutylammonium   (3-hydroxypropylsulfonyl)(trifluoromethylsulfonyl)imide*

Product 5 (23.2 g, 0.075 mol) was suspended in water (20 mL) and mixed with TBAB (24.434 g, 0.082 mol). The product was extracted with DCM/ethylacetate (4:1, 300 mL) and washed with water (40 times × 20 mL) until it gave negative halogenide test (with 1 % AgNO$_3$ solution). After drying with sodium sulfate and solvent removal the product was isolated as a liquid, which solidified after a few months storage over phosphorous pentoxide in vacuum. The product was obtained in form of colourless crystals, m.p. : 29 – 31°C. Yield 44.8 %. ^{1}H NMR (400 MHz, DMSO) δ 4.54 (t, 1H, J = 5.5 Hz, HO), 3.46 (m, 2H, CH$_2$OH), 3.17 (m, 8H, Bu-1), 2.99 (m, 2H, CH$_2$SO$_2$), 1.81 (m, 2H, CH$_2$CH$_2$SO$_2$), 1.57 (m, 8H, Bu-2), 1.31 (q, 8H, J = 7.3 Hz, Bu-3), 0.94 (t, 12H, J = 7.3 Hz, Bu-4). ^{13}C NMR (101 MHz, DMSO) δ 120.15 (q, J = 324.4 Hz, CF$_3$), 59.31 (CH$_2$OH), 57.54 (Bu-1), 51.97 (CH$_2$SO$_2$), 27.28 (CH$_2$CH$_2$SO$_2$), 23.04 (Bu-2), 19.14 (Bu-3), 13.38 (Bu-4).

7.   *HO-PEG10-TFSI   TBA   α-hydroxyl-ω-3-(trifluoromethylsulfonylaminosulfonyl)propyl-poly(ethylene   glycol) tetrabutylammonium salt*

Product 6 (4.614 g, 0.09 mol) was dissolved in THF (10ml) in a 100 mL Schlenk, then DBU (0.228 g, 15 mmol) and 1M triethylborane THF solution (2.40

mL) were gradually introduced via syringe to the solution under stirring. Ethylene oxide (4.892 g, 0.111 mol) was distilled via a cannula in the flask at –20 °C. The mixture was warmed up in a water bath and left under stirring overnight at 32 °C. Note: the reaction is exothermic, higher bath temperature and smaller flask volume may lead to overheating and gas leakage. Volatile species were removed under vacuum. In order to quench boranes, 10 ml of acetic acid was added, and then the mixture was briefly heated to 120 °C and mixed for 2 min. Note: the traces of boranes cause direct polymerization in the following step. The oily product was dried under vacuum, washed 4 times with MTBE, dissolved in DCM (50 mL) and washed with water (10 mL × 3 times). The extract was passed through anhydrous sodium sulfate and dried under vacuum. The obtained colourless oily product was stored in vacuum over phosphorous pentoxide. Yield 91.1%. ^{1}H NMR (400 MHz, DMSO) δ 4.54 (t, 1H, J = 5.5 Hz, HO), 3.51 (m, 46H, CH_2O), 3.16 (m, 8H, Bu-1), 2.99 (m, 2H, CH_2SO_2), 1.87 (m, 2H, $CH_2CH_2SO_2$), 1.57 (m, 8H, Bu-2), 1.31 (q, 8H, J = 7.3 Hz, Bu-3), 0.94 (t, 12H, J = 7.3 Hz, Bu-4).

8. *MA-PEG10-TFSI TBA α-methacryloyl-ω-3-(trifluoromethylsulfonylaminosulfonyl)propyl-poly(ethylene glycol) tetrabutylammonium salt*

Product 7 (14.300 g, 15 mmol) was solubilized in THF (40 mL) and added to the mixture of methacrylic acid (12.91 g, 150 mmol), DMAP (0.916 g, 7.5 mmol) and DCC (24.76 g, 120 mmol) in THF (80 mL) at 10 °C gradually in one hour. After 12 h MEHQ (100 mg) was added as a stabilizer, and stirring was continued for 12 h. The white precipitate (DCC) was filtered off and washed with THF. The solvent was removed in vacuum, and the oily product was diluted with methanol (20 mL) and stirred for 10 min at 40 °C (to convert methacrylic anhydride into MMA and MA). The volatile species were removed in vacuum. The residue was redissolved in water (100 mL) and stirred for 1 h with charcoal (c.a. 7 g) for 2 h. After filtration, the product was extracted with DCM (3 times × 100 mL), washed with tetrabutylammonium chloride solution (0.125 g, 0.45 mmol in 30 mL of water) to eliminate traces of DMAP, then with water (4 times × 30 mL) and dried over magnesium sulfate. Evaporation of solvent and drying under vacuum gave colourless oily product. Yield: 43.2 %. NMR ESI MS(-): calc. for $C_{28}H_{51}F_3NO_{16}S_2-$: 778.2607 found: 778.2598. ^{1}H NMR (400 MHz, DMSO) δ 6.03 (s, 1H, =CHH), 5.68 (s, 1H, =CHH), 4.21 (t, 2H, J = 4.7 Hz, $COOCH_2$), 3.66

(t, 2H, J = 4.7 Hz, CH$_2$CH$_2$OOC), 3.51 (m, 42H, CH$_2$O), 3.17 (m, 8H, Bu-1), 2.99 (m, 2H, CH$_2$SO$_2$), 1.89 (m, 5H, CH$_2$CH$_2$SO$_2$, CH$_3$C=), 1.58 (m, 8H, Bu-2), 1.32 (q, 8H, J = 7.3 Hz, Bu-3), 0.94 (t, 12H, J = 7.3 Hz, Bu-4). ^{13}C NMR (151 MHz, DMSO) δ 166.45 (COO), 135.79 (=CCH$_3$), 125.65 (CH$_2$=), 120.13 (q, J = 323.4 Hz, CF$_3$), 69.79 (CH$_2$O), 69.44, 68.55, 68.24, 63.68 (CH$_2$OOC), 57.57 (Bu-1), 51.73 (CH$_2$SO$_2$), 24.29 (CH$_2$CH$_2$SO$_2$), 23.06 (Bu-2), 19.16 (Bu-3), 17.86 (CH$_3$C=), 13.36 (Bu-4). ^{19}F NMR (565 MHz, DMSO) δ -77.32.

6.2.2 Free radical polymerization of homo- and co-polymers

Once completed the synthesis of the novel ionic monomer, NMR spectroscopy and mass spectrometry (MS) were employed as reliable methods to evaluate the monomer structure. Then, free radical homo-polymerization of ILM53 was carried out. Free radical polymerization was performed in DMF with 0.1 wt.% of AIBN at 60 °C and a concentration of 33 wt.% ([monomers]:[DMF]=1:3 by wt.), allowing for the preparation of polymers with high yields of 80-85 %. The resulting polymer electrolyte was characterized by low molecular weight and a suitable polydispersity index (M$_n$ = 30100 g mol^{-1}, PDI = 1.6). Aimed to obtain comparable results with previously synthesized polymer electrolytes,[130,189,219] to achieve good film-forming ability and mechanical properties, the amount of AIBN was decreased to 0.05 wt.%. It resulted in SICPEs with higher molecular weight (cit effect amount AIBN) (see PIL53 in Table 1). As previously mentioned in paragraph 2.1.2, there is already a large volume of information about the copolymerization of the well-known lithium 1-[3-(methacryloyloxy)propylsulfonyl]-1-(trifluoromethylsulfonyl)imide (LiTFSI) with non-ionic monomer prevalently containing ethylene oxide units and meth/acrylate functional groups, such as poly(ethylene glycol) methyl ether methacrylate (PEGM).[189,201,202,207] This study aims to determine the effect of additional –EO– units along the flexible chain of ionic monomers on the resulting copolymer and homopolymer electrochemical performance. Then, ILM53 was copolymerized with PEGM providing a set of copolymers that differ in the molar ratio between ionic monomer and PEGM (Table 1, coPIL 1-3). PEGM was chosen due to the presence of oxyethylene fragments along its side chain, similarly to PEO,[249] expected to improve the solubility of ionic species and facilitate their dissociation, resulting in an overall enhancement of the ionic conductivity of copolymers.

Table 6.1 Properties of homopolymer (PolyIL53) and copolymers (poly(PEGM$_n$-r-ILM53$_m$) obtained by free radical polymerization.

Polymer	M_n (SEC)[a] (g mol^{-1})	[ILM53]/[PEGM] (Theor molar ratio)	Yield (%)	M_w/M_n (SEC)[a]	σ (S cm^{-1})		T_g (°C)[b]	T_{onset} (°C)[c]
					25 °C	70 °C		
PIL53	61900	-	78	1.9	9.2×10^{-8}	9.8×10^{-6}	-14	235
coPIL1	79500	01:01	76	5.5	1.2×10^{-6}	3.1×10^{-5}	-15	210
coPIL2	83900	02:01	74	5.6	3.0×10^{-6}	3.8×10^{-5}	-46	210
coPIL3	85900	04:01	76	5.8	1.2×10^{-6}	1.8×10^{-5}	-49	210

[a] By GPC in 0.1 M solution of LiTFSI in DMF at 50°C with PMMA standards.

Besides both monomers being readily soluble in water, acetonitrile, and aprotic polar solvents (e.g. DMF, DMSO, DMA), DMF was selected as the best option, especially for its solubilization ability towards ILMs and to ensure a reliable comparison with previous literature reports.[189,199] The polymerization was stopped after 36 h by cooling down the reaction tube and adding 4-methoxyphenol inhibitor. The reaction time allowed to obtain copolymer with comparable molecular weight along with suitable polydispersity index (PDI), see Table 6.1. Finally, the cation exchange with LiCl 0.1M solution was performed to replace the triethylammonium with lithium cations. The composition and purity of already synthetized copolymers were confirmed by means of ^{1}H NMR.

Table 6.2 Comparison between homo/copolymers obtained with PEGM and LiMTFSI and ILM53 ionic monomers.

Polymer	M_n (SEC) (g mol^{-1})	[PEGM]/[ILM53] or [LiMTFSI][d]	M_w/M_n (SEC)	σ at 25°C (S cm^{-1})	T_g (°C)[c]	Ref
PIL53	61900 [a]	-	1.9 [a]	**9.2x10^{-8}**	-14	This chapter
poly (LiMTFSI)	52700 [b]	-	1.2 [b]	**1.1x10^{-12}**	95	201
RAFT poly(PEGM)-b-poly(LiMTSI)1	25000 [b]	4.2:1	1.4 [b]	**2.3x10^{-6}**	-61	201
RAFT poly(PEGM)-b-poly(LiMTSI)2	31300 [b]	3.2:1	1.5 [b]	1.5x10^{-6}	-51	201
RAFT poly(PEGM)-b-poly(LiMTSI)3	38300 [b]	02:01	1.5 [b]	1.2x10^{-6}	-41	201
RAFT poly(PEGM)-r-poly(LiMTFSI)	80200 [b]	01:01	1.3 [b]	1.1x10^{-7}	-7	201
poly(PEGM)-r-poly(LiMTFSI)	457000 [b]	9.9:1	4.6 [b]	6.3x10^{-8}	-57	189
coPIL1	79500 [a]	01:01	5.5 [a]	1.2x10^{-6}	-15	This chapter
coPIL2	83900 [a]	02:01	5.6 [a]	**3.0x10^{-6}**	-46	This chapter
coPLI3	85900 [a]	04:01	5.8 [a]	1.2x10^{-6}	-49	This chapter

[a] By GPC in 0.1 M solution of LiTFSI in DMF at 50 °C. [b] By GPC in 0.1 M LiCl acetonitrile/water mixture (1:4 v/v). [c] By DSC. [d] Theoretical PEGM:Ionic monomer molar ratio.

6.2.3 Chemical-physical and electrochemical characterization

Ionic conductivity

Ionic conductivity (σ) values as a function of temperature were recorded by EIS and applying Equation 9 (Table 6.1, chapter 3). Before EIS measurements, samples were heated at 60 °C (1h) and, subsequently, equilibrated at 20 °C for 3h, to ensure optimal interfacial contact with the stainless steel blocking electrodes. As reported in Table 1, coPIL2 shows the highest ionic conductivity values, being 3.0×10^{-6} and 3.8×10^{-5} S cm^{-1}, respectively, at 25 and 70 °C. As shown in Table 6.2, the comparison between PIL53 and poly(LiMTFSI) revealed a substantial improvement in the ionic conductivity of the newly synthesized homopolymer, likely ascribable to the presence of longer ethylene oxide side chain directly linked

to the TFSI⁻ functional groups. As predicted, the copolymerization of IL53 with PEGM enhances the ionic conductivity of the solid-state polymer electrolyte, boosting the mobility and the coordination of lithium cations. The coPILs 1-3 conductivity increased by two orders of magnitude at 25 °C in comparison with the homopolymer, reaching values above 10^{-5} already at 60 °C. The quasi-linear Arrhenius behaviour observed in Figure 6.1 suggests that lithium ions diffusion occurs prevalently through isolated hopping on the pendant sulfonamide groups but also results from the local segmental motion of coordination sites in the polymer main chain. Indeed, the data trend reported in Figure 6.1 evidences a slight decrease in conductivity, increasing the [PEGM]:[ILM53] ratio from 2:1 to 4:1. A possible explanation for this behaviour might be that an excess of non-ionic part limits/hinders the hopping along with the anion moieties, reducing the overall conductivity.

Moreover, considering that the conductivity difference between copolymers prepared either by RAFT or conventional free radical polymerization can be directly linked to the difference in their molecular weights, when the parent homopolymers are completely miscible, we found it of further interest to compare the conductivity values of coPIL1-3 copolymers with that of poly(PEGM)-b-poly(LiMTFSI) block copolymers previously synthesized as reported in Table 6.2.

Noteworthy, ionic conductivity values for block copolymers comprising PEGM and LiMTFSI in different molar ratios are similar or even lower to coPIL1-3. Specifically, in the whole range of investigated temperatures, the ionic conductivity of coPIL2 is higher than the one of poly(PEGM)-b-poly(LiMTSI)1 copolymer (Table 6.2) prepared by RAFT polymerization, although the [EO]/[Li] theoretical ratio is slightly lower (i.e., 30 vs 36). Finally, considering the relatively high molecular mass of newly prepared block copolymers, it may be assumed that the direct insertion of ethylene oxide units into the ionic monomer main chain greatly enhances the ionic conductivity, without the need of increasing the quantity(length) of non-ionic blocks (PEGM monomer).
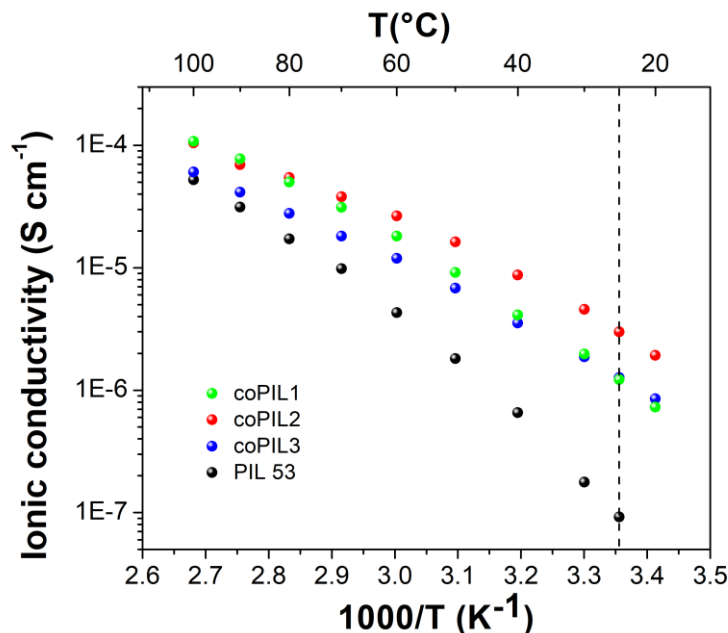
Figure 6.1 Ionic conductivity vs temperature (from 20 to 100 °C) for the copolymer coPIL1-3 and homopolymer PIL 53.

Thermal analysis

The obtained ionic copolymers appeared as rubber or wax-like materials depending on the temperature. The thermal properties of the new set of copolymers were determined by DSC and TGA (Figure 6.2). DSC was used to determine the glass transition temperatures (Table 6.1, Figure 6.2a). The homopolymer PIL53 shows a T_g of –14 °C (Table 6.1, Figure 6.2a). As for the comparison reported in Table 6.2, this value is significantly lower when compared to the previously synthesized PIL based on the LiMTFSI ionic monomer. The short-chain length of LiMTFSI drastically hinders the mobility of the resulting polymer. Indeed after the precipitation/purification step, the poly(LiMTFSI) is white solid/powder material; meanwhile, PIL53 sample is a rubber-like material. As already demonstrated and reported in chapter 2, the increment of ethylene oxide units in the polymer architecture reduces T_g values, which correspondingly enhances the mobility of side chains.[207] Here, for the first time, the same principle was applied directly during the synthesis of the ionic monomer introducing several ethylene oxide units in the main chain, thus having a long and flexible segment with anchored TFSI⁻ moiety. This

preparation allowed the obtainment of homopolymers with low T_g, even without additional PEGM monomers. The coPIL1 sample, although containing a more significant number of –EO– units, showed T_g similar to the PIL53, while coPIL 2 and 3 showed glass transitions at –46 and –50 °C, respectively. The beneficial effect of PEGM on decreasing the T_g is probably mitigated by the already low glass transition temperature of PIL53 homopolymer, and a relatively high amount of co-monomer is necessary to observe a considerable variation. The presence of a single glass transition temperature proves that the newly prepared ionic monomer ILM53 is similar to PEGM in terms of polarity and hydrophilicity, thus they are fully miscible.
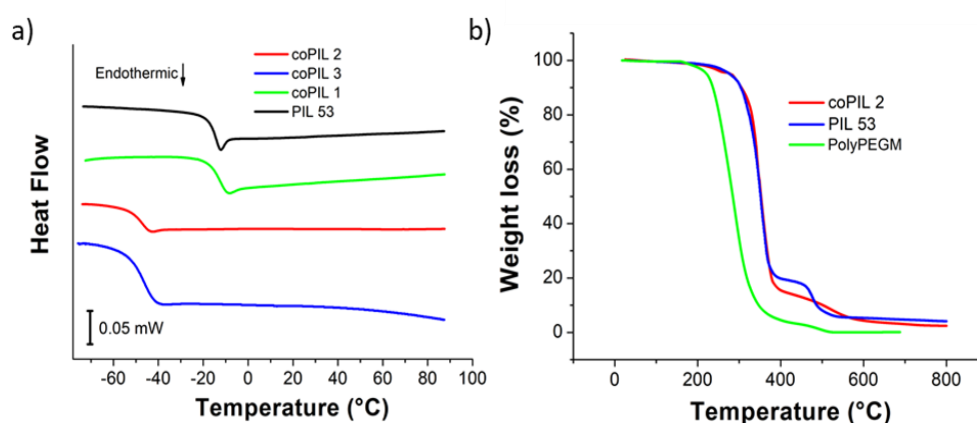
Figure 6.2 DSC (a) and TGA (b) traces of copolymers and homopolymer.

Previous studies reported that the operating temperature range of lithium-based cells is a crucial parameter to be envisaged when developing new materials. Considering the various possible practical applications, from portable electronic devices to the transportation and stationary fields, the thermal stability of the solid-state SICPE should guarantee stable and safe operation in a wide range of temperatures, generally between –20 and 80 °C.[268–270] Therefore, determining the safe temperature operation limits for the new family of copolymers is a fundamental analysis.

The thermal degradation behaviour of the polymer materials under investigation was assessed via thermogravimetric analysis (TGA) in air flow. The coPIL 2 was selected as a reference sample for further characterizations, being the best sample in terms of ionic conductivity. The TGA plot of all the other prepared coPILs is shown in Figure 6.2b. T_{onset} value of coPIL2 is slightly lower when compared to the parent PIL53, but both samples are thermally stable up to at least 220 °C, the temperature at which decomposition starts to occur. These results are especially relevant considering the flammability of conventional organic carbonate electrolyte mixtures commonly used in commercial LIBs, which become thermally unstable already above 80 °C.[49] Indeed, the very flat TGA plateau and the absence of weight loss variations up to 220 °C is an additional benefit that clearly confirms the absence of solvent/water residue from the synthesis, thus the purity of the synthesized samples.

Rheological properties

The rheological properties of sample coPIL2 were analysed in a small amplitude oscillatory flow mode at 25 and 70 °C. Figure 6.3a shows the complex viscosity evolution as a frequency function at 25 and 70 °C. At 1Hz, the complex viscosity of coPIL53 shifts from 750 to 156 Pa.s at 25 and 70 °C, respectively. At both temperatures, the complex viscosity decreases linearly with the frequency. Figure 6.3 b and c show the variation of loss and storage moduli as a function of the frequency at 25 and 70 °C. The absence of a plateau at the lowest frequencies is characteristic of a branched polymer. The loss moduli, both at 25 and 70 °C, are higher than the storage moduli, indicating the viscous contribution predominates over the elastic contribution, which is characteristic of an uncrosslinked polymer. Although both copolymers exhibited viscous behaviour instead of elastic one, the sample coPIL2 showed improved viscosity values in the range of explored frequencies. We could assume that the limited content of PEGM units and the slight T_g increase allowed to achieve enhanced mechanical properties compared to previous copolymers based on LiMTFSI and PEGM (Table 6.2).
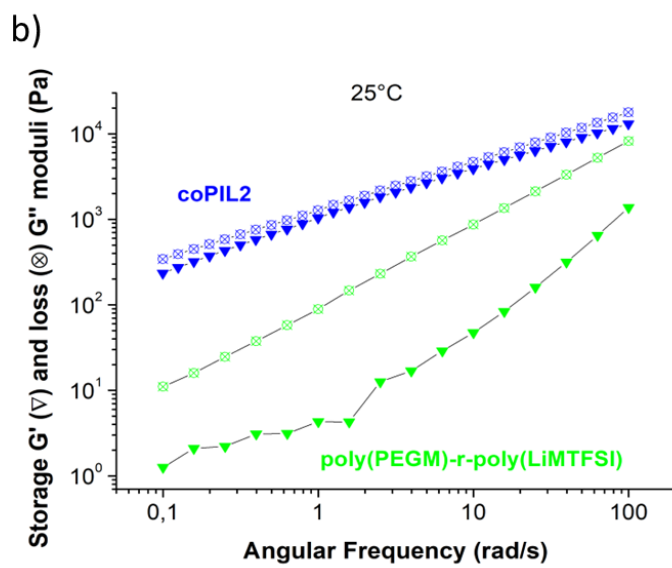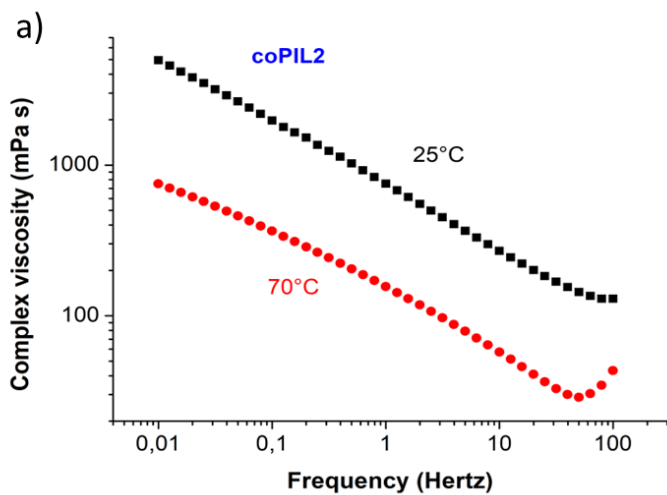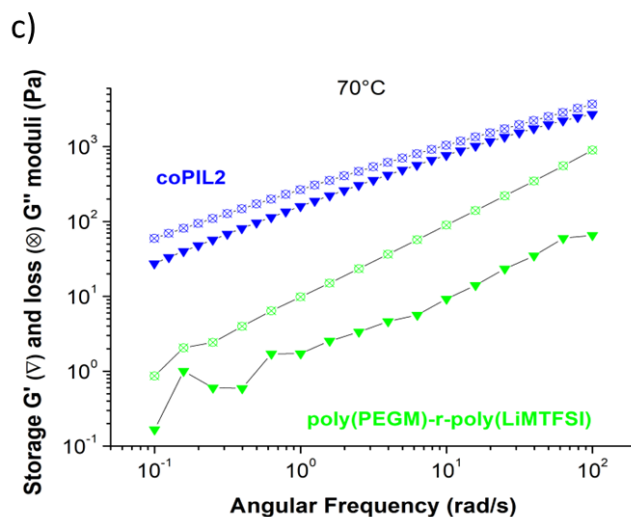
Figure 6.3 Temperature dependence of the complex viscosity of coPIL2 sample (a) and frequency dependence of the storage modulus G' (full symbols) and the loss modulus G" (open symbols) obtained at 25 °C (b) and 70 °C (c) for coPIL2 and poly(LiM-r-PEGM).[189]

Electrochemical stability, transference number and compatibility with Li metal

Evaluating the electrochemical stability window (ESW) is particularly important to establish the voltage range at which the electrolyte can work without undergoing unwanted degradation processes, which may account for performance decay during cycling and cause eventual cell failure. The ESW of coPIL2 was evaluated by cyclic voltammetry at 70 °C of two distinct lithium metal half-cells in which the polymer electrolyte was in contact with the inert copper electrode (cathodic scan) and carbon-coated aluminium electrode (anodic scan): the voltage window was scanned from the open-circuit voltage (OCV) to –0.5 V and +5 V vs Li$^+$/Li redox potential, respectively. The results are shown in Figure 6.4. The anodic breakdown potential of the sample approaches 4.5 V vs Li$^+$/Li, which accounts for suitable stability toward oxidative process at high potential allowing reversible operation with commonly used commercial LIB cathodes, such as LiFePO$_4$ and LiCoO$_2$. Generally, electrolyte anodic stability is determined by the oxidative stability of the anion, and thus, the steep increase of current close to 4.5 V is probably associated with the decomposition of the TFSI$^-$ functional group of the

polymer.[130] During the following voltametric cycles, the anodic limit slightly increased, which is likely explained by the growth of a passivation layer at the electrode/electrolyte interface. At cathodic potential values, a well-defined couple of peaks was clearly observed between −0.5 and +0.5 V vs Li^+/Li, easily ascribed to highly reversible lithium plating/stripping processes. It confirmed the efficient transfer of lithium ions through the polymer network and at the polymer/electrode interface. No additional peaks are visible either during anodic or cathodic scans, confirming the absence of monomer and/or solvent residues from the synthesis or water impurities.
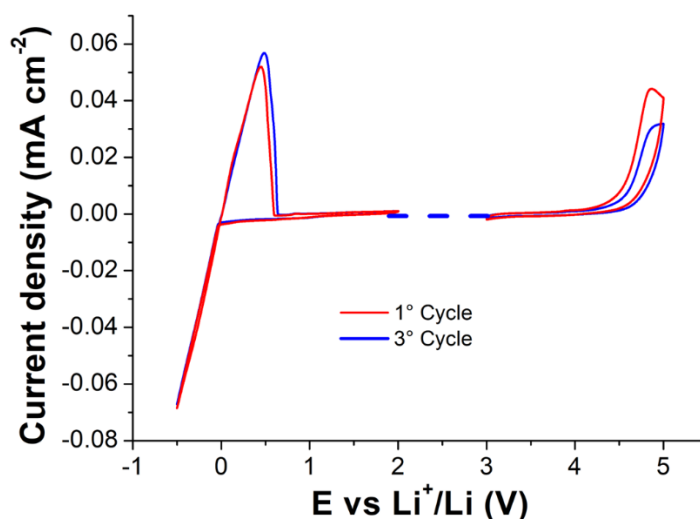
Figure 6.4 Electrochemical stability window for coPIL2 obtained by CV at 70 °C (stainless steel as working electrode and Li foil as counter and reference electrodes, scan rate 0.1 mV s^{-1}).

The stability of coPIL2 at the interface with the lithium metal electrode was investigated utilizing reversible constant current (galvanostatic) plating and stripping tests. The lithium plating/stripping measure was performed at 70 °C and at different current density values, ranging from 0.1 to 0.5 mA cm^{-2} (30 min per step, see Figure 6.5 a,b).Actually, coPIL2 demonstrates excellent stability during reversible plating and stripping with limited overpotential at high current density regimes, without abnormal voltage drifts, thus no short circuit issues. Moreover, as

evidenced in Figure 6.5b even after long-term cycling at 0.1 mA cm^{-2}, either the profile or the potential values are identical to the initial values, proving the outstanding compatibility of coPIL2 with lithium metal and the effective suppression of dendrite growth under the selected testing conditions. Indeed, as shown in Figure 6.5c, the charge transfer resistance at the electrolyte/electrode interface is not subjected to variation upon constant cycling over time even after 323 h of reversible plating and stripping at different current regimes, highlighting the stability of electrolyte due to formation of a stable SEI that allows reversible cycling and prevents battery failure.
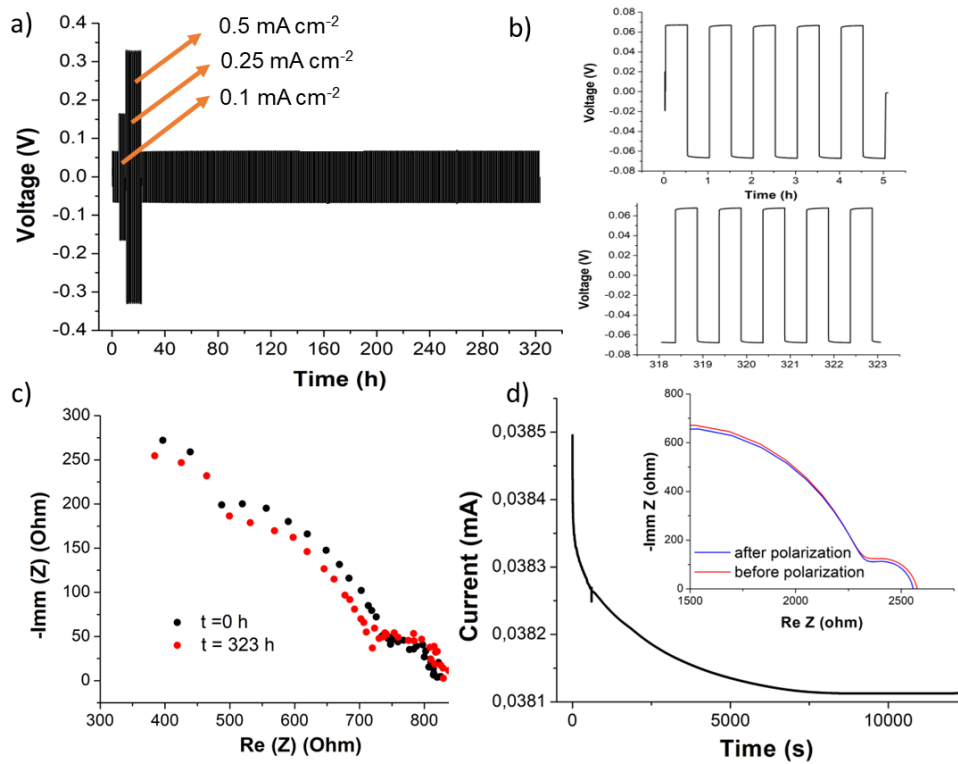
Figure 6.5 Electrochemical characterization performed with symmetrical cell with Li/coPIL2/Li configuration at 70 °C: (a) galvanostatic plating and stripping test at different current densities (0.1, 0.25 and 0.5 mA cm^{-2}); (b) particular of potential vs. test time of lithium stripping/platingand (c) results from EIS at the beginning and at the end of the plating and stripping test; (d) EIS analysis and polarization current variation results from lithium-ion transference number measurement.

The lithium-ion transference number of coPIL2 was evaluated at 70 °C by both the Evans/Vincent/Bruce[220] and Abraham et al.[221] methods, which were in good accordance. The experiments were performed by assembling symmetrical cells with Li/coPIL2/Li configuration. Results from EIS and polarization current variation analysis are given in Figure 6.5d. Through data fitting, it was found that the initial cell resistance value of 252 Ω only decreased to 221 Ω, proving the formation of a stable interface in contact with lithium metal, and the plot of current response as a function of time revealed a small drop from 3.849 to 3.811 µA before the steady-state was reached. Further, by applying the Equation 3, the calculated t_{Li}^+ value is 0.98 (or 0.96 considering the Equation 4). It is worth noticing that both t_{Li}^+ values are close to unity, being at the level of the best single-ion conducting polymer electrolytes reported in the literature[177] and clearly significantly higher compared to many various electrolytes systems under study for Li-based battery devices, which include standard liquid electrolytes containing dissolved salts, RTIL-based electrolytes, cationic PILs/Li salts, salt in polymers (e.g., PEO/Li) and/or composite electrolytes.[157,244] Indeed, the t_{Li}^+ of the novel SICPE is evidently higher with respect to the one reported for RAFT-poly(PEGM)-b-poly(LiMTSI)1,[201] which was 0.83. We could assume that the long EO chain of ionic monomer actively participates in the coordination and mobility of Li^+ cations, resulting in enhanced electrochemical performance, especially in terms of stable galvanostatic cycling and high energy density.

Electrochemical behaviour in laboratory-scale Li metal cell

To further confirm the significance of the newly prepared SICPE as a promising solid-state electrolyte (solvent/additive-free), the lab-scale lithium cell prototypes based on coPIL2 were assembled using a lithium-metal infinite negative electrode and a commercial carbon-coated $LiFePO_4$ as a standard active material for the positive electrode. As detailed in chapter 3, coPIL2 was also used as a binder for the catholyte preparation. The lab-scale lithium metal cell in Li/coPIL2/LFP configuration was tested at 70 °C at different current rates, denoted as C/n. As shown in Figure 6.6a, the first cell was cycled starting from a relatively low current of 15.7 µA (C/20) up to 63.9 µA (C/5) before being subjected to further prolonged C/20 cycling. The initial specific capacity delivered during the first cycles at C/20

($\approx$150 mAh g^{-1}) is close to the practical capacity delivered by the commercial LFP in standard LP30 electrolyte (i.e., 158 mAh g^{-1} at C/20). Excellent cycling stability with outstanding Coulombic efficiency approaching 100% during the whole cycling test is demonstrated, along with remarkable capacity retention of about 94 % after the 25[th] cycle at C/20. Figure 6.6b shows discharge potential profiles versus specific capacity at different current rates, which nicely resemble the typical flat plateaus of the LFP cathode corresponding to the Li$^+$ ion insertion (discharge) into FePO$_4$. The observed profiles remain stable even upon doubling the current rate, with only a slight overpotential increase at C/5, supporting the favourable charge transport properties of the system. Here, the overpotential increase is clearly linked to the thickness of the electrolyte used in this proof-of-concept cell (250 µm), which negatively affects the ion diffusion between cathode and anode throughout the electrolyte and the non-optimised interface engineering and electrode formulation (out of the scope of this Thesis work); moreover, the commercial LFP used in this work is optimized to deliver high energy density rather than high power output. We can assume that increasing the conductive carbon loading in the electrode and, particularly, decreasing the electrolyte thickness and optimising the catholyte formulation and homogeneity may mitigate the overpotential issue.By decreasing the active material loading to 3.35 mg cm^{-2} and the thickness (amount) of the SICPE between the electrodes, the truly solid-state cell could deliver high capacities up to 100 mAh g^{-1} at C/5 upon prolonged reversible cycling (Figure 6.6c), which is definitely remarkable for a truly solid-state single ion conducting polymer electrolyte based Li-metal cell.
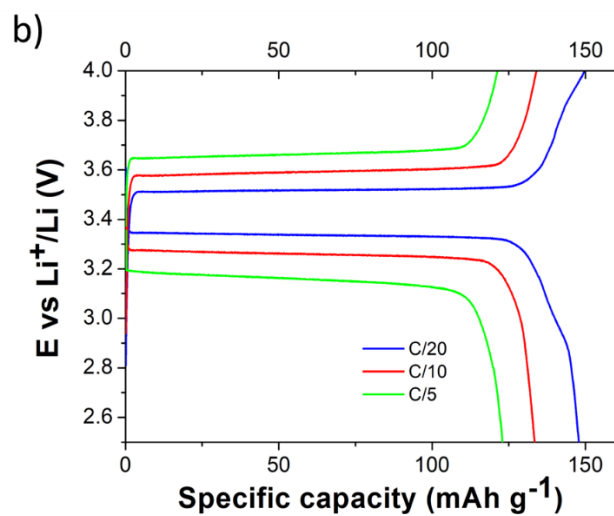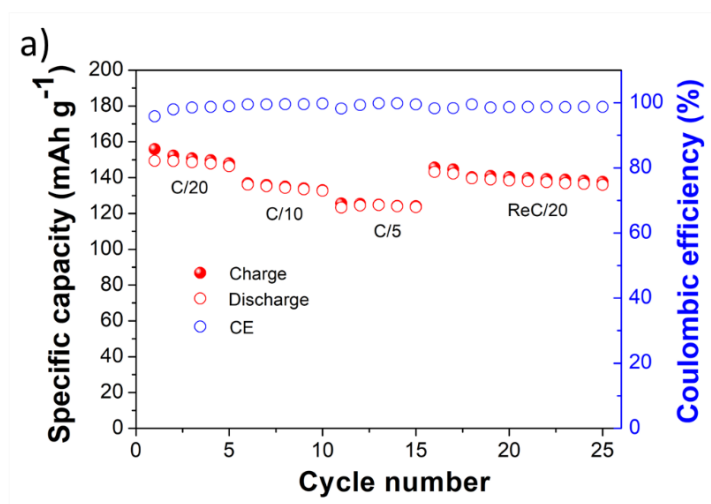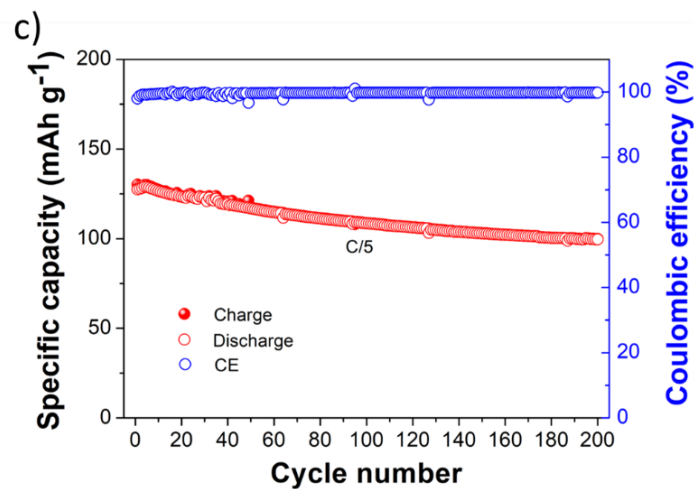
Figure 6.6 Galvanostatic cycling behaviour of Li/coPIL2/LFP solid-state cells at 70 °C. Specific capacity vs cycle number dependence (a) and corresponding voltage vs specific capacity profiles (b). Specific capacity vs. cycle number dependence at C/5 upon prolonged cycling (c).

The efficient ion conduction in the polymer separator and the favourable charge transport at the electrode/electrolyte interface in the cell guarantee remarkable electrochemical performances of the solid-state Li metal lab-scale cell in terms of capacity output and capacity retention after more than 200 consecutive charge/discharge cycles at C/5 rate. Indeed, the comparison with other SICPE systems makes clear that a high transference number value is crucial to filling the ion mobility gap with liquid electrolytes and assuring stable cycling at higher C-rate. Indeed, it is here demonstrated here that working on the nature of the ionic monomer chain is possible to prepare solid-state SICPE with suitable conductivity and improved transference number to allow stable galvanostatic cycling at a relatively high current rate. Optimisation of electrode formulation, electrolyte thickness and overall cell assembly are fundamental steps towards achieving higher current rates at low working temperature, along with the requested long-term cycling stability without any capacity fading, which is fundamental importance for future practical operation of high energy/power Li-metal cells conceived for plug-in and EV applications.

6.3 Conclusions

In this chapter, a new family of SICPE characterized by a novel ILM (ILM53) was prepared via simple free radical polymerization and thoroughly characterized in terms of its chemical-physical characteristics. The elongated monomer chain characterized by several -EO- units allowed to obtain a truly ionic liquid monomer in form of transparent oil-like material. The direct polymerization of ILM53 resulted in homopolymer (PIL53) with improved ionic conductivity (9.2×10^{-8} S cm^{-1} at 25 °C) in comparison with the polyLiMTFSI previously characterized (1.1×10^{-12} S cm^{-1} at 25 °C). The new family of SICPE prepared via simple free radical polymerization of ILM53 and PEGM monomers demonstrated excellent electrochemical performance in comparison with the state of art of solid-state SICPEs.

7 Concluding remarks

In the present scenario, actors such as supportive government policies, improving energy storage economics, and growing renewable energy sector – including hydropower, wind, and solar – are expected to be the major drivers for the continuous expansion of the energy storage market. Indeed, the battery segment is expected to account for the largest spread in the energy storage market, owing to its increasing adoption at the residential, commercial, and industry levels. In this context, the need for advanced batteries able to satisfy different performance requirements depending on the application is evident and urgent for the progress of renewable energy, along with mitigating climate change issues.

This Ph.D. research work faced one of the main challenges in the development of next-gen lithium batteries, namely the design of novel and efficient solid-state electrolyte materials. Considering the relevance of such key battery component, this work was focused on the development of novel strategies to tackle fundamental bottlenecks for the realization of Li-metal solid-state batteries for high-voltage and high energy density applications. In brief, a novel SICPEs comprising carbonate-based polymer backbone was prepared exploiting dual ROP-RAFT polymerization techniques to address the limited electrochemical stability of ethylene oxide-based polymer electrolyte. Then, intrigued by the amelioration of mechanical properties in block copolymers because of phase separation, different SICPEs were prepared by controlled RAFT polymerization. The 2-phenylethyl methacrylate monomer was used instead trimethylene to achieve better control over polymerization, resulting in a newly designed set of single-ion conducting block copolymers (A-b-B) with improved viscoelastic behavior and specific morphology. Finally, aiming at addressing the limited ionic conductivity of truly solid-state SIC polymer electrolyte, a novel Li-ionic monomer was prepared and successfully applied for the preparation of highly conductive SICPEs.

The experimental section starts in chapter 4, where the synthesis and thoroughly characterization of a newly designed poly(carbonate)-*b*-poly(ionic liquid) SICPEs family is detailed. The beneficial effect of combining ROP and RAFT living polymerization was demonstrated, which led to partially immiscible block copolymers with one block responsible for high ionic conductivity and the second one for improved mechanical properties and outstanding electrochemical

stability. The new generation of SICPEs, namely poly[TMC$_n$-b-(LiM$_m$-r-PEGM$_k$)] block copolymers, differed from the single-ion conducting block copolymer polyelectrolytes previously reported by our research group by the presence of poly(TMC) block. Remarkably, while maintaining sufficient ionic conductivity and high lithium-ion transference number (0.91), the polycarbonate block revealed outstanding electrochemical stability up to 5 V vs Li$^+$/Li at 70 °C and significantly enhanced the viscoelastic properties of poly[TMC$_n$-b-(LiM$_m$-r-PEGM$_k$)] block copolymers. The sufficiently high level of ionic conductivity of the SICPE was associated to several factors, including: i) the presence of oxyethylene fragments, that significantly improve the solubility of ionic species and facilitate their dissociation, ii) the two low T_g enabling motion of polymer chains, and iii) the nanophase separation of the casted films responsible for mechanical integrity and effective prevention of dendrite growth. The proof-of-concept lab-scale truly solid-state Li-metal cells assembled with such novel ionic block copolymers using both standard LFP and high voltage NMC-based composite electrodes at high active material loading provided excellent performances in terms of high specific capacity output, stability and reversible cycling even up to 4.8 V vs Li$^+$/Li. The obtained results are very relevant among the literature reports on truly solid-state single-ion conducting systems, which postulates the implementation of this family of polyelectrolytes in next-generation advanced, all-solid Li-metal batteries, conceived for high energy and/or power applications at enhanced safety.

In chapter 5, the synthesis, thermo-mechanical and chemical-physical properties of novel single-ion conducting block copolymers (A-b-B) is reported. The block copolymers possessed randomly distributed Li-conducting and ion-solvating segments in the first block (A), which was accompanied by incompatible poly(2-phenylethyl methacrylate) block (B), providing mechanical strength and initiating phase segregation. Such poly[(LiM$_n$-r-PEGM$_m$)-b-PhEtM$_k$] copolymers were synthesized by segmental RAFT copolymerization, allowing the control of the length of both blocks. AFM images demonstrated two types of morphologies: perpendicular hexagonally packed cylinders (HPC) and perpendicular lamellas. Six block copolymers with low molecular weights showed segregation into HPC morphology, and their ionic conductivity was lower than parent poly[LiM$_n$-r-PEGM$_m$] copolymers. The ionic conductivity of the poly[(LiM$_{17}$-r-PEGM$_{86}$)-b-PhEtM$_{131}$] sample (3.8×10^{-7} S cm^{-1} at 25 °C) was almost approaching the conductivity of initial ionic A-blocks (4.1×10^{-7} S cm^{-1} at 25 °C) despite the significant decrease in the concentration of mobile charges. Moreover, the block

copolymer showed improved viscoelastic performance compared to the parent poly[LiM$_{17}$-r-PEGM$_{86}$] copolymer (an enhancement of four orders of magnitude in complex viscosity and up to five orders of magnitude in storage modulus at 25 $^{\circ}$C). This indicates a correlation between the ionic conductivity in SICPE block copolymers and their morphology. While cylindrical morphology decreased the ionic conductivity, the lamellar samples exhibited conductivity comparable to the parent ionic A-blocks. Such results were attributed to nanosized channels formation with a high concentration of Li cations responsible for conductivity and poly(PhEtM) based phase accountable for toughness. Proof-of-concept lab-scale truly solid-state Li-metal cells were assembled with the optimized poly[(LiM$_{17}$-r-PEGM$_{86}$)-b-PhEtM$_{131}$] block copolymer and LFP-based composite cathodes. The Li/poly[(LiM$_{17}$-r-PEGM$_{86}$)-b-PhEtM$_{131}$]/LiFePO$_4$ cells were studied at 70 $^{\circ}$C and provided excellent performances in terms of high specific capacity output, stability and reversible cycling at high active material loading for a solid-state system. The system delivered 131 mAh g^{-1} after more than 75 cycles at C/20 rate, with a capacity retention of 87%, and stable reversible operation to C/5 current rate.

Finally, in chapter 6, a new family of SICPE characterized by a novel ILM (ILM53) was prepared via simple free radical polymerization and thoroughly characterized in terms of its chemical-physical characteristics. Conversely to well-known and now commercialized LiMTFSI, which appears as a white crystalline powder, the addition of several -EO- units into the main monomer chain of ILM results in the obtainment of a transparent oil-like material. The direct polymerization of ILM53 resulted in homopolymer (PIL53) with improved ionic conductivity (9.2×10^{-8} S cm^{-1} at 25 $^{\circ}$C) in comparison with the polyLiMTFSI previously characterized (1.1×10^{-12} S cm^{-1} at 25 $^{\circ}$C). Moreover, the sample PIL53 had the characteristics of a rubber-like material instead of a solid crystalline powder as polyLiMTSI. The beneficial effect of the elongated -EO- chains terminated with anchored TFSI anion moieties was also demonstrated during the characterization of copolymers (coPIL1-3) prepared by copolymerization of ILM53 and PEGM. The best sample, namely coPIL2, showed ionic conductivity values of 3.0×10^{-6} and 3.8×10^{-5} S cm^{-1} at 25 and 70 $^{\circ}$C, respectively, along with relatively high viscoelastic behaviour, which allowed for the fabrication of a solid-state Li metal lab-scale cell with LFP-based cathode able to perform more than 200 cycles at relatively high current rate (C/5) for a truly solid-state electrolyte and without any observable signs of short circuits and/or dendrite growth. The specific capacity output was close to 100 mAh g^{-1} after 200 charging/discharging cycles, drastically outperforming the

results obtained with the SICPE composed solely of PEGM and LiMTSI reported in the literature and evidenced in the chapter for comparison.

In conclusion, the strategies presented in this Ph.D. work in terms of performance optimization of different SICPEs, as well as the engineering and specific tailoring of the synthetic procedures here suggested, represent reliable solutions/insights for the scientific community in the field, paving the way towards the development of the next-generation of safe, high performing, cost-effective and environmentally friendly lithium metal batteries mainly conceived for electric transportation applications.

References

1. Davis, S. J., Caldeira, K. & Matthews, H. D. Future CO2 emissions and climate change from existing energy infrastructure. *Science (80-.).* **329**, 1330–1333 (2010).

2. Chen, G. Z. Supercapacitor and supercapattery as emerging electrochemical energy stores. *Int. Mater. Rev.* **62**, 173–202 (2017).

3. Winter, M. & Brodd, R. J. What are batteries, fuel cells, and supercapacitors? *Chem. Rev.* **104**, 4245–4269 (2004).

4. Poonam, Sharma, K., Arora, A. & Tripathi, S. K. Review of supercapacitors: Materials and devices. *J. Energy Storage* **21**, 801–825 (2019).

5. Balducci, A. *et al.* High temperature carbon-carbon supercapacitor using ionic liquid as electrolyte. *J. Power Sources* **165**, 922–927 (2007).

6. Brandt, A., Pires, J., Anouti, M. & Balducci, A. An investigation about the cycling stability of supercapacitors containing protic ionic liquids as electrolyte components. *Electrochim. Acta* **108**, 226–231 (2013).

7. Stettner, T., Huang, P., Goktas, M., Adelhelm, P. & Balducci, A. Mixtures of glyme and aprotic-protic ionic liquids as electrolytes for energy storage devices. *J. Chem. Phys.* **148**, 193825 (2018).

8. Lingua, G., Falco, M., Stettner, T., Gerbaldi, C. & Balducci, A. Enabling safe and stable Li metal batteries with protic ionic liquid electrolytes and high voltage cathodes. *J. Power Sources* **481**, 228979 (2021).

9. González, A., Goikolea, E., Barrena, J. A. & Mysyk, R. Review on supercapacitors: Technologies and materials. *Renewable and Sustainable Energy Reviews* vol. 58 1189–1206 (2016).

10. Nishi, Y. The development of lithium ion secondary batteries. *Chem. Rec.* **1**, 406–413 (2001).

11. Tarascon, J.-M. M. & Armand, M. Issues and challenges facing rechargeable lithium batteries. *Mater. Sustain. Energy A Collect. Peer-Reviewed Res. Rev.*

Artic. from Nat. Publ. Gr. **414**, 171–179 (2010).

12. Xu, K. Nonaqueous Liquid Electrolytes for Lithium-Based Rechargeable Batteries. *Chem. Rev.* **104**, 4303–4418 (2004).

13. Peled, E. The Electrochemical Behavior of Alkali and Alkaline Earth Metals in Nonaqueous Battery Systems—The Solid Electrolyte Interphase Model. *J. Electrochem. Soc.* **126**, 2047–2051 (1979).

14. Brandt, K. Historical development of secondary lithium batteries. *Solid State Ionics* **69**, 173–183 (1994).

15. Ilchev, N., Manev, V. & Hampartzumian, K. The lithium-manganese dioxide cell II. behaviour of manganese dioxide in nonaqueous electrolyte. *J. Power Sources* **25**, 177–185 (1989).

16. Whittingham, M. S. Electrical Energy Storage and Intercalation Chemistry. *Science (80-.).* **192**, 1126–1127 (1976).

17. Whittingham, M. S. Mechanism of fast ion transport in solids. *Electrochim. Acta* **20**, 575–583 (1975).

18. Whittingham, M. S. Chemistry of intercalation compounds: Metal guests in chalcogenide hosts. *Prog. Solid State Chem.* **12**, 41–99 (1978).

19. Wang, Q. *et al.* Thermal runaway caused fire and explosion of lithium ion battery. *J. Power Sources* **208**, 210–224 (2012).

20. Lin, D., Liu, Y. & Cui, Y. Reviving the lithium metal anode for high-energy batteries. *Nat. Nanotechnol.* **12**, 194–206 (2017).

21. Kong, L., Li, C., Jiang, J. & Pecht, M. G. Li-ion battery fire hazards and safety strategies. *Energies* **11**, 1–11 (2018).

22. Di Pietro, B., Patriarca, M. & Scrosati, B. On the use of rocking chair configurations for cyclable lithium organic electrolyte batteries. *J. Power Sources* **8**, 289–299 (1982).

23. Murphy, D. W., Di Salvo, F. J., Carides, J. N. & Waszczak, J. V. United States . STRUCTURES WITH LITHIUM. *Mater. Res. Bull.* **13**, 1395–1402 (1978).

24. Whittingham, M. S. & Gamble, F. R. The lithium intercalates of the

transition metal dichalcogenides. *Mater. Res. Bull.* **10**, 363–371 (1975).

25. Batteries, R. L. *et al.* Solid-Solution Oxides for Storage-Battery Electrodes. (1980).

26. Manthiram, A. & Goodenough, J. B. Layered lithium cobalt oxide cathodes. *Nat. Energy* **6**, 323 (2021).

27. Yoshino, A. From polyacetylene to carbonaceous anodes. *Nat. Energy* **6**, 449 (2021).

28. Babu, B. *et al.* Fast Charging Materials for High Power Applications. *Adv. Energy Mater.* **10**, 2001128 (2020).

29. Arora, P. & Zhang, Z. (John). Battery Separators. *Chem. Rev.* **104**, 4419–4462 (2004).

30. Goodenough, J. B. & Park, K. S. The Li-ion rechargeable battery: A perspective. *J. Am. Chem. Soc.* **135**, 1167–1176 (2013).

31. Goodenough, J. B. Evolution of strategies for modern rechargeable batteries. *Acc. Chem. Res.* **46**, 1053–1061 (2013).

32. Zhuang, G. V., Yang, H., Blizanac, B. & Ross, P. N. A study of electrochemical reduction of ethylene and propylene carbonate electrolytes on graphite using ATR-FTIR spectroscopy. *Electrochem. Solid-State Lett.* **8**, 441–445 (2005).

33. Arora, P., White, R. E. & Doyle, M. Capacity Fade Mechanisms and Side Reactions in Lithium-Ion Batteries. *J. Electrochem. Soc.* **145**, 3647–3667 (1998).

34. Liu, J. *et al.* Pathways for practical high-energy long-cycling lithium metal batteries. *Nat. Energy 2019 43* **4**, 180–186 (2019).

35. Pinson, M. B. & Bazant, M. Z. Theory of SEI Formation in Rechargeable Batteries: Capacity Fade, Accelerated Aging and Lifetime Prediction. *J. Electrochem. Soc.* **160**, A243–A250 (2013).

36. Pathan, T. S., Rashid, M., Walker, M., Widanage, W. D. & Kendrick, E. Active formation of Li-ion batteries and its effect on cycle life. *JPhys Energy* **1**, (2019).

37.   Nie, M. & Lucht, B. L. Role of Lithium Salt on Solid Electrolyte Interface
       (SEI) Formation and Structure in Lithium Ion Batteries. *J. Electrochem. Soc.*
       161, A1001–A1006 (2014).

38.   Gu, W. & Yushin, G. Review of nanostructured carbon materials for
       electrochemical capacitor applications: advantages and limitations of
       activated carbon, carbide-derived carbon, zeolite-templated carbon, carbon
       aerogels, carbon nanotubes, onion-like carbon, and graphene. *Wiley
       Interdiscip. Rev. Energy Environ.* **3**, 424–473 (2014).

39.   Candelaria, S. L. *et al.* Nanostructured carbon for energy storage and
       conversion. *Nano Energy* **1**, 195–220 (2012).

40.   Wu, Y. P., Rahm, E. & Holze, R. Carbon anode materials for lithium ion
       batteries. *Journal of Power Sources* vol. 114 228–236 (2003).

41.   Lee, S., Kim, J., Lee, J. & Cho, B. H. State-of-charge and capacity estimation
       of lithium-ion battery using a new open-circuit voltage versus state-of-
       charge. *Journal of Power Sources* vol. 185 1367–1373 (2008).

42.   Gao, J. *et al.* Brief overview of electrochemical potential in lithium ion
       batteries*. *Chinese Phys. B* **25**, 018210 (2015).

43.   Dai, H., Jiang, B. & Wei, X. Impedance Characterization and Modeling of
       Lithium-Ion Batteries Considering the Internal Temperature Gradient.
       Energies 2018, Vol. 11, Page 220 **11**, 220 (2018).

44.   Wang, R., Cui, W., Chu, F. & Wu, F. Lithium metal anodes: Present and
       future. *J. Energy Chem.* **48**, 145–159 (2020).

45.   Roy, P. & Srivastava, S. K. Nanostructured anode materials for lithium ion
       batteries. *J. Mater. Chem. A* **3**, 2454–2484 (2015).

46.   Manthiram, A. A reflection on lithium-ion battery cathode chemistry. *Nat.
       Commun. 2020 111* **11**, 1–9 (2020).

47.   Fergus, J. W. Recent developments in cathode materials for lithium ion
       batteries. *J. Power Sources* **195**, 939–954 (2010).

48.   Xu, J., Dou, S., Liu, H. & Dai, L. Cathode materials for next generation
       lithium ion batteries. *Nano Energy* **2**, 439–442 (2013).

49.   Zhou, D., Shanmukaraj, D., Tkacheva, A., Armand, M. & Wang, G. Polymer

Electrolytes for Lithium-Based Batteries: Advances and Prospects. *Chem* **5**, 2326–2352 (2019).

50.   Yao, P. *et al.* Review on Polymer-Based Composite Electrolytes for Lithium Batteries. *Front. Chem.* **7**, 522 (2019).

51.   Zheng, F., Kotobuki, M., Song, S., Lai, M. O. & Lu, L. Review on solid electrolytes for all-solid-state lithium-ion batteries. *J. Power Sources* **389**, 198–213 (2018).

52.   Cheng, X. B., Zhang, R., Zhao, C. Z. & Zhang, Q. Toward Safe Lithium Metal Anode in Rechargeable Batteries: A Review. *Chem. Rev.* **117**, 10403–10473 (2017).

53.   Xu, W. *et al.* Lithium metal anodes for rechargeable batteries. *Energy Environ. Sci.* **7**, 513–537 (2014).

54.   Wu, F. *et al.* Perspectives for restraining harsh lithium dendrite growth: Towards robust lithium metal anodes. *Energy Storage Mater.* **15**, 148–170 (2018).

55.   Wu, F., Maier, J. & Yu, Y. Guidelines and trends for next-generation rechargeable lithium and lithium-ion batteries. *Chem. Soc. Rev.* **49**, 1569–1614 (2020).

56.   Zheng, G. *et al.* Interconnected hollow carbon nanospheres for stable lithium metal anodes. *Nat. Nanotechnol. 2014 98* **9**, 618–623 (2014).

57.   Cheng, X. B. *et al.* A review of solid electrolyte interphases on lithium metal anode. *Adv. Sci.* **3**, 1–20 (2015).

58.   Kozen, A. C. *et al.* Next-Generation Lithium Metal Anode Engineering via Atomic Layer Deposition. **10**, 41 (2021).

59.   Wu, F. *et al.* An effective approach to protect lithium anode and improve cycle performance for Li-S batteries. *ACS Appl. Mater. Interfaces* **6**, 15542–15549 (2014).

60.   Zhang, L., Zhu, C., Yu, S., Ge, D. & Zhou, H. Status and challenges facing representative anode materials for rechargeable lithium batteries. *J. Energy Chem.* **66**, 260–294 (2022).

61.   Asenbauer, J. *et al.* The success story of graphite as a lithium-ion anode

material – fundamentals, remaining challenges, and recent developments including silicon (oxide) composites. *Sustain. Energy Fuels* **4**, 5387–5416 (2020).

62. De Las Casas, C. & Li, W. A review of application of carbon nanotubes for lithium ion battery anode material. *J. Power Sources* **208**, 74–85 (2012).

63. Claye, A. S., Fischer, J. E., Huffman, C. B., Rinzler, A. G. & Smalley, R. E. Solid-State Electrochemistry of the Li Single Wall Carbon Nanotube System. *J. Electrochem. Soc.* **147**, 2845 (2000).

64. Wang, T. *et al.* Study of Microstructure Change of Carbon Nanofibers as Binder-Free Anode for High-Performance Lithium-Ion Batteries. *ACS Appl. Mater. Interfaces* **8**, 33091–33101 (2016).

65. Wen, Z. S., Yang, J., Wang, B. F., Wang, K. & Liu, Y. High capacity silicon/carbon composite anode materials for lithium ion batteries. *Electrochem. commun.* **5**, 165–168 (2003).

66. Mcdowell, M. T. *et al.* 25th Anniversary Article: Understanding the Lithiation of Silicon and Other Alloying Anodes for Lithium-Ion Batteries. *Adv. Mater.* **25**, 4966–4985 (2013).

67. Falco, M. *et al.* A bilayer polymer electrolyte encompassing pyrrolidinium-based RTIL for binder-free silicon few-layer graphene nanocomposite anodes for Li-ion battery. *Electrochem. commun.* **118**, 106807 (2020).

68. Chan, C. K. *et al.* High-performance lithium battery anodes using silicon nanowires. *Nat. Nanotechnol. 2008 31* **3**, 31–35 (2007).

69. Maranchi, J. P., Hepp, A. F. & Kumta, P. N. High capacity, reversible silicon thin-film anodes for lithium-ion batteries. *Electrochem. Solid-State Lett.* **6**, A198 (2003).

70. Yan, H., Zhang, D., Qilu, Duo, X. & Sheng, X. A review of spinel lithium titanate (Li4Ti5O12) as electrode material for advanced energy storage devices. *Ceram. Int.* **47**, 5870–5895 (2021).

71. Wang, Y. Q. *et al.* Rutile-TiO 2 nanocoating for a high-rate Li 4Ti 5O 12 anode of a lithium-ion battery. *J. Am. Chem. Soc.* **134**, 7874–7879 (2012).

72. Furushima, Y., Yanagisawa, C., Nakagawa, T., Aoki, Y. & Muraki, N. Thermal stability and kinetics of delithiated LiCoO2. *J. Power Sources* **196**,

2260–2263 (2011).

73.   Whittingham, M. S. Lithium batteries and cathode materials. *Chem. Rev.* **104**, 4271–4301 (2004).

74.   Huang, H., Faulkner, T., Barker, J. & Saidi, M. Y. Lithium metal phosphates, power and automotive applications. *J. Power Sources* **189**, 748–751 (2009).

75.   Chang, Z. R. *et al.* Synthesis and characterization of high-density LiFePO4/C composites as cathode materials for lithium-ion batteries. *Electrochim. Acta* **54**, 4595–4599 (2009).

76.   Padhi, A. K., Nanjundaswamy, K. S. & Goodenough, J. B. Phospho-olivines as Positive-Electrode Materials for Rechargeable Lithium Batteries. *J. Electrochem. Soc.* **144**, 1188–1194 (1997).

77.   Ravet, N. *et al.* Electroactivity of natural and synthetic triphylite. *J. Power Sources* **97**–**98**, 503–507 (2001).

78.   Yamada, A., Chung, S. C. & Hinokuma, K. Optimized LiFePO[sub 4] for Lithium Battery Cathodes. *J. Electrochem. Soc.* **148**, A224 (2001).

79.   Ouyang, C., Shi, S., Wang, Z., Huang, X. & Chen, L. First-principles study of Li ion diffusion in LiFePO 4. *Phys. Rev. B* **69**, (1043).

80.   Zhang, W.-J. Structure and performance of LiFePO4 cathode materials: A review. *J. Power Sources* **196**, 2962–2970 (2011).

81.   Gong, Z. & Yang, Y. Recent advances in the research of polyanion-type cathode materials for Li-ion batteries. *Energy Environ. Sci.* **4**, 3223–3242 (2011).

82.   Takahashi, M., Tobishima, S., Takei, K. & Sakurai, Y. Characterization of LiFePO4 as the cathode material for rechargeable lithium batteries. *J. Power Sources* **97**–**98**, 508–511 (2001).

83.   Jugović, D. & Uskoković, D. A review of recent developments in the synthesis procedures of lithium iron phosphate powders. *J. Power Sources* **190**, 538–544 (2009).

84.   Saïdi, M. Y., Barker, J., Huang, H., Swoyer, J. L. & Adamson, G. Performance characteristics of lithium vanadium phosphate as a cathode material for lithium-ion batteries. *J. Power Sources* **119**–**121**, 266–272

(2003).

85.   Saïdi, M. Y., Barker, J., Huang, H., Swoyer, J. L. & Adamson, G. Electrochemical properties of lithium vanadium phosphate as a cathode material for lithium-ion batteries. *Electrochem. Solid-State Lett.* **5**, 149–152 (2002).

86.   Böckenfeld, N. & Balducci, A. On the use of lithium vanadium phosphate in high power devices. *J. Power Sources* **235**, 265–273 (2013).

87.   Wakihara, M. Recent developments in lithium ion batteries. *Mater. Sci. Eng. R Reports* **33**, 109–134 (2001).

88.   Rossen, E., Jones, C. D. W. & Dahn, J. R. Structure and electrochemistry of LixMnyNi1−yO2. *Solid State Ionics* **57**, 311–318 (1992).

89.   Ohzuku, T. & Makimura, Y. Layered lithium insertion material of LiCo1/3Ni1/3Mn1/3O2 for lithium-ion batteries. *Chem. Lett.* 642–643 (2001) doi:10.1246/CL.2001.642.

90.   Xu, J., Lin, F., Doeff, M. M. & Tong, W. A review of Ni-based layered oxides for rechargeable Li-ion batteries. *J. Mater. Chem. A* **5**, 874–901 (2017).

91.   Liu, Z., Yu, A. & Lee, J. Y. Synthesis and characterization of LiNi1−x−yCoxMnyO2 as the cathode materials of secondary lithium batteries. *J. Power Sources* **81**–**82**, 416–419 (1999).

92.   Yoshio, M., Noguchi, H., Itoh, J. ichi, Okada, M. & Mouri, T. Preparation and properties of LiCoyMnxNi1−x−yO2 as a cathode for lithium ion batteries. *J. Power Sources* **90**, 176–181 (2000).

93.   Yu, H. & Zhou, H. Initial Coulombic efficiency improvement of the Li1.2Mn0.567Ni0.166Co0.067O2 lithium-rich material by ruthenium substitution for manganese. *J. Mater. Chem.* **22**, 15507–15510 (2012).

94.   Robert, R., Villevieille, C. & Novák, P. Enhancement of the high potential specific charge in layered electrode materials for lithium-ion batteries. *J. Mater. Chem. A* **2**, 8589–8598 (2014).

95.   Ellis, B. L., Lee, K. T. & Nazar, L. F. Positive electrode materials for Li-Ion and Li-batteries. *Chem. Mater.* **22**, 691–714 (2010).

96. Garcia, J. C. *et al.* Surface Structure, Morphology, and Stability of Li(Ni1/3Mn1/3Co1/3)O2 Cathode Material. *J. Phys. Chem. C* **121**, 8290–8299 (2017).

97. Koyama, Y., Tanaka, I., Adachi, H., Makimura, Y. & Ohzuku, T. Crystal and electronic structures of superstructural Li1−x[Co1/3Ni1/3Mn1/3]O2 (0≤x≤1). *J. Power Sources* **119–121**, 644–648 (2003).

98. Darjazi, H., Rezvani, S. J., Brutti, S. & Nobili, F. Improvement of structural and electrochemical properties of NMC layered cathode material by combined doping and coating. *Electrochim. Acta* **404**, 139577 (2022).

99. Tian, C., Lin, F. & Doeff, M. M. Electrochemical Characteristics of Layered Transition Metal Oxide Cathode Materials for Lithium Ion Batteries: Surface, Bulk Behavior, and Thermal Properties. (2017) doi:10.1021/acs.accounts.7b00520.

100. Kim, J. M. & Chung, H. T. Role of transition metals in layered Li[Ni,Co,Mn]O2 under electrochemical operation. *Electrochim. Acta* **49**, 3573–3580 (2004).

101. Kobayashi, H. *et al.* Investigation on lithium de-intercalation mechanism for Li1−yNi1/3Mn1/3Co1/3O2. *J. Power Sources* **146**, 640–644 (2005).

102. Tsai, Y. W. *et al.* In-Situ X-ray Absorption Spectroscopic Study on Variation of Electronic Transitions and Local Structure of LiNi1/3Co1/3Mn1/3O2 Cathode Material during Electrochemical Cycling. *Chem. Mater.* **17**, 3191–3199 (2005).

103. Yoon, W. S. *et al.* Combined NMR and XAS Study on Local Environments and Electronic Structures of Electrochemically Li-Ion Deintercalated Li1-xCo 1/3Ni1/3Mn1/3O2 Electrode System. *Electrochem. Solid-State Lett.* **7**, A53 (2004).

104. Jung, R., Metzger, M., Maglia, F., Stinner, C. & Gasteiger, H. A. Oxygen Release and Its Effect on the Cycling Stability of LiNi x Mn y Co z O 2 (NMC) Cathode Materials for Li-Ion Batteries . *J. Electrochem. Soc.* **164**, A1361–A1377 (2017).

105. Ngala, J. K. *et al.* The synthesis, characterization and electrochemical behavior of the layered LiNi0.4Mn0.4Co0.2O2 compound. *J. Mater. Chem.* **14**, 214–220 (2004).

106.   Jung, S.-K. *et al.* Understanding the Degradation Mechanisms of LiNi0.5Co0.2Mn0.3O2 Cathode Material in Lithium Ion Batteries. *Adv. Energy Mater.* **4**, 1300787 (2014).

107.   Noh, H. J., Youn, S., Yoon, C. S. & Sun, Y. K. Comparison of the structural and electrochemical properties of layered Li[NixCoyMnz]O2 (x = 1/3, 0.5, 0.6, 0.7, 0.8 and 0.85) cathode material for lithium-ion batteries. *J. Power Sources* **233**, 121–130 (2013).

108.   Li, T. *et al.* Degradation Mechanisms and Mitigation Strategies of Nickel-Rich NMC-Based Lithium-Ion Batteries. *Electrochem. Energy Rev. 2019 31* **3**, 43–80 (2019).

109.   Zheng, J., Kan, W. H. & Manthiram, A. Role of Mn content on the electrochemical properties of Nickel-Rich layered LiNi0.8-xCo0.1Mn0.1+xO2 (0.0 ≤ x ≤ 0.08) cathodes for lithium-ion batteries. *ACS Appl. Mater. Interfaces* **7**, 6926–6934 (2015).

110.   Manthiram, A., Knight, J. C., Myung, S. T., Oh, S. M. & Sun, Y. K. Nickel-Rich and Lithium-Rich Layered Oxide Cathodes: Progress and Perspectives. *Adv. Energy Mater.* **6**, (2016).

111.   Jarvis, K. A., Deng, Z., Allard, L. F., Manthiram, A. & Ferreira, P. J. Atomic structure of a lithium-rich layered oxide material for lithium-ion batteries: Evidence of a solid solution. *Chem. Mater.* **23**, 3614–3621 (2011).

112.   Xu, J. *et al.* Elucidating anionic oxygen activity in lithium-rich layered oxides. *Nat. Commun. 2018 91* **9**, 1–10 (2018).

113.   Xu, K. Electrolytes and interphases in Li-ion batteries and beyond. *Chem. Rev.* **114**, 11503–11618 (2014).

114.   Zhang, Z. *et al.* Fluorinated electrolytes for 5 v lithium-ion battery chemistry. *Energy Environ. Sci.* **6**, 1806–1810 (2013).

115.   Xia, L., Chen, M., Wang, F., Miao, H. & Yuan, J. Partially fluorinated linear carboxylate esters employed as co-solvents for high-voltage lithium-ion batteries. *Journal of Power Sources* vol. 526 (2022).

116.   Goodenough, J. B. & Kim, Y. Challenges for rechargeable Li batteries. *Chem. Mater.* **22**, 587–603 (2010).

117.   Vogdanis, L., Martens, B., Uchtmann, H., Hensel, F. & Heitz, W. Synthetic

and thermodynamic investigations in the polymerization of ethylene carbonate. *Die Makromol. Chemie* **191**, 465–472 (1990).

118.   Hess, S., Wohlfahrt-Mehrens, M. & Wachtler, M. Flammability of Li-Ion Battery Electrolytes: Flash Point and Self-Extinguishing Time Measurements. *J. Electrochem. Soc.* **162**, A3084–A3097 (2015).

119.   Campion, C. L., Li, W. & Lucht, B. L. Thermal Decomposition of LiPF[sub 6]-Based Electrolytes for Lithium-Ion Batteries. *J. Electrochem. Soc.* **152**, A2327 (2005).

120.   Kusachi, Y., Zhang, Z., Dong, J. & Amine, K. Electrode Surface Film Formation in Tris(ethylene glycol)-Substituted TrimethylsilaneÀLithium Bis(oxalate)borate Electrolyte. *J. Phys. Chem. C* **115**, 24013–24020 (2011).

121.   Jia, H. & Xu, W. Nonflammable nonaqueous electrolytes for lithium batteries. *Curr. Opin. Electrochem.* **30**, 100781 (2021).

122.   Nair, J. R. *et al.* Room temperature ionic liquid (RTIL)-based electrolyte cocktails for safe, high working potential Li-based polymer batteries. *J. Power Sources* **412**, 398–407 (2019).

123.   Nakagawa, H. *et al.* Application of nonflammable electrolyte with room temperature ionic liquids (RTILs) for lithium-ion cells. *J. Power Sources* **174**, 1021–1026 (2007).

124.   Wang, Y. *et al.* Design principles for solid-state lithium superionic conductors. *Nat. Mater.* **14**, 1026–1031 (2015).

125.   Manthiram, A., Yu, X. & Wang, S. Lithium battery chemistries enabled by solid-state electrolytes. *Nat. Rev. Mater. 2017 24* **2**, 1–16 (2017).

126.   Payne, D. R. & Wright, P. V. Morphology and ionic conductivity of some lithium ion complexes with poly(ethylene oxide). *Polymer (Guildf).* **23**, 690–693 (1982).

127.   Armand, M. Polymers with Ionic Conductivity. *Adv. Mater.* **2**, 278–286 (1990).

128.   Long, L., Wang, S., Xiao, M. & Meng, Y. Polymer electrolytes for lithium polymer batteries. *J. Mater. Chem. A* **4**, 10038–10039 (2016).

129.   Li, S. *et al.* Progress and Perspective of Ceramic/Polymer Composite Solid

Electrolytes for Lithium Batteries. *Adv. Sci.* **7**, 1903088 (2020).

130. Porcarelli, L. *et al.* Single-Ion Conducting Polymer Electrolytes for Lithium Metal Polymer Batteries that Operate at Ambient Temperature. *ACS Energy Lett.* **1**, 678–682 (2016).

131. Gauthier, M. *et al.* Electrode-Electrolyte Interface in Li-Ion Batteries: Current Understanding and New Insights. *J. Phys. Chem. Lett.* **6**, 4653–4672 (2015).

132. Xue, Z., He, D. & Xie, X. Poly(ethylene oxide)-based electrolytes for lithium-ion batteries. *J. Mater. Chem. A* **3**, 19218–19253 (2015).

133. Méry, A., Rousselot, S., Lepage, D. & Dollé, M. A critical review for an accurate electrochemical stability window measurement of solid polymer and composite electrolytes. *Materials (Basel).* **14**, (2021).

134. MacFarlane, D. R. & Forsyth, M. Plastic crystal electrolyte materials: New perspectives on solid state ionics. *Adv. Mater.* **13**, 957–966 (2001).

135. Fan, J. & Angell, C. A. The preparation, conductivity, viscosity and mechanical properties of polymer electrolytes and new hybrid ionic rubber electrolytes. *Electrochim. Acta* **40**, 2397–2400 (1995).

136. Mindemark, J., Lacey, M. J., Bowden, T. & Brandell, D. Beyond PEO—Alternative host materials for Li+-conducting solid polymer electrolytes. *Prog. Polym. Sci.* **81**, 114–143 (2018).

137. Kim, H.-K., Srinivasan -, V., Agrawal, R. C. & Pandey, G. P. Solid polymer electrolytes: materials designing and all-solid-state battery applications: an overview Status and Targets for Polymer-Based Solid-State Batteries for Electric Vehicle Applications Insights into the use of polyethylene oxide in energy storage/conversion devices: a critical review Anil Arya and A L Sharma-Recent citations Solid polymer electrolytes: materials designing and all-solid-state battery applications: an overview. *J. Phys. D. Appl. Phys.* **41**, 18 (2008).

138. Berthier, C. *et al.* Microscopic investigation of ionic conductivity in alkali metal salts-poly(ethylene oxide) adducts. *Solid State Ionics* **11**, 91–95 (1983).

139. Bruce, P. G. Ion– polyether coordination complexes: crystalline ionic conductors for clean energy storage. *Dalt. Trans.* **0**, 1365–1369 (2006).

140. Croce, F., Appetecchi, G. B., Persi, L. & Scrosati, B. Nanocomposite polymer electrolytes for lithium batteries. *Nat. 1998 3946692* **394**, 456–458 (1998).

141. Zhao, Y. *et al.* Design Strategies for Polymer Electrolytes with Ether and Carbonate Groups for Solid-State Lithium Metal Batteries. *Chem. Mater.* **32**, 6811–6830 (2020).

142. Qiao, L. *et al.* A promising bulky anion based lithium borate salt for lithium metal batteries. *Chem. Sci.* **9**, 3451–3458 (2018).

143. Karuppasamy, K., Antony, R., Alwin, S., Balakumar, S. & Sahaya Shajan, X. A review on PEO based solid polymer electrolytes (SPEs) complexed with LiX (X=Tf, BOB) for rechargeable lithium ion batteries. *Mater. Sci. Forum* **807**, 41–63 (2015).

144. Sutto, T. E. Hydrophobic and Hydrophilic Interactions of Ionic Liquids and Polymers in Solid Polymer Gel Electrolytes. *J. Electrochem. Soc.* **154**, P101 (2007).

145. Kosonen, H. *et al.* Mesomorphic Structure of Poly(styrene)-block-poly(4-vinylpyridine) with Oligo(ethylene oxide)sulfonic Acid Side Chains as a Model for Molecularly Reinforced Polymer Electrolyte. *Macromolecules* **35**, 10149–10154 (2002).

146. Niitani, T. *et al.* Synthesis of Li+ ion conductive PEO-PSt block copolymer electrolyte with microphase separation structure. *Electrochem. Solid-State Lett.* **8**, A385 (2005).

147. Matyjaszewski, K. & Tsarevsky, N. V. Nanostructured functional materials prepared by atom transfer radical polymerization. *Nat. Chem.* **1**, 276–288 (2009).

148. Perrier, S. 50th Anniversary Perspective: RAFT Polymerization - A User Guide. *Macromolecules* **50**, 7433–7447 (2017).

149. Giles, J. R. M., Gray, F. M., MacCallum, J. R. & Vincent, C. A. Synthesis and characterization of ABA block copolymer-based polymer electrolytes. *Polymer (Guildf).* **28**, 1977–1981 (1987).

150. Daigle, J. C. *et al.* Lithium battery with solid polymer electrolyte based on comb-like copolymers. *J. Power Sources* **279**, 372–383 (2015).

151. Khan, I. M., Fish, D., Delaviz, Y. & Smid, J. ABA triblock comb copolymers with oligo(oxyethylene) side chains as matrix for ion transport. *Die Makromol. Chemie* **190**, 1069–1078 (1989).

152. Hirahara, K. *et al.* Fabrication of solid polymer electrolyte based on block-graft copolymer. 1. Precision synthesis and characterization of polystyrene-block-[poly(p-hydroxystyrene)-graft-poly(ethylene   oxide))-block-polystyrene. *React. Funct. Polym.* **37**, 169–182 (1998).

153. Wang, C., Sakai, T., Watanabe, O., Hirahara, K. & Nakanishi, T. All Solid-State Lithium-Polymer Battery Using a Self-Cross-Linking Polymer Electrolyte. *J. Electrochem. Soc.* **150**, A1166 (2003).

154. Sun, B., Mindemark, J., Edström, K. & Brandell, D. Realization of high performance polycarbonate-based Li polymer batteries. *Electrochem. commun.* **52**, 71–74 (2015).

155. Mindemark, J., Mogensen, R., Smith, M. J., Silva, M. M. & Brandell, D. Polycarbonates as alternative electrolyte host materials for solid-state sodium batteries. *Electrochem. commun.* **77**, 58–61 (2017).

156. Zhang, J. J. *et al.* Aliphatic Polycarbonate-Based Solid-State Polymer Electrolytes for Advanced Lithium Batteries: Advances and Perspective. *Small* **14**, 1–16 (2018).

157. Sun, B. *et al.* Ion transport in polycarbonate based solid polymer electrolytes: Experimental and computational investigations. *Phys. Chem. Chem. Phys.* **18**, 9504–9513 (2016).

158. Tominaga, Y. Ion-conductive polymer electrolytes based on poly(ethylene carbonate) and its derivatives. *Polym. J.* **49**, 291–299 (2017).

159. Kimura, K. & Tominaga, Y. Understanding Electrochemical Stability and Lithium Ion-Dominant Transport in Concentrated Poly(ethylene carbonate) Electrolyte. *ChemElectroChem* **5**, 4008–4014 (2018).

160. Meabe, L. *et al.* Polycondensation as a Versatile Synthetic Route to Aliphatic Polycarbonates for Solid Polymer Electrolytes. *Electrochim. Acta* **237**, 259–266 (2017).

161. Pêgo, A. P., Grijpma, D. W. & Feijen, J. Enhanced mechanical properties of 1,3-trimethylene carbonate polymers and networks. *Polymer (Guildf).* **44**, 6495–6504 (2003).

162.   Brandell, D., Mindemark, J. & Hernández, G. *Polymer-based Solid State Batteries*. *Processing of Polymers* (De Gruyter, 2021). doi:10.1515/9781501521140.

163.   Xu, J., Feng, E. & Song, J. Renaissance of aliphatic polycarbonates: New techniques and biomedical applications. *J. Appl. Polym. Sci.* **131**, (2014).

164.   Tominaga, Y., Nanthana, V. & Tohyama, D. Ionic conduction in poly(ethylene carbonate)-based rubbery electrolytes including lithium salts. *Polym. J.* **44**, 1155–1158 (2012).

165.   Tominaga, Y., Yamazaki, K. & Nanthana, V. Effect of Anions on Lithium Ion Conduction in Poly(ethylene carbonate)-based Polymer Electrolytes. *J. Electrochem. Soc.* **162**, A3133–A3136 (2015).

166.   Okumura, T. & Nishimura, S. Lithium ion conductive properties of aliphatic polycarbonate. *Solid State Ionics* **267**, 68–73 (2014).

167.   Commarieu, B. *et al.* Solid-to-liquid transition of polycarbonate solid electrolytes in Li-metal batteries. *J. Power Sources* **436**, 226852 (2019).

168.   Nakamura, M. & Tominaga, Y. Utilization of carbon dioxide for polymer electrolytes [II]: Synthesis of alternating copolymers with glycidyl ethers as novel ion-conductive polymers. *Electrochim. Acta* **57**, 36–39 (2011).

169.   Tominaga, Y., Shimomura, T. & Nakamura, M. Alternating copolymers of carbon dioxide with glycidyl ethers for novel ion-conductive polymer electrolytes. *Polymer (Guildf).* **51**, 4295–4298 (2010).

170.   Helou, M., Miserque, O., Brusson, J. M., Carpentier, J. F. & Guillaume, S. M. Organocatalysts for the controlled 'immortal' ring-opening polymerization of six-membered-ring cyclic carbonates: A metal-free, green process. *Chem. - A Eur. J.* **16**, 13805–13813 (2010).

171.   Smith, M. J., Silva, M. M., Cerqueira, S. & MacCallum, J. R. Preparation and characterization of a lithium ion conducting electrolyte based on poly(trimethylene carbonate). *Solid State Ionics* **140**, 345–351 (2001).

172.   Silva, M. M., Barros, S. C., Smith, M. J. & MacCallum, J. R. Study of novel lithium salt-based, plasticized polymer electrolytes. *J. Power Sources* **111**, 52–57 (2002).

173.   Barbosa, P. C., Rodrigues, L. C., Silva, M. M. & Smith, M. J.

Characterization of pTMCnLiPF6 solid polymer electrolytes. *Solid State Ionics* **193**, 39–42 (2011).

174. Silva, M. M., Barros, S. C., Smith, M. J. & MacCallum, J. R. Characterization of solid polymer electrolytes based on poly(trimethylenecarbonate) and lithium tetrafluoroborate. *Electrochim. Acta* **49**, 1887–1891 (2004).

175. Sun, B., Mindemark, J., Edström, K. & Brandell, D. Polycarbonate-based solid polymer electrolytes for Li-ion batteries. *Solid State Ionics* **262**, 738–742 (2014).

176. Morioka, T., Ota, K. & Tominaga, Y. Effect of oxyethylene side chains on ion-conductive properties of polycarbonate-based electrolytes. *Polymer (Guildf)*. **84**, 21–26 (2016).

177. Doyle, M., Fuller, T. F. & Newman, J. The importance of the lithium ion transference number in lithium/polymer cells. *Electrochim. Acta* **39**, 2073–2081 (1994).

178. Brissot, C., Rosso, M., Chazalviel, J. N. & Lascaud, S. Dendritic growth mechanisms in lithium/polymer cells. *J. Power Sources* **81**–**82**, 925–929 (1999).

179. Tikekar, M. D., Archer, L. A. & Koch, D. L. Stability Analysis of Electrodeposition across a Structured Electrolyte with Immobilized Anions. *J. Electrochem. Soc.* **161**, A847–A855 (2014).

180. Jeong, K., Park, S. & Lee, S. Y. Revisiting polymeric single lithium-ion conductors as an organic route for all-solid-state lithium ion and metal batteries. *J. Mater. Chem. A* **7**, 1917–1935 (2019).

181. Matyjaszewski, K. Atom transfer radical polymerization (ATRP): Current status and future perspectives. Macromolecules 2012, 45, 4015-4039. (2012).

182. Baskaran, D. & Müller, A. H. E. Anionic vinyl polymerization—50 years after Michael Szwarc. *Prog. Polym. Sci.* **32**, 173–219 (2007).

183. Ito, K., Nishina, N. & Ohno, H. Enhanced ion conduction in imidazolium-type molten salts. *Electrochim. Acta* **45**, 1295–1298 (2000).

184. Shaplov, A. S. *et al.* Ionic IPNs as novel candidates for highly conductive

solid polymer electrolytes. *J. Polym. Sci. Part A Polym. Chem.* **47**, 4245–4266 (2009).

185.   Mecerreyes, D. Polymeric ionic liquids: Broadening the properties and applications of polyelectrolytes. *Prog. Polym. Sci.* **36**, 1629–1648 (2011).

186.   Shaplov, A. S., Ponkratov, D. O. & Vygodskii, Y. S. Poly(ionic liquid)s: Synthesis, properties, and application. *Polym. Sci. - Ser. B* **58**, 73–142 (2016).

187.   Macfarlane, D. R. *et al.* Energy applications of ionic liquids. *Energy Environ. Sci.* **7**, 232–250 (2014).

188.   Forsyth, S. A., Pringle, J. M. & MacFarlane, D. R. Ionic Liquids—An Overview. *Aust. J. Chem.* **57**, 113–119 (2004).

189.   Porcarelli, L. *et al.* Design of ionic liquid like monomers towards easy-accessible single-ion conducting polymer electrolytes. *Eur. Polym. J.* **107**, 218–228 (2018).

190.   Mecerreyes, D. *et al.* Single-ion conducting poly(ethylene oxide carbonate) as solid polymer electrolyte for lithium batteries. *Batter. Supercaps* **3**, 1–5 (2019).

191.   KOBAYASHI, N., Uchiyama, M. & Tsuchida, E. Poly[lithium methacrylate-co-oligo(oxyethylene)methacrylate] as a solid electrolyte with high ionic conductivity. *Solid State Ionics* **17**, 307–311 (1985).

192.   Ryu, S.-W. *et al.* Effect of Counter Ion Placement on Conductivity in Single-Ion Conducting Block Copolymer Electrolytes. *J. Electrochem. Soc.* **152**, A158 (2005).

193.   Choi, U. H. *et al.* Influence of solvating plasticizer on ion conduction of polysiloxane single-ion conductors. *Macromolecules* **47**, 3145–3153 (2014).

194.   Liang, S., Choi, U. H., Liu, W., Runt, J. & Colby, R. H. Synthesis and lithium ion conduction of polysiloxane single-ion conductors containing novel weak-binding borates. *Chem. Mater.* **24**, 2316–2323 (2012).

195.   Sun, X. G. & Angell, C. A. New single ion conductors ('polyBOP' and analogs) for rechargeable lithium batteries. *Solid State Ionics* **175**, 743–746 (2004).

196. Hoffmann, J. F., Pulst, M. & Kressler, J. Enhanced ion conductivity of poly(ethylene oxide)-based single ion conductors with lithium 1,2,3-triazolate end groups. *J. Appl. Polym. Sci.* **136**, 1–8 (2019).

197. Onishi, K., Matsumoto, M. & Shigehara, K. Thioaluminate Polymer Complexes as Single-Ionic Solid Electrolytes. *Chem. Mater.* **10**, 927–931 (1998).

198. Meziane, R., Bonnet, J.-P. P., Courty, M., Djellab, K. & Armand, M. Single-ion polymer electrolytes based on a delocalized polyanion for lithium batteries. *Electrochim. Acta* **57**, 14–19 (2011).

199. Shaplov, A. S. *et al.* Design and synthesis of new anionic 'polymeric ionic liquids' with high charge delocalization. *Polym. Chem.* **2**, 2609–2618 (2011).

200. Bouchet, R. *et al.* Efficient electrolytes for lithium-metal batteries. *Nat. Mater.* **12**, 1–6 (2013).

201. Porcarelli, L. *et al.* Single-Ion Block Copoly(ionic liquid)s as Electrolytes for All-Solid State Lithium Batteries. *ACS Appl. Mater. Interfaces* **8**, 10350–10359 (2016).

202. Porcarelli, L. *et al.* Single-ion triblock copolymer electrolytes based on poly(ethylene oxide) and methacrylic sulfonamide blocks for lithium metal batteries. *J. Power Sources* **364**, 191–199 (2017).

203. Feng, S. *et al.* Single lithium-ion conducting polymer electrolytes based on poly[(4-styrenesulfonyl)(trifluoromethanesulfonyl)imide] anions. *Electrochim. Acta* **93**, 254–263 (2013).

204. Inceoglu, S. *et al.* Morphology–Conductivity Relationship of Single-Ion-Conducting Block Copolymer Electrolytes for Lithium Batteries. *ACS Macro Lett.* **3**, 510–514 (2014).

205. Jangu, C. *et al.* Sulfonimide-Containing Triblock Copolymers for Improved Conductivity and Mechanical Performance. *Macromolecules* **48**, 4520–4528 (2015).

206. Nguyen, H. D. *et al.* Nanostructured multi-block copolymer single-ion conductors for safer high-performance lithium batteries. *Energy Environ. Sci.* **11**, 3298–3309 (2018).

207. Zhu, J. *et al.* Single-Ion Conducting Polymer Electrolytes for Solid-State

Lithium–Metal Batteries: Design, Performance, and Challenges. *Adv. Energy Mater.* **11**, 1–18 (2021).

208. Deng, K. *et al.* A Novel Single-Ion-Conducting Polymer Electrolyte Derived from CO 2 -Based Multifunctional Polycarbonate. *ACS Appl. Mater. Interfaces* **8**, 33642–33648 (2016).

209. Keddie, D. J. A guide to the synthesis of block copolymers using reversible-addition fragmentation chain transfer (RAFT) polymerization. *Chem. Soc. Rev.* **43**, 496–505 (2013).

210. Ajellal, N. *et al.* Metal-catalyzed immortal ring-opening polymerization of lactones, lactides and cyclic carbonates. *Dalt. Trans.* **39**, 8363–8376 (2010).

211. Moad, G., Rizzardo, E. & Thang, S. H. RAFT Polymerization and Some of its Applications. *Chem. – An Asian J.* **8**, 1634–1644 (2013).

212. Rokicki, G. Aliphatic cyclic carbonates and spiroorthocarbonates as monomers. *Prog. Polym. Sci.* **25**, 259–342 (2000).

213. Nederberg, F. *et al.* Organocatalytic ring opening polymerization of trimethylene carbonate. *Biomacromolecules* **8**, 153–160 (2007).

214. Sherck, N. J., Kim, H. C. & Won, Y. Y. Elucidating a Unified Mechanistic Scheme for the DBU-Catalyzed Ring-Opening Polymerization of Lactide to Poly(lactic acid). *Macromolecules* **49**, 4699–4713 (2016).

215. Kang, H. U., Yu, Y. C., Shin, S. J. & Youk, J. H. One-step synthesis of block copolymers using a hydroxyl-functionalized trithiocarbonate RAFT agent as a dual initiator for RAFT polymerization and ROP. *J. Polym. Sci. Part A Polym. Chem.* **51**, 774–779 (2013).

216. Isik, M., Sardon, H., Saenz, M. & Mecerreyes, D. New amphiphilic block copolymers from lactic acid and cholinium building units. *RSC Adv.* **4**, 53407–53410 (2014).

217. Capasso Palmiero, U., Sponchioni, M., Manfredini, N., Maraldi, M. & Moscatelli, D. Strategies to combine ROP with ATRP or RAFT polymerization for the synthesis of biodegradable polymeric nanoparticles for biomedical applications. *Polym. Chem.* **9**, 4084–4099 (2018).

218. Göktaş, M. & Olgun, B. One-Step Synthesis and Characterization of Poly(ε-caprolactone)-b-poly(N-isopropylacrylamide) Thermo-Responsive Block

Copolymers via RAFT and ROP Techniques. *Polym. Sci. - Ser. B* **61**, 421–429 (2019).

219.   Lingua, G. *et al.* Unique Carbonate-Based Single Ion Conducting Block Copolymers Enabling High-Voltage, All-Solid-State Lithium Metal Batteries. *Macromolecules* **54**, 6911–6924 (2021).

220.   Evans, J., Vincent, C. A. & Bruce, P. G. Electrochemical measurement of transference numbers in polymer electrolytes. *Polymer (Guildf).* **28**, 2324–2328 (1987).

221.   Abraham, K. M., Jiang, Z. & Carroll, B. Highly Conductive PEO-like Polymer Electrolytes. *Chem. Mater.* **9**, 1978–1988 (1997).

222.   Yuan, J., Mecerreyes, D. & Antonietti, M. Poly(ionic liquid)s: An update. *Prog. Polym. Sci.* **38**, 1009–1036 (2013).

223.   Zhang, H. *et al.* Single lithium-ion conducting solid polymer electrolytes: Advances and perspectives. *Chem. Soc. Rev.* **46**, 797–815 (2017).

224.   Yuan, J., Mecerreyes, D. & Antonietti, M. Progress in Polymer Science Poly (ionic liquid) s : An update. *Prog. Polym. Sci.* **38**, 1009–1036 (2013).

225.   Qian, W., Texter, J. & Yan, F. Frontiers in poly(ionic liquid)s: Syntheses and applications. *Chem. Soc. Rev.* **46**, 1124–1159 (2017).

226.   Brinkkötter, M. *et al.* Influence of anion structure on ion dynamics in polymer gel electrolytes composed of poly(ionic liquid), ionic liquid and Li salt. *Electrochim. Acta* **237**, 237–247 (2017).

227.   Bouchet, R. *et al.* Single-ion BAB triblock copolymers as highly efficient electrolytes for lithium-metal batteries. *Nat. Mater.* **12**, 452–457 (2013).

228.   Devaux, D. *et al.* Comparison of single-ion-conductor block-copolymer electrolytes with Polystyrene-TFSI and Polymethacrylate-TFSI structural blocks. *Electrochim. Acta* **269**, 250–261 (2018).

229.   Shaplov, A. S. *et al.* Polymeric ionic liquids: Comparison of polycations and polyanions. *Macromolecules* **44**, 9792–9803 (2011).

230.   Lozinskaya, E. I. *et al.* Expanding the chemistry of single-ion conducting poly(ionic liquid)s with polyhedral boron anions. *Polym. Int.* **68**, 1570–1579 (2019).

231. Elmore, C. T. *et al.* Ion transport in solvent-free, crosslinked, single-ion conducting polymer electrolytes for post-lithium ion batteries. *Batteries* **4**, 1–17 (2018).

232. Eschen, T., Kösters, J., Schönhoff, M. & Stolwijk, N. A. Ionic transport in polymer electrolytes based on PEO and the PMImI ionic liquid: Effects of salt concentration and iodine addition. *J. Phys. Chem. B* **116**, 8290–8298 (2012).

233. Reiter, J., Dominko, R., Nádherná, M. & Jakubec, I. Ion-conducting lithium bis(oxalato)borate-based polymer electrolytes. *J. Power Sources* **189**, 133–138 (2009).

234. Weber, R. L. *et al.* Effect of nanoscale morphology on the conductivity of polymerized ionic liquid block copolymers. *Macromolecules* **44**, 5727–5735 (2011).

235. Ye, Y., Sharick, S., Davis, E. M., Winey, K. I. & Elabd, Y. A. High hydroxide conductivity in polymerized ionic liquid block copolymers. *ACS Macro Lett.* **2**, 575–580 (2013).

236. Nykaza, J. R. *et al.* Polymerized ionic liquid diblock copolymers: impact of water/ion clustering on ion conductivity. *Soft Matter* **12**, 1133–1144 (2016).

237. Shi, Z., Newell, B. S., Bailey, T. S. & Gin, D. L. Ordered, microphase-separated, noncharged-charged diblock copolymers via the sequential ATRP of styrene and styrenic imidazolium monomers. *Polymer (Guildf).* **55**, 6664–6671 (2014).

238. Rojas, A. A. *et al.* Effect of Lithium-Ion Concentration on Morphology and Ion Transport in Single-Ion-Conducting Block Copolymer Electrolytes. *Macromolecules* **48**, 6589–6595 (2015).

239. Zhang, W. *et al.* Internal Morphology-Controllable Self-Assembly in Poly(Ionic Liquid) Nanoparticles. *ACS Nano* **10**, 7731–7737 (2016).

240. Li, L., Li, S. & Lu, Y. Suppression of dendritic lithium growth in lithium metal-based batteries. *Chem. Commun.* **54**, 6648–6661 (2018).

241. Liu, J. *et al.* A functional-gradient-structured ultrahigh modulus solid polymer electrolyte for all-solid-state lithium metal batteries. *J. Mater. Chem. A* **7**, 24477–24485 (2019).

242. Chang, W. *et al.* Understanding Adverse Effects of Temperature Shifts on Li-Ion Batteries: An Operando Acoustic Study. *J. Electrochem. Soc.* **167**, 090503 (2020).

243. Eshetu, G. G., Mecerreyes, D., Forsyth, M., Zhang, H. & Armand, M. Polymeric ionic liquids for lithium-based rechargeable batteries. *Mol. Syst. Des. Eng.* **4**, 294–309 (2019).

244. Manuel Stephan, A. & Nahm, K. S. Review on composite polymer electrolytes for lithium batteries. *Polymer (Guildf).* **47**, 5952–5964 (2006).

245. Deng, K. *et al.* Single-ion conducting artificial solid electrolyte interphase layers for dendrite-free and highly stable lithium metal anodes. *J. Mater. Chem. A* **7**, 13113–13119 (2019).

246. Lain, M. J., Brandon, J. & Kendrick, E. Design strategies for high power vs. High energy lithium ion cells. *Batteries* **5**, (2019).

247. Li, D. & Zhou, H. Two-phase transition of Li-intercalation compounds in Li-ion batteries. *Mater. Today* **17**, 451–463 (2014).

248. Sadoway, D. R. Block and graft copolymer electrolytes for high-performance, solid-state, lithium batteries. *J. Power Sources* **129**, 1–3 (2004).

249. Shaplov, A. S., Marcilla, R. & Mecerreyes, D. Recent Advances in Innovative Polymer Electrolytes based on Poly(ionic liquid)s. *Electrochim. Acta* **175**, 18–34 (2015).

250. Ye, Y., Choi, J.-H., Winey, K. I. & Elabd, Y. A. Polymerized Ionic Liquid Block and Random Copolymers: Effect of Weak Microphase Separation on Ion Transport. *Macromolecules* **45**, 7027–7035 (2012).

251. Choi, J.-H. H., Ye, Y., Elabd, Y. A. & Winey, K. I. Network Structure and Strong Microphase Separation for High Ion Conductivity in Polymerized Ionic Liquid Block Copolymers. *Macromolecules* **46**, 5290–5300 (2013).

252. Meek, K. M. & Elabd, Y. A. Polymerized ionic liquid block copolymers for electrochemical energy. *J. Mater. Chem. A* **3**, 24187–24194 (2015).

253. Nykaza, J. R., Ye, Y. & Elabd, Y. A. Polymerized ionic liquid diblock copolymers with long alkyl side-chain length. *Polymer (Guildf).* **55**, 3360–3369 (2014).

254. Thelen, J. L., Inceoglu, S., Venkatesan, N. R., Mackay, N. G. & Balsara, N. P. Relationship between Ion Dissociation, Melt Morphology, and Electrochemical Performance of Lithium and Magnesium Single-Ion Conducting Block Copolymers. *Macromolecules* **49**, 9139–9147 (2016).

255. Devaux, D. *et al.* Comparison of single-ion-conductor block-copolymer electrolytes with Polystyrene- TFSI and Polymethacrylate- TFSI structural blocks. *Electrochim. Acta* **269**, 250–261 (2018).

256. Lozinskaya, E. I. *et al.* Self-assembly of Li single-ion-conducting block copolymers for improved conductivity and viscoelastic properties. *Electrochim. Acta* 140126 (2022) doi:10.1016/J.ELECTACTA.2022.140126.

257. Mai, Y. & Eisenberg, A. Self-assembly of block copolymers. *Chem. Soc. Rev.* **41**, 5969 (2012).

258. Scalfani, V. F. *et al.* Morphological Phase Behavior of Poly(RTIL)-Containing Diblock Copolymer Melts. *Macromolecules* **45**, 4262–4276 (2012).

259. Forsyth, M., Porcarelli, L., Wang, X., Goujon, N. & Mecerreyes, D. Innovative Electrolytes Based on Ionic Liquids and Polymers for Next-Generation Solid-State Batteries. *Acc. Chem. Res.* **52**, 686–694 (2019).

260. Zhu, J. *et al.* Single-Ion Conducting Polymer Electrolytes for Solid-State Lithium–Metal Batteries: Design, Performance, and Challenges. *Adv. Energy Mater.* **11**, 2003836 (2021).

261. Di Noto, V., Lavina, S., Giffin, G. A., Negro, E. & Scrosati, B. Polymer electrolytes: Present, past and future. *Electrochim. Acta* **57**, 4–13 (2011).

262. Yue, L. *et al.* All solid-state polymer electrolytes for high-performance lithium ion batteries. *Energy Storage Mater.* **5**, 139–164 (2016).

263. Osada, I., de Vries, H., Scrosati, B. & Passerini, S. Ionic-Liquid-Based Polymer Electrolytes for Battery Applications. *Angew. Chemie Int. Ed.* **55**, 500–513 (2016).

264. Park, M. J., Choi, I., Hong, J. & Kim, O. Polymer electrolytes integrated with ionic liquids for future electrochemical devices. *J. Appl. Polym. Sci.* **129**, 2363–2376 (2013).

265.   Yang, X. *et al.* Determining the limiting factor of the electrochemical stability window for PEO-based solid polymer electrolytes: main chain or terminal –OH group? *Energy Environ. Sci.* **13**, 1318–1325 (2020).

266.   Quartarone, E. & Mustarelli, P. Electrolytes for solid-state lithium rechargeable batteries: recent advances and perspectives. *Chem. Soc. Rev.* **40**, 2525 (2011).

267.   Moshtev, R. & Johnson, B. State of the art of commercial Li ion batteries. *J. Power Sources* **91**, 86–91 (2000).

268.   Li, Z. *et al.* Interfacial engineering for stabilizing polymer electrolytes with 4V cathodes in lithium metal batteries at elevated temperature. *Nano Energy* **72**, 104655 (2020).

269.   Rodrigues, M.-T. F. *et al.* A materials perspective on Li-ion batteries at extreme temperatures. *Nat. Energy 2017 28* **2**, 1–14 (2017).

270.   Cheng, L., Ke, C., Fengchun, S., Tang, P. & Zhao, H. *Research on thermo-physical properties identification and thermal analysis of EV Li-ion battery; Research on thermo-physical properties identification and thermal analysis of EV Li-ion battery*. *2009 IEEE Vehicle Power and Propulsion Conference* (2009). doi:10.1109/VPPC.2009.5289653.

Acknowledgements